

## REVIEW ARTICLE

# An alternative menaquinone biosynthetic pathway operating in microorganisms: an attractive target for drug discovery to pathogenic *Helicobacter* and *Chlamydia* strains

Tohru Dairi

Menaquinone is an essential vitamin as an obligatory component of the electron transfer pathway in microorganisms. Menaquinone has been shown to be derived from chorismate by eight enzymes, designated MenA to -H in *Escherichia coli*. However, bioinformatic analyses of whole-genome sequences have suggested that some microorganisms, such as *Helicobacter pylori* and *Campylobacter jejuni*, which are known to cause gastric carcinoma and diarrhea, respectively, do not have orthologs of most of the *men* genes, although they synthesize menaquinone. The <sup>13</sup>C-labeling pattern of menaquinone purified from *Streptomyces coelicolor* A3(2) grown on [U-<sup>13</sup>C]glucose was quite different from that of *E. coli*, suggesting that an alternative pathway was operating in the strain. We searched for candidate genes participating in the alternative pathway by *in silico* screening, and the involvement of these genes in the pathway was confirmed by gene-disruption experiments. We also used mutagenesis to isolate mutants that required menaquinone for their growth and used these mutants as hosts for shotgun cloning experiments. Metabolites that accumulated in the culture broth of mutants were isolated and their structures were determined. Taking these results together, we deduced the outline of the alternative pathway, which branched at chorismate in a similar manner to the known pathway but then followed a completely different pathway. As humans and some useful intestinal bacteria, such as lactobacilli, lack the alternative pathway, it would be an attractive target for the development of chemotherapeutics. *The Journal of Antibiotics* (2009) 62, 347–352; doi:10.1038/ja.2009.46; published online 26 June 2009

**Keywords:** biosynthesis; futasoline pathway; menaquinone; vitamin K

## INTRODUCTION

In prokaryotes, ubiquinone and menaquinone (MK; vitamin K) are lipid-soluble molecules that shuttle electrons between membrane-bound protein complexes in the electron transport chain.<sup>1,2</sup> For example, *Escherichia coli*, a facultative anaerobe, utilizes ubiquinone (CoQ-8) under aerobic conditions, but uses MK (MK-8) when grown anaerobically.<sup>2</sup> On the other hand, *Bacillus subtilis*, a Gram-positive aerobe, only contains MK (MK-7). Therefore, MK biosynthesis is essential for the survival of *B. subtilis*.<sup>1,2</sup> In mammalian cells, ubiquinone has a single role in the electron transport chain, which is located in the inner mitochondrial membrane.<sup>2</sup> On the other hand, MK functions as an essential vitamin for the biological activation of a family of proteins involved in blood coagulation,<sup>3</sup> bone metabolism,<sup>4</sup> tissue calcification and cell cycle regulation.<sup>5</sup>

The biosynthesis of MK has mainly been studied in *E. coli*.<sup>1,2</sup> Chorismate, derived from the shikimate pathway, is initially converted into isochorismate by MenE, isochorismate synthase, and then into 2-succinyl-6-hydroxy-2,4-cyclohexadiene-1-carboxylate by MenD, a thiamin-dependent enzyme. The latter compound is dehydrated by

MenC to yield an aromatic compound, *o*-succinylbenzoate (OSB), followed by the attachment of coenzyme A by MenE to yield *o*-succinylbenzoyl-CoA. *o*-Succinylbenzoyl-CoA is then converted into 1,4-dihydroxy 2-naphthoic acid by MenB. In the last two steps of the pathway, MK is synthesized by MenA and MenG, which catalyze a prenylation and an *S*-adenosylmethionine-dependent methylation, respectively (Figure 1A).

Approximately 6 years ago, however, I found that some bacteria do not possess orthologs of the *menB*, -C, -D, -E and -F genes by bioinformatic analyses and started to investigate an alternative pathway. On the basis of bioinformatic screenings, gene knockouts, shotgun cloning with isolated mutants and *in vitro* studies with recombinant enzymes, we have deduced the outline of the alternative pathway.<sup>6,7</sup> In this review, I introduce this alternative pathway, which we designated as the futasoline pathway.<sup>7</sup>

## HOW IT STARTED

I have been studying the enzymes and genes responsible for the biosyntheses of isoprenoids produced by actinomycetes.<sup>8</sup> Approxi-

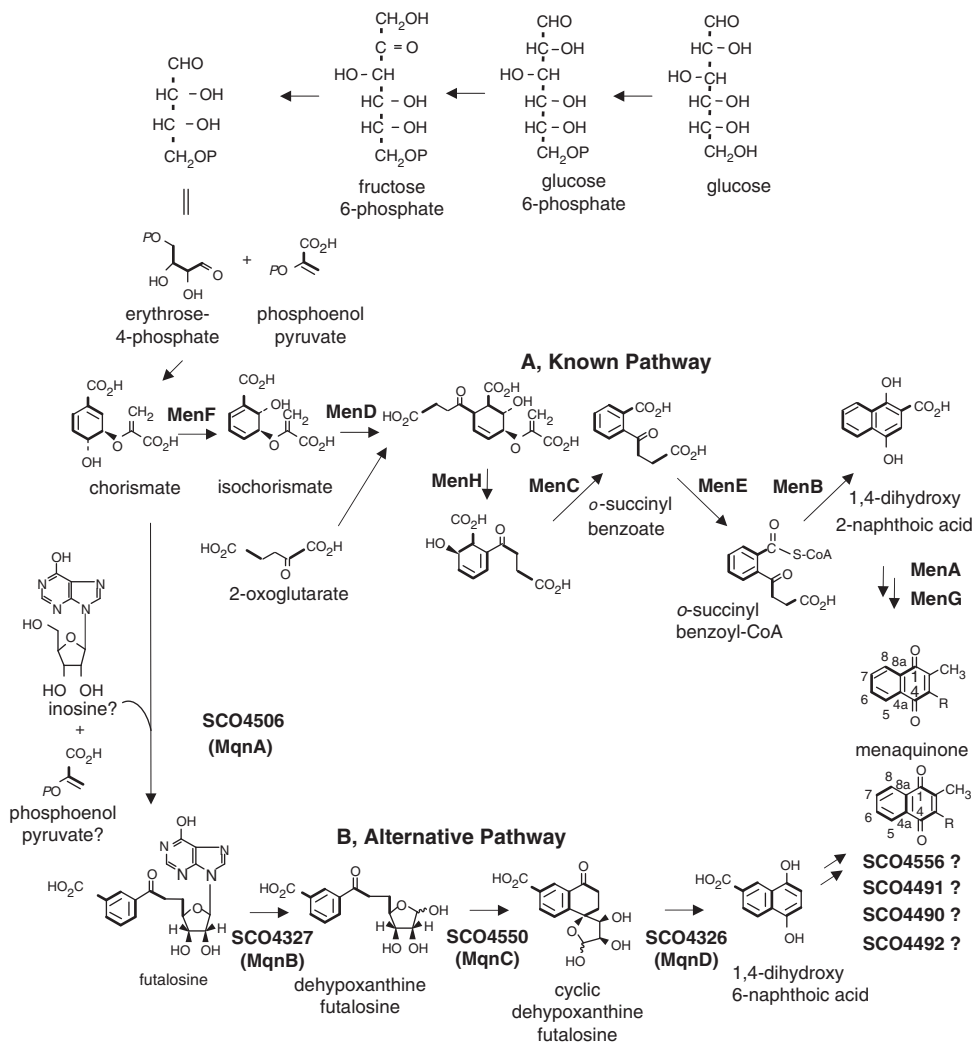


**Figure 1** MK biosynthetic pathways. Known pathway (A). Alternative pathway (B). Bold lines in (A) indicate two, three and four carbon units derived from acetate, phosphoenol pyruvate and erythrose-4-phosphate, respectively. Bold lines in (B) show two and four carbon units that were perhaps derived from C-5 and C-6 glucose and C-3 to C-6 glucose (erythrose-4-phosphate), respectively, by the tracer experiment with [U- $^{13}\text{C}_6$ ]glucose.

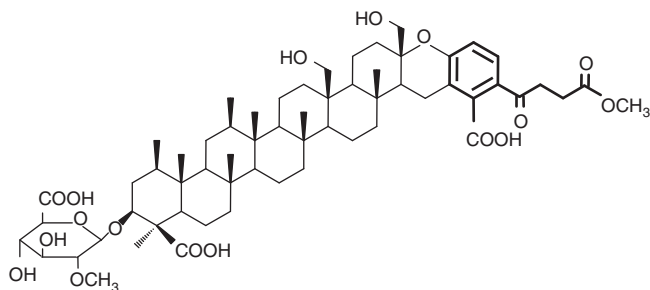


**Figure 2** Structure of KS-505a.  $\alpha$ -Succinylbenzoate moiety is shown in bold lines.

mately 6 years ago, I tried to clone a gene cluster participating in the biosynthesis of KS-505a (Figure 2), which is produced by *Streptomyces argenteolus* strain A-2 and has a unique cyclized tetraterpene moiety and an aromatic moiety derived from OSB.<sup>9</sup> Antibiotic biosynthetic genes cloned from actinomycetes are usually clustered in a genomic DNA region,<sup>8</sup> and OSB is synthesized by the MenF, -D and -C enzymes in the known MK biosynthetic pathway.<sup>1,2</sup> Therefore, I first

tried to clone *menF*, -D and -C orthologs from the KS505a producer, as actinomycetes are known to synthesize MK and the length of the prenyl side chain of MK has been used for taxonomic studies of actinomycetes.<sup>10</sup> To design PCR primers, I searched for the orthologs in databases of *Streptomyces coelicolor* A3(2)<sup>11</sup> and *Streptomyces avermitilis*,<sup>12</sup> the entire genomes of which have been sequenced. Very curiously, however, I did not detect any orthologs in the two strains. Besides these three orthologs, *menE* and *menB* orthologs were also absent in both strains.<sup>11,12</sup> Some pathogenic microorganisms, such as *Helicobacter pylori*<sup>13</sup> and *Campylobacter jejuni*,<sup>14</sup> which are known to cause gastric carcinoma and diarrhea, respectively, also lacked these five *men* gene orthologs, although they synthesize MK.<sup>15,16</sup> In contrast, these microorganisms possessed orthologs of *menA* and *menG*,<sup>13,14</sup> which catalyze a prenylation and a methylation, respectively, suggesting that the naphthoquinone moiety of MK would be synthesized through an alternative pathway.

#### TRACER EXPERIMENTS USING [U- $^{13}\text{C}$ ]GLUCOSE AND *S. COELICOLOR* A3(2)

To investigate whether an alternative pathway was operating in some bacteria, we first analyzed  $^{13}\text{C}$ -labeled MK prepared from *S. coelicolor*

A3(2).<sup>6</sup> The <sup>13</sup>C-NMR spectrum of MK labeled with [U-<sup>13</sup>C<sub>6</sub>]glucose showed a labeling pattern that could be explained by the incorporation of [U-<sup>13</sup>C<sub>6</sub>]glucose into MK through the shikimate pathway by the condensation of phosphoenolpyruvate (PEP) and erythrose-4-phosphate (E4P). These two compounds used for A-ring formation were the same as those in the known pathway, but the incorporated positions (PEP into C-7 and -8, and E4P into C-8a, -4a, -5 and -6) differed from those in the known pathway (Figure 1). Therefore, we carried out further experiments using glucose labeled with <sup>13</sup>C at different positions. The specific incorporation of [3-<sup>13</sup>C]-, [4-<sup>13</sup>C]-, [5-<sup>13</sup>C]- and [6-<sup>13</sup>C]glucose into C-8a, -4a, -5 and -6, respectively, was observed. This labeling pattern is compatible with the above-mentioned findings. The enrichment of C-7 and C-8 by [5-<sup>13</sup>C]glucose and [6-<sup>13</sup>C]glucose, respectively, supported the incorporation of these precursors by PEP through the shikimate pathway. These results established the formation mechanism for the A ring of MK from the shikimate pathway.

In contrast to the known pathway, no specific incorporation of [1,2-<sup>13</sup>C<sub>2</sub>]acetate into the B ring of MK was observed. However, the precursors of the B ring could perhaps be PEP (into C-3/C-4) and a currently unknown metabolite originating from C-5 and C-6 of glucose (into C-1/C-2). Taking these results together, we concluded that an alternative pathway was operating, at least *S. coelicolor* A3(2).

### IN SILICO SCREENING FOR CANDIDATE GENES RESPONSIBLE FOR THE ALTERNATIVE PATHWAY

We searched for genes responsible for the alternative pathway using two strategies. One was *in silico* screening, which utilized genome databases, and the other was screening of mutants, which required MK for their growth. First, we searched for candidate genes by comparing two groups of genome sequences. To date, sequencing of the entire genomes of more than 800 microorganisms has been completed.<sup>17</sup> Among them, we found that some microorganisms belonging to the epsilon and delta categories in Proteobacteria, such as *H. pylori*, *Wolinella succinogenes*, *C. jejuni* and *Geobacter sulfurreducens*, a part of actinobacteria, such as *S. coelicolor* and *S. avermitilis*, and certain Deinococcus-Thermus bacteria, such as *Thermus thermophilus* and *Deinococcus radioduran* and so on, had no *men* gene orthologs despite the fact that these strains synthesize MKs. Among them, we selected four microorganisms, *H. pylori*,<sup>13</sup> *C. jejuni*,<sup>14</sup> *T. thermophilus*<sup>18</sup> and *S. coelicolor*,<sup>11</sup> as query microorganisms. With regard to subject microorganisms, in which the known MK biosynthetic pathway was operating, *E. coli*,<sup>19</sup> *B. subtilis*,<sup>20</sup> *Corynebacterium glutamicum*<sup>21</sup> and *Mycobacterium tuberculosis*<sup>22</sup> were selected. First, we searched for orthologs in each of the groups by reciprocal best-hit pairs using the blastp program<sup>23</sup> with a cutoff value of less than 10<sup>-10</sup>. Next, we searched for candidate genes present in the former group but absent in the latter group. We selected approximately 50 genes in *S. coelicolor* A3(2). Among them, putative transcriptional regulator genes and putative membrane proteins for the transportation of small molecules were excluded and four genes, *SCO4326*, *SCO4327*, *SCO4506* and *SCO4550*, were selected as final candidates, all of which were reported to be encoded as hypothetical proteins.

### GENE DISRUPTION OF THE CANDIDATE GENES

To examine whether the candidate genes indeed participated in the alternative pathway, we disrupted these genes by homologous recombination. We are experienced at handling *Streptomyces* strains<sup>24</sup> and therefore used *S. coelicolor* A3(2) as a model microorganism. Each of the candidate genes was replaced with a thiostrepton resistance gene by a double-crossover homologous recombination. We were only able

to knock out all of the candidate genes when disruptants were selected on agar plates containing MK4 (prenyl side-chain length of C20), which is commercially available and can be substituted for MK8 (prenyl side-chain length of C40) usually found in *S. coelicolor* A3(2).<sup>25</sup> The disruption of each of the mutants was confirmed by PCR using specific primers. The *SCO4326*, *SCO4327*, *SCO4506* and *SCO4550* disruptants obligatorily required MK4 for their growth and the MKs purified from these disruptants were confirmed to be MK4 rather than MK8 by HPLC analysis. Considering that *SCO4506* and *SCO4326* can be mono-cistronically transcribed and exist in the most downstream region of an operon,<sup>11</sup> the polar effects of the disruptions of these genes would be negligible. Hence, *SCO4506* and *SCO4326* are essential. In contrast, *SCO4550* and *SCO4327* were judged to be possibly co-transcribed with *SCO4551* and *SCO4326* in that order,<sup>11</sup> respectively, suggesting that the phenotypes of the *SCO4550* and *SCO4327* disruptants may reflect polar effects. To examine this possibility, plasmids carrying *SCO4551* and *SCO4326* were introduced into the *SCO4550* and *SCO4327* disruptants, respectively, and the cell growth rates of the transformants were examined with or without MK4. Eventually, the transformants again required MK4 for their growth, thereby showing that *SCO4550* and *SCO4327* are also indispensable for the biosynthesis of MK. In summary, we identified four genes (*SCO4326*, *SCO4327*, *SCO4506* and *SCO4550*) as alternative MK biosynthetic pathway genes by *in silico* screenings and gene-disruption experiments.

### ISOLATION OF MUTANTS BY MUTAGENESIS

We could not narrow down any additional candidate genes by bioinformatics and therefore tried to isolate mutants that required MK4 for their growth by *N*-methyl-*N'*-nitro-*N*-nitrosoguanidine mutagenesis to obtain all the genes participating in the alternative pathway. We were able to isolate 26 mutants, and most of these were complemented by plasmids carrying the genes identified by the *in silico* screening. A few mutants that were not complemented were used as hosts for shotgun cloning experiments, and all of these were complemented by a plasmid carrying the *SCO1490*–*SCO1501* genes. By subcloning experiments, these mutants were again complemented by the *SCO1494*, *SCO1495* and *SCO1496* genes, which encode 3-dehydroquinate synthase, shikimate kinase I and chorismate synthase, respectively (Figure 3). The mutant was then spread on a plate containing shikimate and chorismate instead of MK4, and its

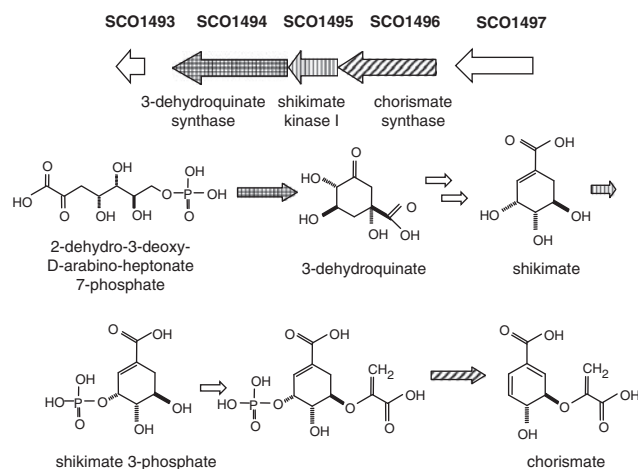


**Figure 3** SCO genes that complemented MK auxotroph. Organization of the genes and their functions in the shikimate pathway are shown.

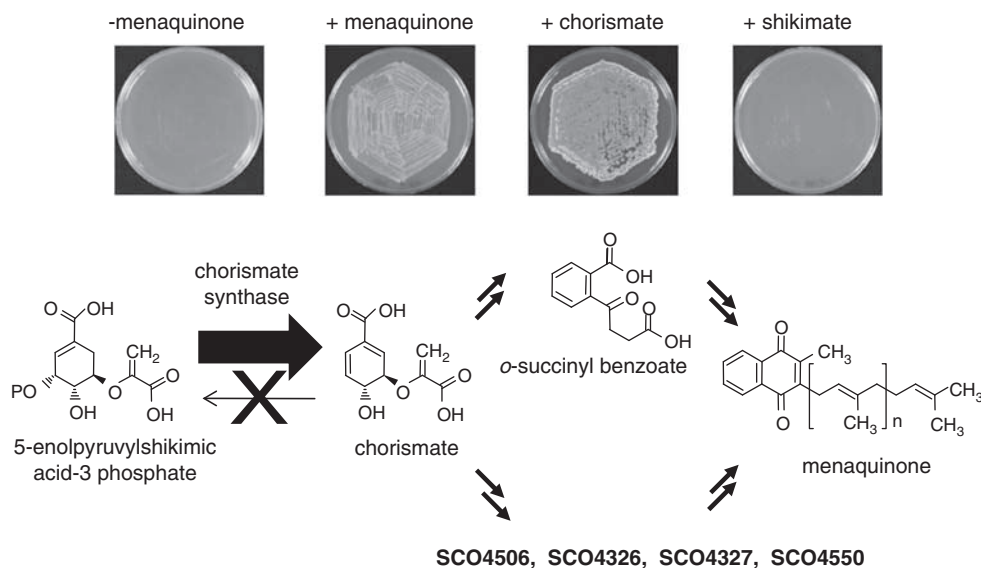


**Figure 4** Phenotypes of MK auxotroph. The mutant used for shotgun cloning experiment was spread onto a yeast extract–malt extract (YEME) plate, and a YEME plate containing MK4, chorismate or shikimate. After cultivation at 30 °C for 1 week, photographic images of each plate were taken. Irreversible reaction catalyzed by chorismate synthase is schematically shown.

growth was examined. The mutant only grew in the presence of chorismate (Figure 4), suggesting that it lacked a functional chorismate synthase or shikimate kinase. As the biosynthetic reaction catalyzed by chorismate synthase is irreversible,<sup>26</sup> the alternative pathway appeared to be branched at chorismate in a similar manner to the known pathway, but then becomes diverged.

#### RELATIVE BLOCKED POINTS OF THE DISRUPTANTS

As described above, we constructed *SCO4326*, *SCO4327*, *SCO4506* and *SCO4550* disruptants. We investigated whether intermediates accumulated in the culture broth of these disruptants. We cultivated each of the mutants in the presence of MK4. The culture broth was centrifuged and MK4 was removed by ethyl acetate extraction. The aqueous layer concentrated by freeze-drying was added into agar plates and the growth of the other mutants was examined. When plates containing the extract from the *SCO4506* disruptant were used, the other disruptants showed no growth, suggesting that the *SCO4506* product may participate in the most upstream step in the pathway. In contrast, at least one disruptant became able to grow on plates containing the extracts from the other disruptants. On the basis of these results, the relative blocked points of the mutants in MK biosynthesis were estimated to be in the following order: *SCO4506*, *SCO4327*, *SCO4550* and *SCO4326*.

#### INTERMEDIATE COMPOUNDS IN THE ALTERNATIVE PATHWAY Isolation of the accumulated metabolite in the culture broth of the *SCO4327* disruptant

Next, we purified the accumulated intermediate in the culture broth of the *SCO4327* disruptant using the assay method described above. The intermediate was purified from the MK4-free aqueous layer of the culture broth of the *SCO4327* disruptant by Dowex ion-exchange resin column chromatography (Dow Chemical Company, Midland, MI, USA) and a successive DIAION HP20 resin column chromatography (Mitsubishi Chemical Corporation, Tokyo, Japan). Finally, the compound was fractionated by preparative HPLC. By NMR and mass spectra analyses, the compound was confirmed to be futasoline, which had previously been isolated from the culture broth of a *Streptomyces* strain.<sup>27</sup>

#### Conversion of futasoline by a recombinant enzyme

As futasoline was isolated from the culture broth of the *SCO4327* disruptant, the *SCO4327* product should catalyze the conversion of futasoline into the next intermediate. Hence, we performed *in vitro* assays using a recombinant enzyme. We first prepared *SCO4327* as a recombinant *N*-terminal His-tagged protein and subjected it to an *in vitro* assay with futasoline as a substrate. However, no products were formed despite the addition of various cofactors and metals to the reaction mixture. We do not know the exact reason why the recombinant protein showed no enzymatic activity, but we assume that it may have been unstable. Therefore, we prepared a recombinant TTHA0556, which is an ortholog of *SCO4327* in *T. thermophilus* HB8,<sup>18</sup> an extreme thermophile, expecting that the recombinant protein would be highly thermostable. When purified *N*-terminal maltose-binding protein (MBP)-fused TTHA0556 was incubated with futasoline, the substrate was quickly consumed and two reaction products emerged in the absence of cofactors and metals. As *SCO4327* and TTHA0556 products have very weak similarities to some nucleosidases, we expected that the TTHA0556 product may release hypoxanthine from futasoline. Indeed, one product was confirmed to be hypoxanthine by liquid chromatography–mass spectrometry (LC–MS) analysis. The other product was purified by reverse-phase preparative HPLC and its structure was determined by mass spectra and NMR spectra analyses to be dehypoxanthine futasoline (DHFL). DHFL was also confirmed to be a real intermediate in the alternative pathway by a bioassay using the *SCO4506* disruptant.

#### Isolation of the accumulated metabolite in the culture broth of the *SCO4326* disruptant

As described above, the reaction next to *SCO4327* was judged to be possibly catalyzed by *SCO4550*. Indeed, a small amount of DHFL was accumulated in the culture broth of the *SCO4550* disruptant. Hence, we carried out an *in vitro* enzyme assay with a recombinant enzyme. We prepared both recombinant *SCO4550* and recombinant TTHA1092, an ortholog of *SCO4550* in *T. thermophilus* HB8, and incubated them with DHFL. However, we did not detect any products

**Table 1** Distribution of the alternative pathway

<i>Eubacteria</i>		<i>Genus</i>	<i>Archaea</i>	<i>Genus</i>		
Proteobacteria	Epsilon category	<i>Helicobacter</i>	Euryarchaeota	<i>Archaeoglobus</i>		
		<i>Wolinella</i>		<i>Thermoplasma</i>		
		<i>Thiomicrospira</i>	Crenarchaeota	<i>Ignicoccus</i>		
		<i>Campylobacter</i>		<i>Pyrobaculum</i>		
		<i>Arcobacter</i>		<i>Caldivirga</i>		
		<i>Nitratiruptor</i>		<i>Thermoproteus</i>		
		<i>Sulfurovum</i>		<i>Nitrosopumilus</i>		
	Delta category	<i>Geobacter</i>				
		<i>Pelobacter</i>				
		<i>Desulfovibrio</i>				
		<i>Desulfococcus</i>				
		<i>Desulfobacterium</i>				
		<i>Anaeromyxobacter</i>				
		<i>Syntrophobacter</i>				
Acidobacteria	Acidobacteria	<i>Acidobacteria</i>				
		<i>Solibacter</i>				
Firmicutes	Bacillales	<i>Bacillus halodurans</i>				
		<i>Bacillus clausii</i>				
	Clostridia	<i>Symbiobacterium</i>				
		<i>Syntrophomonas</i>				
		<i>Carboxydotherrmus</i>				
		<i>Desulfotomaculum</i>				
		<i>Pelotomaculum</i>				
		<i>Desulforudis</i>				
		<i>Heliobacterium</i>				
		<i>Moorella</i>				
		Actinobacteria		<i>Streptomyces</i>		
				<i>Frankia</i>		
				<i>Acidotherrmus</i>		
<i>Salinispora</i>						
Planctomyces		<i>Rhodopirellula</i>				
Chlamydia		<i>Chlamydia</i>				
		<i>Chlamydotherrmus</i>				
Spirochete		<i>Leptospira</i>				
Green nonsulfur bacteria		<i>Herpetosiphon</i>				
		<i>Deinococcus</i>				
Thermus		<i>Thermus</i>				
		<i>Aquifex</i>				
Hyperthermophilic bacteria		<i>Hydrogenobaculum</i>				
		<i>Sulfurihydrogenibium</i>				
		<i>Thermodesulfovibrio</i>				

with both proteins, even under the various conditions examined. Therefore, we decided to isolate an intermediate from the culture broth of the *SCO4326* disruptant, because the reaction product generated by TTHA1092 (*SCO4550*) would be the same as the intermediate accumulated in the culture broth of the *SCO4326* disruptant. The intermediate was purified by almost the same methods as those used for the *SCO4327* disruptant. Finally, we isolated one compound and its structure was determined to be cyclic DHFL, as shown in Figure 1.

#### Conversion of cyclic DHFL by a recombinant enzyme

Next, we examined whether recombinant *SCO4326* would convert cyclic DHFL into the next intermediate. In this experiment, we again

used a recombinant enzyme of *T. thermophilus* HB8, expecting that the recombinant protein would be more stable than *SCO4326*. Recombinant TTHA1568, an ortholog of *SCO4326* in *T. thermophilus* HB8, was prepared as an *N*-terminal MBP-fused protein and was used for an *in vitro* assay with cyclic DHFL as a substrate. We clearly detected a specific product by HPLC analysis and its structure was confirmed to be 1,4-dihydroxy 6-naphthoic acid (DHNA) by LC-MS analysis.

#### BIOSYNTHESIS IN THE EARLY STEPS

As described above, the alternative pathway appeared to branch at chorismate, and the *SCO4506* enzyme would participate in the most upstream step. On the basis of the structure of futasoline, the nucleoside moiety would be derived from inosine derivatives. Furthermore, a C2 unit, such as pyruvate or PEP, was previously implicated as a building block between chorismate and inosine (C6' and C7' positions of futasoline) by tracer experiments.<sup>6</sup> Therefore, we examined whether recombinant TTHA0803, an ortholog of *SCO4506* in *T. thermophilus* HB8, catalyzed the formation of futasoline. We incubated the recombinant enzyme with a combination of the substrates. We did not detect the formation of futasoline, but 3-(1-carboxyvinyl)benzoate and *m*-hydroxybenzoate were formed from chorismate in the absence and presence of flavin mononucleotide, respectively. It was unclear why the recombinant enzyme showed unexpected activities at this stage. As recombinant TTHA0803 accepted chorismate as a substrate, the nucleosides and C2 units used in this assay may not be the actual substrates, or additional enzymes may be necessary to complete the reaction. Further studies are necessary to clarify this unique biosynthetic step.

#### BIOSYNTHESIS IN THE LATE STEPS

Although we did not investigate the biosynthetic steps from DHNA to MK, a putative route can be estimated as follows: *SCO4491* and *SCO4556* are annotated as the UbiA homolog (prenylation enzyme in ubiquinone biosynthesis and its function would be the same as that of MenA) and MenG homolog (methylation), respectively.<sup>11</sup> The *SCO4491* gene is assumed to constitute an operon with the *SCO4490*, *SCO4492* and *SCO4493* genes. Among these, the *SCO4493* gene is annotated as an AsnC family transcriptional regulator, which would not directly participate in metabolic reactions. In contrast, *SCO4490* and *SCO4492* are homologous to UbiX and UbiD, respectively, both of which are known to be decarboxylation enzymes in the ubiquinone biosynthetic pathway,<sup>2</sup> although *S. coelicolor* A3(2) never synthesizes ubiquinones.<sup>10</sup> Taking these findings together, the prenylation, methylation and decarboxylation reactions would be catalyzed by *SCO4491*, *SCO4556* and *SCO4490/SCO4492*, respectively. Moreover, we previously showed that symmetrical compounds, such as 1,4-naphthoquinone, were not true intermediates using tracer experiments,<sup>6</sup> and methylation is reported to occur in the final step in the known pathway. Therefore, the order of the later steps could be prenylation, decarboxylation and methylation.

#### DISTRIBUTION OF THE ALTERNATIVE PATHWAY

We re-investigated the distribution of the alternative pathway in microorganisms with completely sequenced genomes.<sup>17</sup> Of the four genes identified in this study (*SCO4506*, *SCO4326*, *SCO4327* and *SCO4550*), we identified at least three orthologs in the microorganisms, including Gram-negative/positive microorganisms and Archaea (Table 1). As described above, *E. coli* has both ubiquinone biosynthetic genes and the known MK biosynthetic genes. However, there were no bacteria possessing both ubiquinone biosynthetic genes and the alternative MK biosynthetic genes. We were also unable

to find any bacteria equipped with both the known and alternative pathways.

### ENZYMATIC PROPERTIES OF FUTALOSINE HYDROLASE

In addition to *H. pylori* and *C. jejuni*, the following pathogenic bacteria also possess the alternative pathway:<sup>17</sup> *Chlamydia*, such as *Chlamydomphila abortus*, *Chlamydomphila caviae*, *Chlamydomphila felis*, *Chlamydia muridarum* and *Chlamydia trachomatis*, which cause eye and lung infections and genital diseases; and spirochetes, such as *Leptospira borgpetersenii* and *Leptospira interrogans*, which are the most common causes of bovine leptospirosis and also cause zoonotic infections in humans. As humans and commensal intestinal bacteria, including lactobacilli, lack the alternative pathway, a compound that inhibits the alternative pathway would specifically prevent the growth of pathogenic *Helicobacter* strains without affecting intestinal bacterial flora. Moreover, a rapid and easy diagnosis of *H. pylori* infection that is represented by the urea breath test has been developed. Therefore, a timely medical care for an individual patient with antibiotics specific to the alternative pathway might become possible.

As a first step toward developing such antibiotics, we investigated the enzymatic properties of compounds participating in the futasoline pathway; recombinant TTHA0556 of *T. thermophilus*, which participates in the second step of the pathway and catalyzes the reaction releasing hypoxanthine from futasoline (we named the enzyme futasoline hydrolase and EC number EC3.2.2.26 was recently assigned to the enzyme), was prepared and used in functional analyses.<sup>28</sup> Recombinant TTHA0556 formed a homotetramer and only reacted with futasoline. Other structurally related nucleotides and nucleosides were not accepted. Recombinant TTHA0556 required no cofactors or metals, and the optimum pH and temperature were 4.5 (almost the same activity was observed up to pH 6.0) and 80 °C, respectively. The  $K_m$  value was calculated to be  $154.0 \pm 5.3 \mu\text{M}$  and the  $k_{\text{cat}}$  value was  $1.02 \text{ s}^{-1}$ . Although recombinant TTHA0556 was not inhibited by DHFL, cyclic DHFL or DHNA, it was slightly inhibited by hypoxanthine, with a  $K_i$  value of 1.1 mM. As described above, futasoline hydrolase only reacted with futasoline, and was essential for survival. Taking these results together, compounds such as derivatives of hypoxanthine that inhibit enzyme activity can be developed as anti-*H. pylori* drugs.

### ACKNOWLEDGEMENTS

This study was performed in my laboratory, together with Dr T Hiratsuka in collaboration with Professor H Seto (Tokyo University of Agriculture; tracer experiments), Dr K Furihata (The University of Tokyo; structural analyses of intermediates) and Dr J Ishikawa (National Institute of Infectious Diseases; bioinformatic analyses). This work was supported, in part, by Grants-in-Aid for Scientific Research on Priority Areas 'Applied Genomics' from the Ministry of Education, Culture, Sports, Science, and Technology of Japan, the Urakami Foundation, the Skylark Food Science Institute and the Asahi Glass Foundation to TD.

- Bentley, R. & Maganathan, R. Biosynthesis of vitamin K (menaquinone) in bacteria. *Microbiol. Rev.* **46**, 241–280 (1982).
- Meganathan, R. Biosynthesis of menaquinone (vitamin K2) and ubiquinone (coenzyme Q): a perspective on enzymatic mechanisms. *Vitam. Horm.* **61**, 173–218 (2001).
- Dahlbäck, B. & Villoutreix, B. O. Regulation of blood coagulation by the protein c anticoagulant pathway: novel insights into structure–function relationships and molecular recognition. *Artern. Thromb. Vasc. Biol.* **25**, 1311–1320 (2005).
- Adams, J. & Pepping, J. Vitamin K in the treatment and prevention of osteoporosis and arterial calcification. *Am. J. Health Syst. Pharm.* **62**, 1574–1581 (2005).
- Lamson, D. W. & Plaza, S. M. The anticancer effects of vitamin K. *Altern. Med. Rev.* **8**, 303–318 (2003).
- Seto, H. *et al.* Studies on a new biosynthetic pathway for menaquinone. *J. Am. Chem. Soc.* **130**, 5614–5615 (2008).
- Hiratsuka, T. *et al.* An alternative menaquinone biosynthetic pathway operating in microorganisms. *Science* **321**, 1670–1673 (2008).
- Dairi, T. Studies on biosynthetic genes and enzymes of isoprenoids produced by actinomycetes. *J. Antibiot.* **58**, 227–243 (2005).
- Nakanishi, S. *et al.* KS-505a, a novel inhibitor of bovine brain Ca<sup>2+</sup> and calmodulin-dependent cyclic-nucleotide phosphodiesterase from *Streptomyces argenteolus*. *J. Antibiot.* **45**, 341–347 (1992).
- Embley, T. M. & Stackebrandt, E. The molecular phylogeny and systematics of the actinomycetes. *Annu. Rev. Microbiol.* **48**, 257–289 (1994).
- Bentley, S. D. *et al.* Complete genome sequence of the model actinomycete *Streptomyces coelicolor* A3(2). *Nature* **417**, 141–147 (2002).
- Omura, S. *et al.* Genome sequence of an industrial microorganism *Streptomyces avermitilis*: deducing the ability of producing secondary metabolites. *Proc. Natl. Acad. Sci. USA* **98**, 12215–12220 (2001).
- Tomb, J. F. *et al.* The complete genome sequence of the gastric pathogen *Helicobacter pylori*. *Nature* **388**, 539–547 (1997).
- Parkhill, J. *et al.* The genome sequence of the food-borne pathogen *Campylobacter jejuni* reveals hypervariable sequences. *Nature* **403**, 665–666 (2000).
- Marcelli, S. W. *et al.* The respiratory chain of *Helicobacter pylori*: identification of cytochromes and the effects of oxygen on cytochrome and menaquinone levels. *FEMS Microbiol. Lett.* **138**, 59–64 (1996).
- Moss, C. W., Lambert-Fair, M. A., Nicholson, M. A. & Guerrant, G. O. Isoprenoid quinones of *Campylobacter cryaerophila*, *C. cinaedi*, *C. fennelliae*, *C. hyointestinalis*, *C. pylori*, and *C. upsaliensis*. *J. Clin. Microbiol.* **28**, 395–397 (1990).
- [http://www.genome.ad.jp/kegg/catalog/org\\_list.html](http://www.genome.ad.jp/kegg/catalog/org_list.html).
- Henne, A. *et al.* The genome sequence of the extreme thermophile *Thermus thermophilus*. *Nat. Biotechnol.* **22**, 547–553 (2004).
- Blattner, F. R. *et al.* The complete genome sequence of *Escherichia coli* K-12. *Science* **277**, 1453–1474 (1997).
- Kunst, F. *et al.* The complete genome sequence of the Gram-positive bacterium *Bacillus subtilis*. *Nature* **390**, 249–256 (1997).
- Ikeda, M. & Nakagawa, S. The *Corynebacterium glutamicum* genome: features and impacts on biotechnological processes. *Appl. Microbiol. Biotechnol.* **62**, 99–109 (2003).
- Cole, S. T. *et al.* Deciphering the biology of *Mycobacterium tuberculosis* from the complete genome sequence. *Nature* **393**, 537–544 (1998).
- Altschul, S. F., Gish, W., Miller, W., Myers, E. W. & Lipman, D. J. Basic local alignment search tool. *J. Mol. Biol.* **215**, 403–410 (1990).
- Hopwood, D. A. *et al.* *Gene Manipulation of Streptomyces, A Laboratory Manual* (The John Innes Foundation, Norwich, UK, 1985).
- Collins, M. D., Pirouz, T., Goodfellow, M. & Minnikin, D. E. Distribution of menaquinones in actinomycetes and corynebacteria. *J. Gen. Microbiol.* **100**, 221–230 (1977).
- Macheroux, P., Schmid, J., Amrhein, N. & Schaller, A. A unique reaction in a common pathway: mechanism and function of chorismate synthase in the shikimate pathway. *Planta* **207**, 325–334 (1999).
- Hosokawa, N. *et al.* Futasoline and its derivatives, new nucleoside analogs. *Chem. Pharm. Bull. (Tokyo)* **47**, 1032–1034 (1999).
- Hiratsuka, T., Itoh, N., Seto, H. & Dairi, T. Enzymatic properties of futasoline hydrolase, an enzyme essential to a newly identified menaquinone biosynthetic pathway. *Biosci. Biotechnol. Biochem.* **73**, 1137–1141 (2009).

## ORIGINAL ARTICLE

# Absolute stereostructures of chaetomugilins G and H produced by a marine-fish-derived *Chaetomium* species

Takeshi Yamada, Muroga Yasuhide, Hirohumi Shigeta, Atsushi Numata and Reiko Tanaka

Chaetomugilins G and H were isolated from a strain of *Chaetomium globosum* that was originally isolated from the marine fish, *Mugil cephalus*, and their absolute stereostructures were elucidated on the basis of spectroscopic analyses, including 1D and 2D NMR techniques, and chemical transformation. In addition, the absolute configuration of chaetoviridin C was established by derivatization from chaetomugilin A. These compounds exhibited a growth inhibitory activity against cultured P388, HL-60, L1210 and KB cells.

*The Journal of Antibiotics* (2009) 62, 353–357; doi:10.1038/ja.2009.39; published online 22 May 2009

**Keywords:** azaphilones; *Chaetomium* sp.; cytotoxicity; chaetomugilin; chaetoviridin; fungus; marine fish

## INTRODUCTION

Marine microorganisms are potentially prolific sources of highly bioactive secondary metabolites that might serve as useful leads in the development of new pharmaceutical agents. On the basis of the fact that some of the bioactive materials isolated from marine animals have been produced by bacteria, we focused our attention on new antitumor agents from microorganisms separated from marine organisms.<sup>1–5</sup> As part of this endeavor, we conducted a search for antitumor compounds from a strain of *Chaetomium globosum* OUPS-T106B-6 that was originally isolated from the marine fish, *Mugil cephalus*, and reported six new cytotoxic metabolites designated as chaetomugilins A (1), B, C, D (2), E and F from the culture broth of this fungal strain.<sup>6,7</sup> These compounds are azaphilones and they have various bioactivities, including antimicrobial, nitric oxide inhibitory, gp120-CD4-binding inhibitory, monoamine oxidase inhibitory and platelet-derived growth factor-binding inhibitory activities.<sup>7</sup> An examination of a disease-oriented panel of 39 human cancer cell lines (HCC panel)<sup>8,9</sup> suggested the possibility that the mode of action of chaetomugilins A (1), C and F might be different from that shown by any other anticancer drugs developed to date.<sup>7</sup> Our continuing search for cytotoxic metabolites from this fungal strain yielded two new azaphilones designated as chaetomugilins G (3) and H (4), along with the known compound, chaetoviridin C (5)<sup>10</sup> (Figure 1). These compounds exhibited moderate cytotoxic activity against the murine P388 leukemia cell line, the human HL-60 leukemia cell line, the murine L1210 leukemia cell line and the human KB epidermoid carcinoma cell line. We describe herein the absolute stereostructures and biological activities of these compounds.

## RESULTS AND DISCUSSION

The microorganism from *M. cephalus* fish was cultured at 27 °C for 6 weeks in a medium (100l) containing 1% soluble starch and 0.1% casein in 50% artificial seawater adjusted to pH 7.5. This fermentation was carried out on twice the volume than that used in previous reports<sup>6,7</sup> to obtain minor metabolites. After incubation, the AcOEt extract of the culture filtrate was purified by bioassay-directed fractionation (cytotoxicities against the P388 cell line) using a stepwise combination of Sephadex LH-20, silica gel column chromatography and reversed-phase HPLC to afford chaetomugilins G (3), H (4) and chaetoviridin C (5), together with chaetomugilins A–F. The physico-chemical properties of chaetomugilins G (3) and H (4) are summarized in Table 1.

Chaetomugilin G (3) had the molecular formula, C<sub>24</sub>H<sub>29</sub>ClO<sub>7</sub>, which was established from the [M+H]<sup>+</sup> peak in high-resolution fast atom bombardment mass spectrometry and from the ratio of the intensity of isotope peaks (MH<sup>+</sup>/[MH+2]<sup>+</sup>). Its IR spectrum exhibited bands at 3423, 1700 and 1687 cm<sup>-1</sup>, which are characteristic of hydroxyl, ester and conjugated carbonyl groups, respectively. A close inspection of the <sup>1</sup>H and <sup>13</sup>C NMR spectra (Table 2) of 3 by DEPT and heteronuclear multiple quantum coherence (HMQC) experiments revealed the presence of four secondary methyls (11-CH<sub>3</sub>, C-13, 4'-CH<sub>3</sub> and C-6'), one tertiary methyl (7-CH<sub>3</sub>), one ester methyl (1'-OCH<sub>3</sub>), four sp<sup>2</sup>-hybridized methines (C-1, C-4, C-9 and C-10) including oxygen-bearing carbon (C-1), five sp<sup>3</sup>-methines (C-8, C-11, C-12, C-4' and C-5') including two oxymethines (C-12 and C-5'), one quaternary oxygen-bearing sp<sup>3</sup>-carbon (C-7), six quaternary sp<sup>2</sup>-carbons (C-3, C-4a, C-5, C-8a, C-2' and C-3')

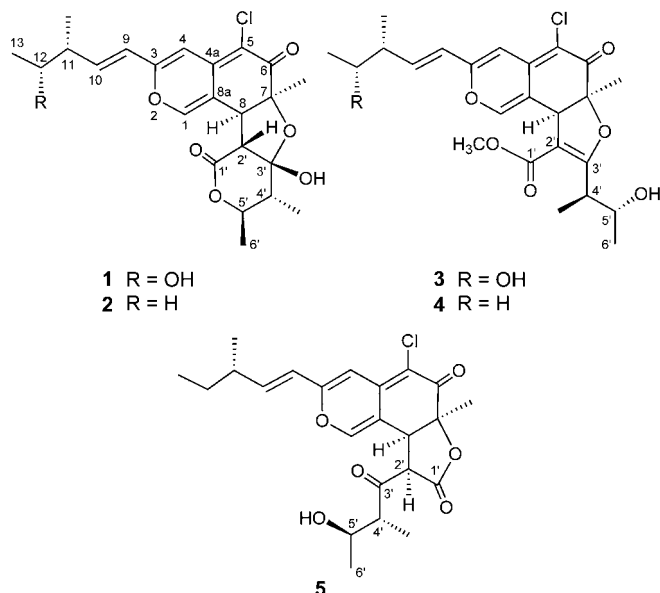


**Figure 1** Structures of chaetomugilins A (1), D (2), G (3) and H (4) and chaetoviridin C (5).

**Table 1** Physico-chemical properties of chaetomugilins G (3) and H (4)

	3	4
Appearance	Yellow powder	Yellow powder
M.p.	165–167 °C	119–121 °C
$[\alpha]_D^{22}$	–80.1 ( <i>c</i> 0.13, EtOH)	–175.0 ( <i>c</i> 0.09, EtOH)
<i>HRFAB-MS</i>		
Found:	465.1679 (M+H) <sup>+</sup>	449.1729 (M+H) <sup>+</sup>
Calcd:	465.1685 (for C <sub>24</sub> H <sub>30</sub> <sup>35</sup> ClO <sub>7</sub> )	449.1731 (for C <sub>24</sub> H <sub>30</sub> <sup>35</sup> ClO <sub>6</sub> )
Molecular formula	C <sub>24</sub> H <sub>29</sub> ClO <sub>7</sub>	C <sub>24</sub> H <sub>29</sub> ClO <sub>6</sub>
UV $\lambda_{\max}$ (EtOH) nm	255 (3.91), 292 (3.86), 391 (3.93), 408 (3.90)	252 (3.90), 290 (3.86), 392 (3.94), 408 (3.94)
IR $\nu_{\max}$ (KBr) cm <sup>-1</sup>	3423, 1700, 1687, 1613, 1564, 1522	3444, 1717, 1700, 1686, 1622, 1561, 1523
TLC R <sub>f</sub> <sup>a</sup>	0.47	0.65
<i>Solubility</i>		
Soluble	DMSO, MeOH, CHCl <sub>3</sub>	DMSO, MeOH, CHCl <sub>3</sub>
Insoluble	H <sub>2</sub> O	H <sub>2</sub> O

<sup>a</sup>Silica gel (10% MeOH in CHCl<sub>3</sub>).

including one oxygen-bearing carbon (C-3') and two carbonyls (C-6 and C-1'). The <sup>1</sup>H-<sup>1</sup>H COSY analysis of **3** revealed two partial structural units as shown by bold-faced lines in Figure 2. The geometrical configuration of the double bond moiety (C-9–C-10) was deduced to be *trans* from the coupling constants of the olefinic protons ( $J_{9,10}$  = 15.8 Hz). The connection of these units and of the remaining functional groups was determined on the basis of the key heteronuclear multiple-bond connectivity (HMBC) correlations summarized in Figure 2. The connection of a chlorine atom to C-5 was reasonable from its chemical shift ( $\delta_C$  110.43). Thus, the planar structure of **3** was elucidated as shown in Figure 2.

The relative stereochemistry of **3** was examined by conducting NOESY experiments (Table 2). NOE correlations (6'-H/8-H and 6'-H/7-CH<sub>3</sub>) implied that 8-H is oriented *cis* to the 7-methyl group. However, the relative configuration of C-11, C-12, C-4' and C-5' could not be elucidated. Treatment with *p*-TsOH of chaetomugilin A (**1**) in MeOH gave chaetomugilins B and C, as reported previously.<sup>6,7</sup> This time, the above reaction was carried out on the condition that more *p*-TsOH was used, which then resulted in **3** together with chaetomugilins B and C (Scheme 1). Product **3** was confirmed to be identical to natural **3** on the basis of IR, UV and NMR spectra and optical rotations. This result allowed us to assign the absolute configuration of all the asymmetric centers (7*S*, 8*R*, 11*R*, 12*R*, 4'*R* and 5'*R*) in chaetomugilin G (**3**).

Chaetomugilin H (**4**), which contained one oxygen atom less than **3**, was assigned the molecular formula, C<sub>24</sub>H<sub>29</sub>ClO<sub>6</sub>. The general features of its UV, IR and NMR spectra (Table 3) closely resembled those of **3**, except that the proton signals for H-11 ( $\delta_H$  2.25, sept), H-12 ( $\delta_H$  1.43, quint) and H-13 ( $\delta_H$  0.90, t), and the carbon signals for C-10 ( $\delta_C$  146.04), C-11 ( $\delta_C$  38.76), C-12 ( $\delta_C$  29.18), C-13 ( $\delta_C$  11.68) and 11-CH<sub>3</sub> ( $\delta_C$  19.35) in **4** revealed a chemical shift difference relative to those of **3**. The above evidence implied that the hydroxyl methine at C-12 in **3** was replaced with a methylene in **4**. The planar structure of **4** was confirmed by analyzing <sup>1</sup>H-<sup>1</sup>H COSY correlations and HMBC correlations (Table 3). In NOESY experiments, the same NOE correlations (6'-H/8-H and 6'-H/7-CH<sub>3</sub>) as those of **3** were observed. As in compound **3**, treatment with *p*-TsOH of chaetomugilin D (**2**) in MeOH gave product **4** (Scheme 1), which was confirmed to be identical to natural **4** on the basis of IR, UV and NMR spectra and optical rotations. The above lines of evidence revealed the absolute stereostructure of chaetomugilin H (**4**). Treatment of chaetomugilins C and F with *p*-TsOH also gave **3** and **4**, respectively (Scheme 1). This fact implied that the transformation from **1** and **2** to **3** and **4** proceeded through chaetomugilins C and E, respectively.

The planar structure of chaetoviridin C (**5**), which was confirmed to be identical in terms of IR, UV and NMR spectra, as well as optical rotation, has already been reported by Natori and co-workers,<sup>10</sup> but the stereochemistry has remained undecided. To determine the absolute configuration of **5**, the derivatization from chaetoviridin C (**5**) to chaetomugilin D (**2**) was carried out. Treatment with *p*-TsOH of **5** in MeOH gave product **2**, which was confirmed to be identical to natural **2** on the basis of IR, UV and NMR spectra and optical rotations.<sup>7</sup> This result allowed us to assign the absolute configuration of all the asymmetric centers (7*S*, 8*S*, 11*S*, 2'*R*, 4'*R* and 5'*R*) in chaetoviridin C (**5**).

Chaetomugilins A (**1**) and D (**2**) were stable in the mixture, MeOH/CHCl<sub>3</sub>, for several days. In the process of isolation, the time that **1** was exposed to MeOH on the silica gel column chromatography was very short (6–7 h, the longest time). In addition, **2** was not exposed to MeOH in this procedure. These results suggested that chaetomugilins G (**3**) and H (**4**) were not artifacts of chaetomugilins A (**1**) and D (**2**), respectively.

Assays for the growth inhibitory activity of other azaphilones using various cancer cell lines are rarely reported. As a primary screen for antitumor activities, the cancer cell growth inhibitory activities of chaetomugilins G (**3**) and H (**4**) were examined using the murine P388 leukemia cell line, the human HL-60 leukemia cell line, the murine L1210 leukemia cell line and the human KB epidermoid carcinoma cell line. Compound **3** exhibited significant cytotoxicity to P388 and HL-60 cell lines. In addition, compound **4** also showed moderate activity against KB cell lines (Table 4). These results implied that the presence of the hydroxyl group at C-12 reduced activity.

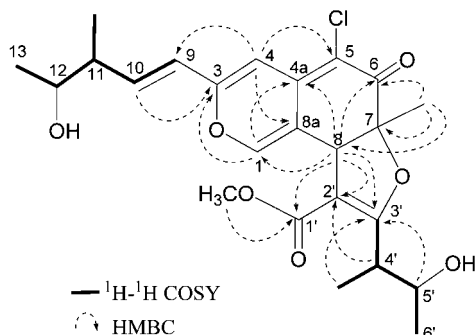


**Table 2** NMR spectral data of chaetomugilin G (3) in CDCl<sub>3</sub>

Position	$\delta_H^a$		$J/Hz$	$^1H-^1H$ COSY	NOE	$\delta_C$	HMBC (C) <sup>b</sup>
1	7.55	s			8, 1'-OCH <sub>3</sub>	147.4	(CH) 3, 4a, 8, 8a
3						156.6	(C)
4	6.52	s			9	105.3	(CH) 3, 5, 8a, 9
4a						141.2	(C)
5						110.4	(C)
6						185.0	(C)
7						87.9	(C)
8	4.19	s			1, 7-CH <sub>3</sub> , 6'	47.6	(CH) 1, 4a, 6, 7, 8a, 7-CH <sub>3</sub> , 1', 2', 3'
8a						113.5	(C)
9	6.13	d	15.8 (10)	10	4, 11, 13, 11-CH <sub>3</sub>	122.2	(CH) 3, 4, 10, 11
10	6.60	dd	15.8 (9), 7.0 (11)	9, 11	11, 12, 13, 11-CH <sub>3</sub>	141.8	(CH) 3, 11, 12, 11-CH <sub>3</sub>
11	2.45	sex	7.0 (10, 12, 11-CH <sub>3</sub> )	10, 12, 11-CH <sub>3</sub>	9, 10, 12, 13, 11-CH <sub>3</sub>	44.1	(CH) 9, 10, 12, 13, 11-CH <sub>3</sub>
12	3.82	quint	7.0 (11, 13)	11, 13	10, 11, 13, 11-CH <sub>3</sub>	70.9	(CH) 10, 11, 13, 11-CH <sub>3</sub>
13	1.20	d	7.0 (12)	12	9, 10, 11, 12	20.4	(CH <sub>3</sub> ) 11, 12
7-CH <sub>3</sub>	1.62	s			8, 6', 4'-CH <sub>3</sub>	22.9	(CH <sub>3</sub> ) 6, 7, 8
11-CH <sub>3</sub>	1.13	d	7.0 (11)	11	9, 10, 11, 12	14.8	(CH <sub>3</sub> ) 10, 11, 12
1'						165.3	(C)
2'						104.7	(C)
3'						173.9	(C)
4'	3.33	quint	6.8 (5', 4'-CH <sub>3</sub> )	5', 4'-CH <sub>3</sub>	5', 4'-CH <sub>3</sub> , 6', 1'-OCH <sub>3</sub>	40.7	(CH) 2', 3', 5', 6', 4'-CH <sub>3</sub>
5'	3.92	quint	6.8 (4', 6')	4', 6'	4', 6', 4'-CH <sub>3</sub>	69.7	(CH) 3', 4', 6', 4'-CH <sub>3</sub>
6'	1.22	d	6.8 (5')	5'	8, 7-CH <sub>3</sub> , 4', 5', 4'-CH <sub>3</sub>	21.5	(CH <sub>3</sub> ) 4', 5'
4'-CH <sub>3</sub>	1.13	d	6.8 (4')	4'	7-CH <sub>3</sub> , 4', 5', 6'	14.8	(CH <sub>3</sub> ) 3', 4', 5'
1'-OCH <sub>3</sub>	3.71	s			1', 4'	51.1	(CH <sub>3</sub> ) 1'

<sup>a</sup> $^1H$  chemical shift values ( $\delta$  ppm from SiMe<sub>4</sub>) followed by multiplicity and then the coupling constants ( $J/Hz$ ). Figures in parentheses indicate the proton coupling with that position.

<sup>b</sup>Long range  $^1H-^{13}C$  correlations from H to C observed in the HMBC experiments.

**Figure 2** Selected  $^1H-^1H$  COSY and HMBC correlations of chaetomugilin G (3).

## EXPERIMENTAL SECTION

### General

The m.ps. were determined on a Yanagimoto micro-melting point apparatus (Yanagimoto Ltd., Kyoto, Japan) and are uncorrected. UV spectra were recorded on a Hitachi U-2000 spectrophotometer (Hitachi Ltd., Tokyo, Japan), and IR spectra on a JASCO FT/IR-680 Plus (JASCO Corporation, Tokyo, Japan). NMR spectra were recorded at 27 °C on Varian UNITY INOVA-500 and MERCURY spectrometers (Varian Technologies Japan Ltd., Tokyo, Japan), with tetramethylsilane as an internal reference. FABMS data were obtained using a JEOL JMS-700 (Ver. 2) mass spectrometer (JEOL Ltd., Tokyo, Japan). Optical rotations were recorded on a JASCO J-820 polarimeter (JASCO Corporation). Liquid chromatography over silica gel (mesh 230–400) (NACARAI Tesque, inc., Kyoto, Japan) was performed at medium pressure. HPLC was run on a Waters ALC-200 (Nihon Waters K.K., Tokyo, Japan) instrument equipped with a differential refractometer (R 401) (Nihon Waters K.K.) and Shim-pack PREP-ODS (25 cm × 20 mm i.d.) (Shimadzu Corporation, Kyoto, Japan). Analytical

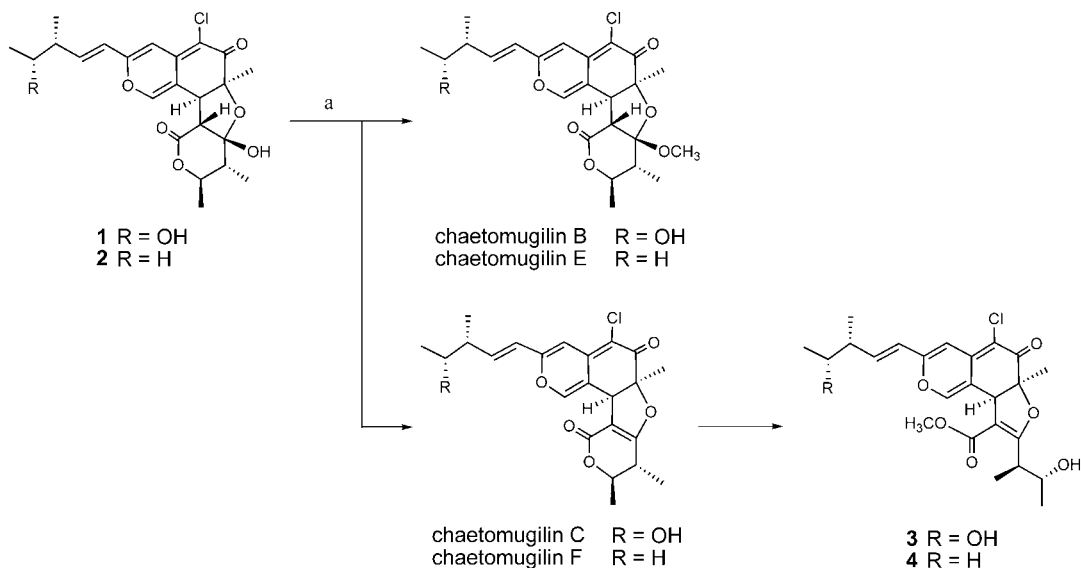
TLC was performed on precoated Merck aluminum sheets (DC-Alufolien Kieselgel 60 F254, 0.2 mm) (Merck Ltd. Japan, Tokyo, Japan) with the solvent system, CH<sub>2</sub>Cl<sub>2</sub>-MeOH (9:1), and compounds were viewed under a UV lamp and sprayed with 10% H<sub>2</sub>SO<sub>4</sub>, followed by heating.

### Culture and isolation of metabolites

A strain of *C. globosum* was initially isolated from the marine fish, *Mugil cephalus*, collected from the Katsura Bay of Japan in October 2000. The marine fish was wiped with EtOH and its gastrointestinal tract was applied to the surface of nutrient agar layered in a Petri dish. Serial transfers of one of the resulting colonies provided a pure strain of *C. globosum*. The fungal strain was cultured at 27 °C for 6 weeks in a liquid medium (100 l) containing 1% soluble starch and 0.1% casein in 50% artificial seawater adjusted to pH 7.5. The culture was filtered under suction and extracted thrice with AcOEt. The combined extracts were evaporated *in vacuo* to afford a mixture of crude metabolites (20.3 g). The AcOEt extract was passed through Sephadex LH-20 (Amersham Pharmacia Biotech Inc., Piscataway, NJ, USA), using CHCl<sub>3</sub>-MeOH (1:1) as eluent. The second fraction (7.2 g) was chromatographed on a silica gel column with a CHCl<sub>3</sub>-MeOH gradient as eluent. The CHCl<sub>3</sub> eluate (1.3 g) was purified by HPLC using MeCN-H<sub>2</sub>O (80:20) as eluent to afford Fr. 1 (160.3 mg), 2 (121.3 mg), 5 (21.7 mg), chaetomugilin E (34.1 mg) and chaetomugilin F (32.2 mg). Fr. 1 was purified by HPLC using MeCN-H<sub>2</sub>O (60:40) as eluent to afford 4 (20.8 mg). The MeOH-CHCl<sub>3</sub> (1:99) eluate (1.8 g) was purified by HPLC using MeOH-H<sub>2</sub>O (70:30) as eluent to afford Fr. 2 (134.7 mg), Fr. 3 (323.8 mg) and Fr. 4 (122.9 mg). Fr. 2 was purified by HPLC using MeCN-H<sub>2</sub>O (35:65) as eluent to afford 3 (22.5 mg). Fr. 3 was purified by HPLC using MeOH-H<sub>2</sub>O (60:40) as eluent to afford 1 (220.5 mg). Fr. 4 was purified by HPLC using MeCN-H<sub>2</sub>O (55:45) as eluent to afford chaetomugilin B (38.5 mg) and chaetomugilin C (44.1 mg).

### Derivatization of 3 from 1

*p*-TsOH (22.7 mg) was added to a MeOH solution (5 ml) of chaetomugilin A (1) (27.2 mg) and the reaction mixture was left at room temperature for 6 h.



**Scheme 1** Reagents and conditions: (a) MeOH, *p*-TsOH, 20 °C, 6 h.

**Table 3** NMR spectral data of chaetomugilin H (4) in CDCl<sub>3</sub>

Position	δ <sub>H</sub> <sup>a</sup>		J/Hz	<sup>1</sup> H- <sup>1</sup> H COSY	NOE	δ <sub>C</sub>	HMBC (C) <sup>b</sup>
1	7.55	s			8, 1'-OCH <sub>3</sub>	147.4	(CH) 3, 4a, 8, 8a
3						157.2	(C)
4	6.49	s			9	104.8	(CH) 3, 5, 8a, 9
4a						141.4	(C)
5						110.1	(C)
6						184.8	(C)
7						87.9	(C)
8	4.19	s			1, 7-CH <sub>3</sub> , 6'	47.6	(CH) 1, 4a, 6, 7, 8a, 7-CH <sub>3</sub> , 2', 3'
8a						113.5	(C)
9	6.04	d	15.8 (10)	10	4, 11, 11-CH <sub>3</sub>	120.3	(CH) 3, 4, 10, 11
10	6.50	dd	15.8 (9), 7.5 (11)	9, 11	11, 12, 13, 11-CH <sub>3</sub>	146.0	(CH) 3, 11, 12, 11-CH <sub>3</sub>
11	2.25	sept	7.5 (10, 12, 11-CH <sub>3</sub> )	10, 12, 11-CH <sub>3</sub>	9, 10, 12, 13, 11-CH <sub>3</sub>	38.8	(CH) 9, 10, 12, 13, 11-CH <sub>3</sub>
12	1.43	quint	7.5 (11, 13)	11, 13	10, 11, 13, 11-CH <sub>3</sub>	29.2	(CH <sub>2</sub> ) 10, 11, 13, 11-CH <sub>3</sub>
13	0.90	t	7.5 (12)	12	10, 11, 12	11.7	(CH <sub>3</sub> ) 11, 12
7-CH <sub>3</sub>	1.62	s			8, 6', 4'-CH <sub>3</sub>	23.0	(CH <sub>3</sub> ) 6, 7, 8
11-CH <sub>3</sub>	1.08	d	7.5 (11)	11	9, 10, 11, 12	19.4	(CH <sub>3</sub> ) 10, 11, 12
1'						165.4	(C)
2'						104.8	(C)
3'						173.9	(C)
4'	3.33	quint	6.9 (5', 4'-CH <sub>3</sub> )	5', 4'-CH <sub>3</sub>	5', 4'-CH <sub>3</sub> , 6', 1'-OCH <sub>3</sub>	40.8	(CH) 3', 5', 6', 4'-CH <sub>3</sub>
5'	3.92	quint	6.9 (4', 6')	4', 6'	4', 6', 4'-CH <sub>3</sub>	69.7	(CH) 3', 4'-CH <sub>3</sub>
6'	1.22	d	6.9 (5')	5'	8, 7-CH <sub>3</sub> , 4', 5', 4'-CH <sub>3</sub>	21.5	(CH <sub>3</sub> ) 4', 5'
4'-CH <sub>3</sub>	1.13	d	6.9 (4')	4'	7-CH <sub>3</sub> , 4', 5', 6'	14.8	(CH <sub>3</sub> ) 3', 4', 5'
1'-OCH <sub>3</sub>	3.71	s			1', 4'	51.1	(CH <sub>3</sub> ) 1'

<sup>a</sup>As in Table 2.

<sup>b</sup>As in Table 2.

The solvent was evaporated off under reduced pressure and the residue was purified by HPLC using MeCN-H<sub>2</sub>O (55:45) as eluent to afford **3** (3.1 mg), chaetomugilin B (7.2 mg) and chaetomugilin C (6.7 mg).

#### Derivatization of 4 from 2

Using the same procedure as above with **1**, chaetomugilin D (**2**) (32.7 mg) was treated with *p*-TsOH (25.8 mg) in MeOH (8 ml), and the products were

purified by HPLC using MeCN-H<sub>2</sub>O (70:30) as eluent to afford **4** (4.1 mg), chaetomugilin E (8.9 mg) and chaetomugilin F (8.2 mg).

#### Derivatization of 2 from chaetomugilin C

Using the same procedure as above with **1**, chaetomugilin C (12.6 mg) was treated with *p*-TsOH (18.6 mg) in MeOH (3 ml) and the products were purified by HPLC using MeCN-H<sub>2</sub>O (55:45) as eluent to afford **3** (4.8 mg).

**Table 4** Cytotoxicity of the metabolites against P388, HL-60, L1210 and KB cell lines

Compound	Cell line P388 $IC_{50}(\mu M)^a$	Cell line HL-60 $IC_{50}(\mu M)^a$	Cell line L1210 $IC_{50}(\mu M)^a$	Cell line KB $IC_{50}(\mu M)^a$
<i>Chaetomugilin</i>				
G (3)	24.1	19.8	123.6	137.8
H (4)	12.3	10.3	93.3	18.8
5-FU <sup>b</sup>	1.7	2.7	3.0	6.0

<sup>a</sup>DMSO was used as vehicle.<sup>b</sup>Positive control.

#### Derivatization of 4 from chaetomugilin F

Using the same procedure as above with **1**, chaetomugilin F (15.5 mg) was treated with *p*-TsOH (20.6 mg) in MeOH (4 ml) and the products were purified by HPLC using MeCN–H<sub>2</sub>O (70:30) as eluent to afford **4** (6.3 mg).

#### Derivatization of 2 from 5

Using the same procedure as above with **1**, *p*-TsOH (10.5 mg) was added to a MeOH solution (3 ml) of chaetoviridin C (**5**) (18.7 mg) and the reaction mixture was left at room temperature for 1 h. The solvent was evaporated off under reduced pressure and the residue was purified by HPLC using MeCN–H<sub>2</sub>O (80:20) as eluent to afford **2** (12.8 mg).

#### Assay for cytotoxicity to P388 and HL-60 cell lines

Cytotoxicity of chaetomugilins G (**3**) and H (**4**) was examined using the 3-(4,5-dimethyl-2-thiazolyl)-2,5-diphenyl-2H-tetrazolium bromide method. P388, HL-60, L1210 and KB cells were cultured in Eagle's Minimum Essential Medium (10% fetal calf serum) at 37 °C in 5% CO<sub>2</sub>. The test material was dissolved in DMSO to give a concentration of 10 mM, and the solution was diluted with the Essential Medium to give concentrations of 200, 20 and 2 μM. Each solution was combined with each cell suspension (1 × 10<sup>5</sup> cells ml<sup>-1</sup>) in the medium. After incubating at 37 °C for 72 h in 5% CO<sub>2</sub>, the grown cells were labeled with 5 mg ml<sup>-1</sup> 3-(4,5-dimethyl-2-thiazolyl)-2,5-diphenyl-2H-tetrazolium bromide in phosphate-buffered saline, and the absorbance of formazan dissolved in 20% SDS in 0.1 N HCl was measured at 540 nm using a microplate reader (Model 450) (Bio-Rad Laboratories, Inc., Tokyo, Japan). Each absorbance value was expressed as a percentage relative to the control

cell suspension that was prepared without the test substance, using the same procedure as that described above. All assays were performed thrice. Semilogarithmic plots were constructed from the averaged data and the effective dose of the substance required to inhibit cell growth by 50% (IC<sub>50</sub>) was determined.

#### ACKNOWLEDGEMENTS

We thank Dr T Ito (National Institute of Technology and Evaluation, Biological Resource Center) for identification of the fungal strain. We are grateful to Ms M Fujitake and Dr K Minoura of this university for MS and NMR measurements, respectively. This study was supported by a Grant-in-Aid for High Technology from the Ministry of Education, Culture, Sports, Science and Technology, Japan.

- 1 Iwamoto, C., Yamada, T., Ito, Y., Minoura, K. & Numata, A. Cytotoxic cytochalasins from a *Penicillium* species separated from a marine alga. *Tetrahedron* **57**, 2997–3004 (2001).
- 2 Yamada, T. *et al.* Absolute stereostructures of cell-adhesion inhibitors, macrospheptides C, E–G and I, produced by a *Periconia* species separated from an *Aplysia* sea hare. *J. Chem. Soc. Perkin. Trans.* **1**, 3046–3053 (2001).
- 3 Yamada, T., Iritani, M., Minoura, K., Kawai, K. & Numata, A. Peribysins A–D, potent cell-adhesion inhibitors from a sea hare-derived culture of *Periconia* species. *Org. Biomol. Chem.* **2**, 2131–2135 (2004).
- 4 Yamada, T., Imai, E., Nakatani, K., Numata, A. & Tanaka, R. Cephalimysin A, a potent cytotoxic metabolite from an *Aspergillus* species separated from a marine fish. *Tetrahedron Lett.* **48**, 6294–6296 (2007).
- 5 Yamada, T. *et al.* Pericosines, antitumor metabolites from the sea hare-derived fungus *Periconia byssoides*. Structures and biological activities. *Org. Biomol. Chem.* **5**, 3079–3086 (2007) and references cited therein.
- 6 Yamada, T. *et al.* Absolute stereostructures of cytotoxic metabolites, chaetomugilins A–C, produced by a *Chaetomium* species separated from a marine fish. *Tetrahedron Lett.* **49**, 4192–4195 (2008).
- 7 Muroga, Y., Yamada, T., Numata, A. & Tanaka, R. Chaetomugilins, new selectively cytotoxic metabolites, produced by a marine fish-derived *Chaetomium* species. *J. Antibiotics* **61**, 615–622 (2008) and references on other azaphilones cited therein.
- 8 Yamori, T. *et al.* Potent antitumor activity of MS-247, a novel DNA minor groove binder, evaluated by an *in vitro* and *in vivo* human cancer cell line panel. *Cancer Res.* **59**, 4042–4049 (1999).
- 9 Yamori, T. Panel of human cancer cell lines provides valuable database for drug discovery and bioinformatics. *Cancer Chemother Pharmacol.* **52**(Suppl 1), S74–S79 (2003).
- 10 Takahashi, M., Koyama, K. & Natori, S. Four new azaphilones from *Chaetomium globosum* var. *flavo-viridae*. *Chem. Pharm. Bull.* **38**, 625–628 (1990).

ORIGINAL ARTICLE

# Ascotricins A and B, novel antagonists of sphingosine-1-phosphate receptor 1 from *Ascotricha chartarum* Berk. SANK 14186

Kiyoaki Yonesu<sup>1</sup>, Takashi Ohnuki<sup>2</sup>, Yasunori Ono<sup>2</sup>, Toshio Takatsu<sup>2</sup> and Futoshi Nara<sup>1</sup>

Ascotricins A and B were isolated as novel sphingosine-1-phosphate receptor 1 (S1P<sub>1</sub>) antagonists from a cultured broth of a fungus identified as *Ascotricha chartarum* Berk. SANK 14186. The two compounds were purified by solvent extraction, reversed-phase (RP) column chromatography and a preparative RP-HPLC. The structures were determined by various NMR experiments and by LC/MS and GC/MS analyses. The S1P<sub>1</sub> antagonist activities were measured by a cyclic AMP assay using S1P<sub>1</sub>-expressing cells and the IC<sub>50</sub> values were 8.2 and 1.8 μM, respectively. In a [<sup>33</sup>P]sphingosine-1-phosphate/S1P<sub>1</sub>-binding assay, those values were 120 and 39 μM, and in a migration assay using human umbilical vein endothelial cells (HUVECs), they were 94 and 28 μM, respectively. Thus, ascotricins A and B are novel S1P<sub>1</sub> antagonists showing an inhibition activity toward HUVEC migration.

*The Journal of Antibiotics* (2009) 62, 359–364; doi:10.1038/ja.2009.40; published online 22 May 2009

**Keywords:** *Ascotricha chartarum*; ascotricins A and B; HUVEC; S1P<sub>1</sub> antagonist; sphingosine-1-phosphate

## INTRODUCTION

Sphingosine-1-phosphate (Sph-1-P) is an intermediate in the sphingomyelin degradation pathway<sup>1</sup> and is also a bioactive lipid messenger. Sph-1-P provokes a variety of cellular responses, including proliferation, prolongation of survival, cytoskeleton rearrangement, etc.<sup>2,3</sup> The first breakthrough in Sph-1-P research was finding its receptor, the endothelial differentiation gene-1/Sphingosine-1-phosphate receptor 1 (Edg-1/S1P<sub>1</sub>)<sup>4</sup>. Sph-1-P promoted proliferation, migration and tube formation of vascular endothelial cells through S1P<sub>1</sub>,<sup>5–7</sup> and the phenotype of S1P<sub>1</sub> homozygous knockout mice strongly indicated that S1P<sub>1</sub> was indispensable for angiogenesis.<sup>8,9</sup> The second expansion of Sph-1-P research was re-finding S1P<sub>1</sub> as a pharmacological target of a new immunosuppressant, FTY720 (Fingolimod).<sup>10,11</sup> The active metabolite of FTY720 stimulated S1P<sub>1</sub> as do other synthetic S1P<sub>1</sub> agonists and caused lymphopenia and the resultant immunosuppression.<sup>10–12</sup> Currently, FTY720 is in an ongoing developmental stage in clinical trials as a novel immunosuppressant for multiple sclerosis.

Although the current physiological research for Sph-1-P has shifted to S1P<sub>1</sub> agonists and to lymphopenia, the relationship of S1P<sub>1</sub> and angiogenesis has not yet been sufficiently studied. A few potent S1P<sub>1</sub> antagonists have been discovered,<sup>13,14</sup> but their capacity as angiogenesis inhibitors has not yet been examined. To obtain a functional S1P<sub>1</sub> antagonist, we searched for one in microorganisms because several microorganisms have sphingolipid synthesis systems, and microbial secondary metabolites are thought to be attractive sources of Sph-1-P analogs.

In this study, we discovered ascotricins A (1) and B (2) (Figure 1) in a cultured broth of the strain, *Ascotricha chartarum* Berk. SANK 14186. Thus, the identification of the producing organism, the isolation, physico-chemical properties, structure elucidation and biological activities of ascotricins are described herein.

## RESULTS

### Identification of the producing organism

The producing microorganism, SANK 14186, shown in Figure 2, was isolated from a soil sample collected from Okinawa Prefecture, Japan.

Colonies on modified Weitzman and Silva–Hutner<sup>15</sup> agar attained 27–33 mm in diameter by 14 days at 23 °C. They were floccose, consisting of short aerial mycelia and submerged vegetative hyphae, white at first, becoming dark green as they produced ascospores and conidiophores. Ascospores were superficial or sometimes immersed, dark brown to black, subglobose, ostiolate, 450–456 μm in height and 330–350 μm in diameter. The terminal hairs were erect, geniculate, often dichotomously branched, euseptate, dark brown to black and 3–4 μm in diameter at the base; short sterile hyaline branches were at the geniculate nodes, clavate, 6.5–13.6 μm in length and 2.8–4.0 μm in diameter. The lateral hairs were similar to the terminal hairs. Asci were linear-cylindrical, thin walled, deliquescing after the spores have matured, 8 spored, 52–72 μm in length and 5.8–7.8 μm in diameter. The ascospores were uniseriate, dark brown to black when mature, discoid, with a single distinct equatorial slit and 7.4–9.2 μm in length and 5.9–8.3 μm in width. The conidiophores were erect, arose from

<sup>1</sup>Exploratory Research Laboratories II, Daiichi Sankyo Co. Ltd., Kitakasai, Edogawa-ku, Tokyo, Japan and <sup>2</sup>Exploratory Research Laboratories I, Daiichi Sankyo Co. Ltd., Hiromachi, Shinagawa-ku, Tokyo, Japan

Correspondence: K Yonesu, Exploratory Research Laboratories II, Daiichi Sankyo Co. Ltd., 1-16-13, Kitakasai, Edogawa-ku, Tokyo 134-8630, Japan.

E-mail: yonesu.kiyoaki.t8@daiichisankyo.co.jp

Received 11 March 2009; revised 4 April 2009; accepted 7 May 2009; published online 22 May 2009

the basal mycelium or the terminal hairs, were olive brown to dark brown, becoming pale brown to hyaline toward the apex, euseptate, similar to the terminal hairs, simple or dichotomous and 2.2–4.0  $\mu\text{m}$  in diameter. Conidiogenous cells arose terminally from the branches, were pale brown, 5.6–12.8  $\mu\text{m}$  in length, 2.4–3.6  $\mu\text{m}$  in diameter and bore conidia-producing denticles. Conidia were produced sympodially from the denticles, were pale brown with age, irregularly globose, the walls conspicuously roughened with minute warts and were 4–7  $\mu\text{m}$  in diameter (Figure 2).

On the basis of these taxonomic properties, the strain, SANK 14186, was identified as *A. chartarum* Berk.<sup>16</sup> This strain has been deposited at the International Patent Organism Depository, National Institute of Advanced Industrial Science and Technology, Japan, under the accession no. FERM BP-08506.

### Fermentation

One loopful of the culture of the strain, *A. chartarum* SANK 14186, on an agar slant was inoculated into 30 ml of a sterilized seed medium consisting of glycerol 3%, glucose 3%, soluble starch 2%, soybean meal 1%, gelatin 0.25%, yeast extract 0.25% and  $\text{NH}_4\text{NO}_3$  0.25% in a 100-ml Erlenmeyer flask. The flask was incubated at 23°C on a rotary shaker at 210 r.p.m. for 5 days. The seed culture (2 ml) was transferred into two 500-ml Erlenmeyer flasks containing 80 ml of sterilized producing medium consisting of glycerol 5%, fresh mashed potato 5%, malt extract 0.5% and yeast extract 0.5%, and incubated at 23°C on a rotary shaker at 210 r.p.m. for 7 days.

### Isolation

After the fermentation broth (400 ml) was adjusted to pH 3, the active substance was extracted from the broth with an equal volume of acetone and the mixture was filtered. The filtrate was extracted with

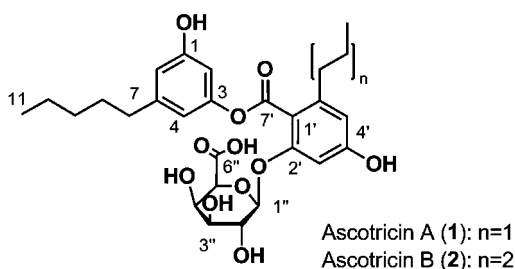


Figure 1 Structures of ascotricins A (1) and B (2).

EtOAc (400 ml) and then the organic layer was dried over anhydrous  $\text{Na}_2\text{SO}_4$  and concentrated *in vacuo* to give crude oil (900 mg). The crude oil was dissolved in MeOH and applied to a COSMOSIL 140C18-OPN column (25 ml, Nacalai Tesque Inc., Kyoto, Japan). The column was developed with acetonitrile–water containing 0.05% formic acid and the active substance was eluted with 50% aqueous acetonitrile containing 0.05% formic acid. The eluate was concentrated *in vacuo* to give a crude residue and further purified by preparative HPLC using a Develosil-packed column (Develosil C30UG-5, 20×150 mm, Nomura Chemical Co. Ltd., Seto, Japan), with 55% aqueous acetonitrile containing 0.05% formic acid as a mobile phase, with a flow rate of 11 ml  $\text{min}^{-1}$ . Fractions containing compounds 1 and 2 were separately concentrated *in vacuo* and lyophilized to give compounds 1 (94.7 mg) and 2 (51.9 mg) as colorless powders, respectively.

### Physico-chemical properties and structural elucidation

The physico-chemical properties of compounds 1 and 2 are summarized in Table 1. These data suggested that they are structurally related homologs. The molecular formula of compound 1 was determined to be  $\text{C}_{27}\text{H}_{34}\text{O}_{11}$  on the basis of HRFAB-MS and  $^1\text{H}$  and  $^{13}\text{C}$  NMR

Table 1 Physico-chemical properties of ascotricin A (1) and B (2)

	1	2
Appearance	Colorless powder	Colorless powder
Molecular formula	$\text{C}_{27}\text{H}_{34}\text{O}_{11}$	$\text{C}_{29}\text{H}_{38}\text{O}_{11}$
HR-FAB-MS ( $m/z$ )		
Found	579.1814 [ $\text{M}+2\text{Na}-\text{H}$ ] <sup>+</sup>	607.2132 [ $\text{M}+2\text{Na}-\text{H}$ ] <sup>+</sup>
Calcd	579.182	607.213
$[\alpha]_D^{25}$	−21.7 (MeOH, $c$ 1.0)	−18 (MeOH, $c$ 0.5)
UV $\lambda_{\text{max}}$	260 nm (MeOH, $\epsilon$ 7800)	261 nm (MeOH, $\epsilon$ 9000)
Solubility		
Soluble	MeOH, acetone	MeOH, acetone
Insoluble	$\text{H}_2\text{O}$ , $n$ -hexane	$\text{H}_2\text{O}$ , $n$ -hexane
IR $\nu_{\text{max}} \text{cm}^{-1}$	3377, 2958, 2930, 2872, 1726, 1612, 1590	3376, 2956, 2929, 2871, 2860, 1726, 1615

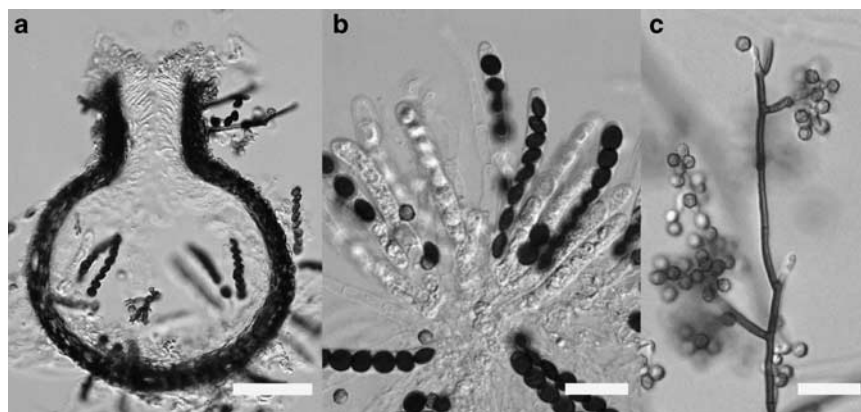


Figure 2 *A. chartarum* Berk. SANK 14186. (a) Ascoma; (b) Paraphyses and asci with ascospores; (c) Conidiophores and conidia. Scales:  $a=50\mu\text{m}$ ,  $b, c=20\mu\text{m}$ .

**Table 2** <sup>1</sup>H and <sup>13</sup>C NMR spectral data of ascotricin A (1) and B (2)

Position	1			2				
	$\delta_c^a$	mult.	$\delta_H^b$	mult.(J Hz)	$\delta_c^a$	mult.	$\delta_H^b$	mult.(J Hz)
1	158.2	s			158.0	s		
2	106.7	d	6.48	1H, m	106.6	d	6.50	1H, m
3	151.5	s			151.4	s		
4	112.1	d	6.35	1H, m	112.1	d	6.45	1H, m
5	144.5	s			144.6	s		
6	112.7	d	6.39	1H, m	112.7	d	6.47	1H, m
7	35.0	t	2.44	2H, m	35.0	t	2.56	m, o
8	30.3	t	1.44	2H, m	30.2	t	1.54	m, o
9	30.9	t	1.15	2H, m	30.8	t	1.55	m, o
10	22.0	t	1.21	2H, m	21.9	t	1.28	m, o
11	14.0	q	0.76	3H, t (7.1)	13.9	q	0.85	m, o
1'	114.0	s			113.9	s		
2'	156.3	s			156.0	s		
3'	100.3	d	6.43	1H, d (1.4)	99.8	d	6.46	1H, brs
4'	159.6	s			159.5	s		
5'	109.5	d	6.23	1H, d (1.4)	109.3	d	6.34	1H, brs
6'	141.8	s			142.2	s		
7'	166.1	s			166.0	s		
8'	34.9	t	2.41	2H, m	32.3	t	2.55	m, o
9'	24.0	t	1.48	2H, m	31.1	t	1.55	m, o
10'	13.8	q	0.80	3H, t (7.3)	30.5	t	1.55	m, o
11'					21.9	t	1.28	m, o
12'					13.8	q	0.84	m, o
1''	100.9	d	4.74	1H, d (7.6)	100.0	d	4.91	1H, d (7.3)
2''	70.1	d	3.49	1H, dd (7.6, 9.3)	69.8	d	3.57	1H, dd (7.3, 9.5)
3''	73.4	d	3.34	1H, dd (2.2, 9.3)	73.0	d	3.52	1H, dd (2.3, 9.5)
4''	69.8	d	3.82	1H, dd (0.7, 2.2)	69.7	d	3.97	1H, dd (0.6, 2.3)
5''	75.1	d	3.95	1H, d (0.7)	73.8	d	4.36	1H, d (0.6)
6''	170.7	s			169.5	s		

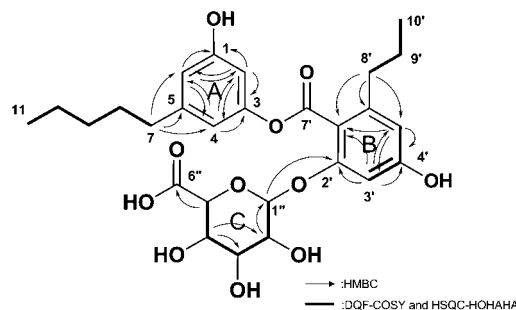
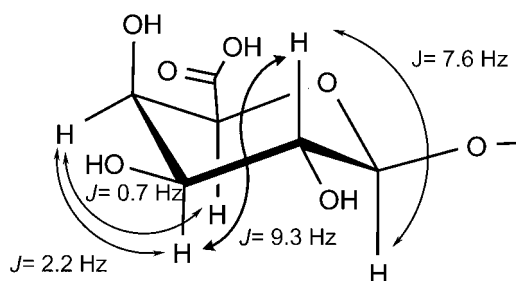
<sup>a</sup>Chemical shifts are shown with reference to DMSO-*d*<sub>6</sub> as  $\delta_H$  2.50.

<sup>b</sup>Chemical shifts are shown with reference to DMSO-*d*<sub>6</sub> as  $\delta_C$  39.5.  
 o: overlapped.

spectral data. The IR spectra of **1** suggested the presence of hydroxyl (3377 cm<sup>-1</sup>), alkyl (2958 and 2930 cm<sup>-1</sup>) and ester or carboxylic acid groups (1726 cm<sup>-1</sup>). The <sup>1</sup>H and <sup>13</sup>C NMR spectral data are summarized in Table 2.

The <sup>1</sup>H NMR spectrum of compound **1** showed signals attributed to two methyl, six methylene, five methine and two sets of *meta*-coupled aromatic protons. The <sup>13</sup>C NMR spectrum of compound **1** showed 27 resolved signals, which were classified into one ester carbonyl, one carboxyl, six methylene, five *O*-methine, five *sp*<sup>2</sup> methine, seven *sp*<sup>2</sup> quaternary and two methyl carbons by an analysis of the DEPT spectra. Twelve *sp*<sup>2</sup> carbon signals indicated the existence of two aromatic ring moieties. As shown in Figure 3, five methine carbons ( $\delta_c$  100.9, 75.1, 73.4, 70.1 and 69.8), substituted by hetero atoms, and a correlated carboxyl carbon ( $\delta_c$  170.7) in the HMBC spectrum indicated the presence of uronic acid moiety. DQF COSY and HSQC-HOHAHA experiments of **1** showed the connectivity from H-7 to H-11, from H-8' to H-10' and from H-1'' to H-5''. From these results, the presence of 1,3,5-tri-substituted and 1,2,4,6-tetra-substituted benzen moieties was revealed, as well as one propyl, one pentyl and one uronic acid moiety.

Identification of the uronic acid moiety was performed by a GC/MS analysis of an acid hydrolysate of **1**. Compound **1** was treated with 6N


**Figure 3** Significant correlations observed in the 2D NMR spectra of ascotricin A (**1**).

**Figure 4** Stereochemistry of the galacturonic acid moiety of ascotricin A (**1**).

HCl for 8 h at 110 °C, and the resulting hydrolysate was converted into a TMS derivative by *N,O*-bis-(trimethylsilyl)trifluoroacetamide (BSTFA) and was then analyzed by GC/MS. The retention time of the TMS derivative was identical to that of the authentic galacturonic acid (derivative of **1**, 14.58 min; authentic sample, 14.61 min). The relative configuration at C-1'' was elucidated to be  $\beta$  by the coupling constants of H-1'' ( $J_{1'',2''}=7.6$  Hz) as shown in Figure 4.

The structural elucidation of two aromatic ring moieties was achieved as follows. Of the four oxygenated aromatic carbons, two appeared relatively downfield at  $\delta_c$  159.6 and  $\delta_c$  158.2, respectively, which were assigned to C-1 and C-4' having free phenolic groups. The anomeric proton (H-1'',  $\delta_H$  4.74) of the uronic acid moiety was long-range coupled to C-2' and it was thereby revealed that C-1'' was linked to C-2' on the aromatic ring B in Figure 3. The signals for two methylene groups of the propyl and pentyl moieties at C-7 and C-8' were downfield shifted ( $\delta_c$  35.0 and 34.9) and were suggested to be because of two sets of benzyl positions. In the HMBC spectrum of **1**, the long-range couplings from H-7 to C-4, C-5 and to C-6 (Figure 3) revealed that the pentyl moiety was connected to C-5. The observed HMBC correlations from H-2 to C-1, C-3, C-4 and to C-6, from H-4 to C-2, C-3 and to C-6, and from H-6 to C-1, C-2 and C-4 established a 1,3-dioxy-5-pentylbenzen substitution for the aromatic ring A of the structure. The structure of aromatic ring B was revealed by similar HMBC experiments. The observed HMBC correlations from H-3' to C-2', C-4' and C-5', from H-5' to C-3', C-4' and C-1', and from H-8' to C-1', C-5' and to C-6' revealed that the propyl moieties were connected to C-6'. The *sp*<sup>2</sup> quaternary carbon (C-1',  $\delta_c$  114.0) had no long-range correlation with any substituent directly linking to C-1'. However, considering the molecular formula, the remaining ester carbonyl carbon must be directly attached to C-1. From these results, a 2,3-dioxy-6-propyl-benzoate was determined as the aromatic ring B in the structure of **1**. The oxygenated *sp*<sup>2</sup> carbon, C-3 ( $\delta_c$  151.5), must be esterified to form depside with C-7'. This assignment is consistent

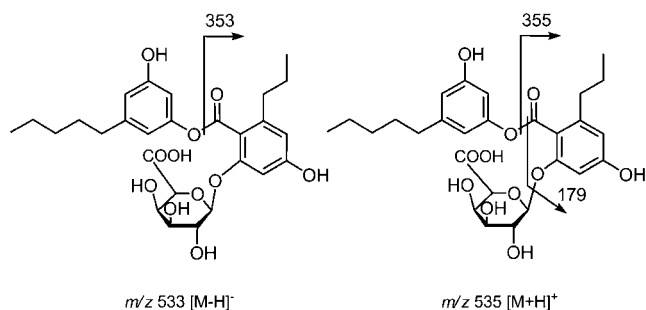


Figure 5 ESIMS fragmentations of ascotricin A (1).

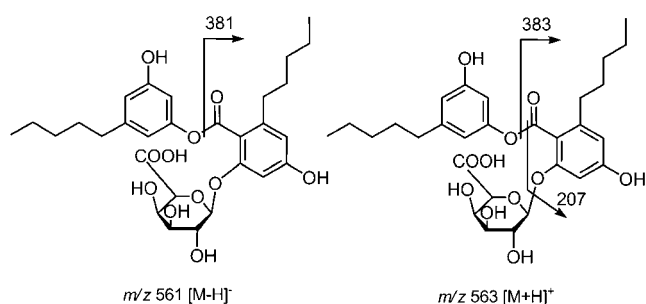


Figure 6 ESIMS fragmentations of ascotricin B (2).

with the observed relative upfield chemical shift of C-3 ( $\delta_c$  151.5) due to benzoate ester substitution, compared with phenolic C-1 ( $\delta_c$  158.2) and C-4' ( $\delta_c$  159.6) and the glycosylated carbon, C-2' ( $\delta_c$  156.3).

Although there was no direct proof of the connectivity of ring A and B obtained from the NMR experiments, the ESIMS of **1** showed a fragment ion that serves to confirm the depside linkage shown in Figure 5. A weak ion at  $m/z$  353 in the negative mode ESIMS spectrum is due to a fragment ion by cleavage of the ester bond. Correspondingly, the positive mode ESIMS spectrum produced fragment ions at  $m/z$  355 and 179, originating from the fragmentation of the cleavage of the ester bond with or without the uronic acid moiety. Thus, the structure of **1** was determined as shown in Figure 1.

The molecular formula of **2** was determined as C<sub>29</sub>H<sub>38</sub>O<sub>11</sub> by HRFAB-MS, indicating that it is larger than **1** by the C<sub>2</sub>H<sub>4</sub> unit. The <sup>1</sup>H NMR data of **2** were similar to those of **1**, except for two methylene signals. DQF COSY and HMBC experiments revealed the presence of two pentyl moieties in **2**. In the HMBC spectrum, long-range correlations were observed between H-8' and C-1', C-5' and C-6', thus it was revealed that one pentyl moiety was connected to C-6' on the aromatic ring B in **2** instead of the propyl moiety in **1**. From these results, the structure of **2** was determined as shown in Figure 1. The mass spectral data also supported the determined structure of **2** (Figure 6). These results revealed that compounds **1** and **2** were novel microbial metabolites and therefore we named them ascotricins A (**1**) and B (**2**), respectively (Figure 1).

### Biological activities

Several papers have shown that Sph-1-P induced the decrease of intracellular cyclic AMP (cAMP) concentration through the receptor S1P<sub>1</sub>; therefore, we examined the S1P<sub>1</sub> antagonist activity of ascotricins in a cAMP assay using S1P<sub>1</sub>-expressing cells.<sup>17,18</sup> Ascotricins A and B inhibited the cAMP concentration decrease induced by 100 nM Sph-1-P, and the IC<sub>50</sub> values were 8.2 and 1.8 μM, respectively

Table 3 Inhibitory activities of each compound in a cAMP assay using S1P<sub>1</sub>-expressing cells

Compound	IC <sub>50</sub> values (μM)
Ascotricin A (1)	8.2
Ascotricin B (2)	1.8
KS-501 (3)	— <sup>a</sup>
Aquastatin A (4)	— <sup>b</sup>

<sup>a</sup>No inhibition at 17 μM.

<sup>b</sup>No inhibition at 15 μM.

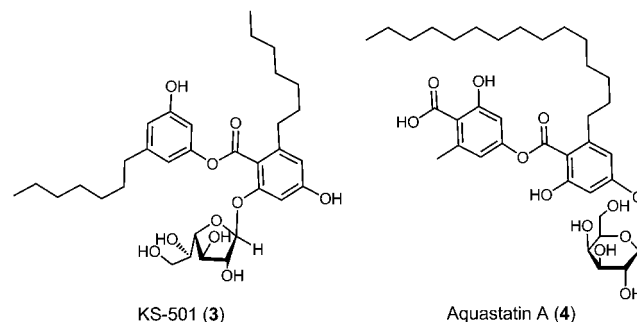


Figure 7 Structures of KS-501 (3) and aquastatin A (4).

Table 4 IC<sub>50</sub> values (μM) of ascotricins A (1) and B (2) in a [<sup>33</sup>P] Sph-1-P/S1P<sub>1</sub> binding assay and an HUVECs migration assay

	Binding	Migration
Ascotricin A (1)	120	94
Ascotricin B (2)	39	28

(Table 3). Ascotricin analogs, such as KS-501 (**3**) and aquastatin A (**4**)<sup>19–21</sup> did not show any inhibition at 17 and 15 μM, respectively (Figure 7 and Table 3). Next, we checked whether ascotricins inhibited [<sup>33</sup>P]Sph-1-P binding to S1P<sub>1</sub> in a receptor-binding assay. According to the results, both ascotricins A and B inhibited [<sup>33</sup>P]Sph-1-P/S1P<sub>1</sub> binding, and the IC<sub>50</sub> values were 120 and 39 μM, respectively (Table 4). Finally, to test whether ascotricins could suppress the biological effect of Sph-1-P on vascular endothelial cells, we performed a migration assay of human umbilical vein endothelial cells (HUVECs), the primary vascular endothelial cells that endogenously express S1P<sub>1</sub>, and the inhibition activity of ascotricins was evaluated in the assay. According to the results, ascotricins A and B suppressed HUVEC migration by 100 nM Sph-1-P, and the IC<sub>50</sub> values were 94 and 28 μM, respectively (Table 4).

### DISCUSSION

*A. chartarum* Berk. SANK 14186, *Sporothrix* sp. KAC-1985 and *Fusarium aquaeductuum* SANK 11089 are fungi that belong to a different order. Nevertheless, their products, ascotricins, KS-501 (**3**) (as an inhibitor of Ca<sup>2+</sup> and calmodulin-dependent cyclic nucleotide phosphatase) and aquastatin A (**4**) (as an inhibitor of mammalian adenosine triphosphatase), have similar glycoside structures and resemble one another (Figure 7)<sup>19–21</sup>. On the other hand, there are distinct structural differences between them. As KS-501 and aquastatin A were ineffective in a cAMP assay using S1P<sub>1</sub>-expressing cells,

the galacturonylated depside structure of ascotricins is necessary for S1P<sub>1</sub> antagonism. Therefore, ascotricins A and B are novel antagonists of S1P<sub>1</sub>. We also found that aranorosin,<sup>22</sup> analogs of caloporoside<sup>23</sup> and cinatrans<sup>24,25</sup> had S1P<sub>1</sub> antagonist activity (data not shown). All of these, including ascotricins, are amphipathic compounds and are also thought to be analogs of Sph-1-P.

Ascotricins inhibited HUVEC migration, and this indicates that ascotricins and their related S1P<sub>1</sub> antagonists might have anti-angiogenic activity. Ascotricins A and B would be useful tools for the elucidation of the function and role of S1P<sub>1</sub> on vascular endothelial cells.

## METHODS

### General

Cell culture media and antibiotics were purchased from Invitrogen Japan KK (Tokyo, Japan). HUVECs were purchased from Kurabo Industries Ltd. (Osaka, Japan). Sph-1-P and sphingosine were purchased from Biomol International LP (Plymouth Meeting, PA, USA). [ $\gamma$ -<sup>33</sup>P]ATP was purchased from PerkinElmer Japan Co. Ltd. (Yokohama, Japan). All other reagents were supplied by Sigma-Aldrich Japan (Tokyo, Japan) unless otherwise stated. NMR spectra were recorded on a Bruker AVANCE 500 spectrometer equipped with a Bruker Biospin cryogenic probe (Bruker Biospin, Osaka, Japan). The data set acquired for each sample consisted of 1D <sup>1</sup>H, <sup>13</sup>C NMR, gs-DQF-COSY, gs-HSQC, gs-HMBC and gs-HSQC-HOHAHA experiments. HR-FABMS data were recorded on a Micromass Autospec mass spectrometer (Nihon Waters KK, Tokyo, Japan). Optical rotations were measured with a JASCO DIP-370 spectropolarimeter (Jasco, Tokyo, Japan). IR spectra were obtained on a JASCO FT/IR-8900 spectrometer. UV spectra were recorded on a Shimadzu UV-265FW spectrometer (Shimadzu Corp., Kyoto, Japan). GC/MS analysis was performed using an Agilent GC/MSD spectrometer (Agilent Technologies, Tokyo, Japan) (EI-MS detector, 5973; GC system, 6890; carrier gas, He). HPLC analysis was performed with an Agilent 1100 system with a photo diode array detector.

### LC/MS analyses

LC/MS analysis of ascotricins was performed using an Agilent LC/MSD equipped with an ESI ion source and a Unison UK-C18 column (75×4.6 mm. i.d., Imtakt Corp., Kyoto, Japan), with aqueous acetonitrile containing 10 mM HCOONH<sub>4</sub> and 0.01% HCOOH, with a flow rate of 1 ml min<sup>-1</sup>. The fragmentor voltage for in-source fragmentation was 140 V in both the ESI-positive- and -negative-mode experiments.

### GC/MS analysis of ascotricin A (1) hydrolysate

Compound **1** was treated with methanol containing 5% HCl at 80 °C for 4 h in a sealed ampoule and the mixture was dried in a stream of N<sub>2</sub> gas. The residue was dissolved in pyridine, BSTFA was then added and the mixture was allowed to stand at room temperature for 5 min. The reaction mixture was analyzed by GC/MS analysis under the following conditions: an HP-5 MS capillary column (Agilent, 0.25×30 mm) coated with 0.25 mm film thickness; the column temperature programed to rise by 5 °C/min from 130 to 300 °C; and the flow rate of the He carrier gas set at 1.5 ml min<sup>-1</sup>.

### cAMP and receptor-binding assay

The cAMP assay was performed as described earlier.<sup>26</sup>

For the receptor-binding assay, [<sup>33</sup>P]Sph-1-P was enzymatically synthesized from sphingosine and [ $\gamma$ -<sup>33</sup>P]ATP using a recombinant murine sphingosine kinase.<sup>27</sup> Human S1P<sub>1</sub>-expressing cells<sup>28</sup> were seeded into 12-well plates (1×10<sup>6</sup> cells per well) and cultured overnight. The next day, the plates were set on ice and the cells were washed thrice with 3 ml of an ice-cold assay buffer ( $\alpha$ -Minimum Essential Medium containing 100 U ml<sup>-1</sup> penicillin-G sodium, 100  $\mu$ g ml<sup>-1</sup> streptomycin sulfate, 1 mg ml<sup>-1</sup> fatty acid-free bovine serum albumin, 15 mM NaF and 2 mM 4-deoxyypyridoxine) and kept on ice for 10 min. The buffer was exchanged for 0.49 ml of a new one and 5  $\mu$ l of one of the buffers; for example, solvent, 50  $\mu$ M unlabeled Sph-1-P or various concentrations of ascotricin A or B solutions, was added. Then, 5  $\mu$ l of 50 nM [<sup>33</sup>P]Sph-1-P (1800 Ci mmol<sup>-1</sup>) was supplied and the plates were left for 1 h on

ice. The cells were washed thrice with 3 ml of an ice-cold wash buffer (50 mM Tris-HCl, pH 7.4, 150 mM NaCl and 1 mg ml<sup>-1</sup> fatty acid-free bovine serum albumin) and lysed with 0.5 ml of 1 N NaOH-0.1% Triton X-100. The radioactivity of the lysate was measured using a liquid scintillation counter ( $n=3$ ).

### Migration assay

A HUVEC migration assay was performed by the method of Takuwa *et al.*,<sup>29</sup> with modification. A serum-free F-12 nutrient mixture medium with or without 100 nM Sph-1-P was added to the lower wells of a 96-well chemotaxis chamber (Neuro Probe Inc., Gaithersburg, MD, USA), and a polycarbonate filter with 5  $\mu$ m pores (Neuro Probe Inc.) was set. HUVECs were suspended into the medium without Sph-1-P. DMSO or various concentrations of ascotricin A or B were added into the HUVEC suspension and then incubated for 10 min at 37 °C in 5% CO<sub>2</sub>. Each HUVEC suspension (6×10<sup>4</sup> cells) was loaded into the upper wells and the chamber was incubated for 4 h under the same conditions. The cells on the filter were fixed and stained with Diff-Quik (Sysmex, Kobe, Japan) and the number of migrated HUVECs that had passed through the filter was determined by measuring OD<sub>595</sub> ( $n=4$ ).

## ACKNOWLEDGEMENTS

We thank Dr Takuwa for his instruction regarding the migration assay.

- 1 Stoffel, W. & Assmann, G. Metabolism of sphingosine bases. XV. Enzymatic degradation of 4t-sphinganine 1-phosphate (sphingosine 1-phosphate) to 2t-hexadecen-1-al and ethanolamine phosphate. *Hoppe. Seylers. Z. Physiol. Chem.* **351**, 1041–1049 (1970).
- 2 Goetzl, E. J. & An, S. Diversity of cellular receptors and functions for the lysophospholipid growth factors lysophosphatidic acid and sphingosine 1-phosphate. *FASEB. J.* **12**, 1589–1598 (1998).
- 3 Goetzl, E. J. *et al.* Mechanisms of lysolipid phosphate effects on cellular survival and proliferation. *Ann. N. Y. Acad. Sci.* **905**, 177–187 (2000).
- 4 Lee, M. J. *et al.* Sphingosine-1-phosphate as a ligand for the G protein-coupled receptor EDG-1. *Science* **279**, 1552–1555 (1998).
- 5 Kimura, T. *et al.* Sphingosine 1-phosphate stimulates proliferation and migration of human endothelial cells possibly through the lipid receptors, Edg-1 and Edg-3. *Biochem. J.* **348**, 71–76 (2000).
- 6 Lee, M. J. *et al.* Akt-mediated phosphorylation of the G protein-coupled receptor EDG-1 is required for endothelial cell chemotaxis. *Mol. Cell.* **8**, 693–704 (2001).
- 7 Krump-Konvalinkova, V. *et al.* Stable knock-down of the sphingosine 1-phosphate receptor S1P<sub>1</sub> influences multiple functions of human endothelial cells. *Arterioscler. Thromb. Vasc. Biol.* **25**, 546–552 (2005).
- 8 Liu, Y. *et al.* Edg-1, the G protein-coupled receptor for sphingosine-1-phosphate, is essential for vascular maturation. *J. Clin. Invest.* **106**, 951–961 (2000).
- 9 Chae, S. S., Paik, J. H., Allende, M. L., Proia, R. L. & Hla, T. Regulation of limb development by the sphingosine 1-phosphate receptor S1P<sub>1</sub>/EDG-1 occurs via the hypoxia/VEGF axis. *Dev. Biol.* **268**, 441–447 (2004).
- 10 Mandala, S. *et al.* Alteration of lymphocyte trafficking by sphingosine-1-phosphate receptor agonists. *Science* **296**, 346–349 (2002).
- 11 Brinkmann, V. *et al.* The immune modulator FTY720 targets sphingosine 1-phosphate receptors. *J. Biol. Chem.* **277**, 21453–21457 (2002).
- 12 Sanna, M. G. *et al.* Sphingosine 1-phosphate (S1P) receptor subtypes S1P<sub>1</sub> and S1P<sub>3</sub>, respectively, regulate lymphocyte recirculation and heart rate. *J. Biol. Chem.* **279**, 13839–13848 (2004).
- 13 Davis, M. D., Clemens, J. J., Macdonald, T. L. & Lynch, K. R. Sphingosine 1-phosphate analogs as receptor antagonists. *J. Biol. Chem.* **280**, 9833–9841 (2005).
- 14 Sanna, M. G. *et al.* Enhancement of capillary leakage and restoration of lymphocyte egress by a chiral S1P<sub>1</sub> antagonist *in vivo*. *Nat. Chem. Biol.* **2**, 434–441 (2006).
- 15 Ono, Y. & Kobayashi, T. Notes on new and noteworthy plant-inhabiting fungi from Japan (2): *Griphosphaerium zelkovicola* sp. nov. with *Sarcostroma* anamorph isolated from bark of *Zelkova serrata*. *Mycoscience* **44**, 109–114 (2003).
- 16 Hawksworth, D. L. A revision of genus *Ascotricha* Berk. *Mycological Papers* **126**, 1–28 (1971).
- 17 Van Brocklyn, J. R. *et al.* Dual actions of sphingosine-1-phosphate: extracellular through the G<sub>i</sub>-coupled receptor Edg-1 and intracellular to regulate proliferation and survival. *J. Cell. Biol.* **142**, 229–240 (1998).
- 18 Okamoto, H. *et al.* EDG1 is a functional sphingosine-1-phosphate receptor that is linked via a G<sub>i/o</sub> to multiple signaling pathways, including phospholipase C activation, Ca<sup>2+</sup> mobilization, Ras-mitogen-activated protein kinase activation, and adenylate cyclase inhibition. *J. Biol. Chem.* **273**, 27104–27110 (1998).



- 19 Nakanishi, S., Ando, K., Kawamoto, I. & Kase, H. KS-501 and KS-502, new inhibitors of Ca<sup>2+</sup> and calmodulin-dependent cyclic-nucleotide phosphodiesterase from *Sporothrix* sp. *J. Antibiot.* **42**, 1049–1055 (1989).
- 20 Yasuzawa, T., Saitoh, Y. & Sano, H. Structures of KS-501 and KS-502, the new inhibitors of Ca<sup>2+</sup> and calmodulin-dependent cyclic nucleotide phosphodiesterase. *J. Antibiot.* **43**, 336–343 (1990).
- 21 Hamano, K. *et al.* Aquastatin A, an inhibitor of mammalian adenosine triphosphatases from *Fusarium aquaeductuum*. Taxonomy, fermentation, isolation, structure determination and biological properties. *J. Antibiot.* **46**, 1648–1657 (1993).
- 22 Roy, K. *et al.* Aranorosin, a novel antibiotic from *Pseudoarachniotus roseus*. I. Taxonomy, fermentation, isolation, chemical and biological properties. *J. Antibiot.* **41**, 1780–1784 (1988).
- 23 Weber, W., Schu, P., Anke, T., Velten, R. & Steglich, W. Caloporside, a new inhibitor of phospholipases C from *Caloporus dichrous* (Fr) Ryv. *J. Antibiot.* **47**, 1188–1194 (1994).
- 24 Itazaki, H. *et al.* Cinatrins, a novel family of phospholipase A<sub>2</sub> inhibitors. I. Taxonomy and fermentation of the producing culture, isolation and structures of Cinatrins. *J. Antibiot.* **45**, 38–49 (1992).
- 25 Tanaka, K., Itazaki, H. & Yoshida, T. Cinatrins, a novel family of phospholipase A<sub>2</sub> inhibitors. II. Biological activities. *J. Antibiot.* **45**, 50–55 (1992).
- 26 Nakamura, T. *et al.* Synthesis and SAR studies of a novel class of S1P<sub>1</sub> receptor antagonists. *Bioorg. Med. Chem.* **15**, 3548–3564 (2007).
- 27 Kohama, T. *et al.* Molecular cloning and functional characterization of murine sphingosine kinase. *J. Biol. Chem.* **273**, 23722–23728 (1998).
- 28 Yonesu, K. *et al.* Involvement of sphingosine-1-phosphate and S1P<sub>1</sub> in angiogenesis: Analyses using a new S1P<sub>1</sub> antagonist of non-sphingosine-1-phosphate analog. *Biochem. Pharmacol.* **77**, 1011–1020 (2009).
- 29 Arikawa, K. *et al.* Ligand-dependent inhibition of B16 melanoma cell migration and invasion via endogenous S1P<sub>2</sub> G protein-coupled receptor. Requirement of inhibition of cellular Rac activity. *J. Biol. Chem.* **278**, 32841–32851 (2003).

## ORIGINAL ARTICLE

# Relationship between peroxisome proliferator-activated receptor- $\gamma$ activation and the ameliorative effects of ascochlorin derivatives on type II diabetes

Junji Magae<sup>1,2</sup>, Mie Tsuruga<sup>2</sup>, Ayako Maruyama<sup>2,3</sup>, Chiharu Furukawa<sup>2</sup>, Shuji Kojima<sup>3</sup>, Hirohiko Shimizu<sup>4</sup> and Kunio Ando<sup>4</sup>

Peroxisome proliferator-activated receptor- $\gamma$  (PPAR- $\gamma$ ) is a crucial factor in the development of insulin resistance associated with type II diabetes. We previously found that 4-*O*-carboxymethyl ascochlorin, a derivative of ascochlorin, ameliorates diabetes and activates PPAR- $\gamma$ . Here, we compared the relationship between the amelioration of type II diabetes in *db/db* mice lacking leptin receptor, and PPAR- $\gamma$  activation by 4-*O*-carboxymethyl-ascochlorin, as well as by 4-*O*-methyl-ascochlorin, a derivative that does not activate PPAR- $\gamma$ . Administration of these compounds significantly reduces blood glucose in a dose-dependent manner, whereas blood cholesterol is significantly elevated in 4-*O*-carboxymethyl-ascochlorin-treated mice but is significantly decreased in 4-*O*-methyl-ascochlorin-treated mice. Pioglitazone, a potent PPAR- $\gamma$  agonist with a thiazolidinedione structure, reduces glucose but elevates cholesterol blood levels. These results suggest that ascochlorin derivatives ameliorate diabetes through a mechanism that is probably independent of PPAR- $\gamma$  activation, although PPAR- $\gamma$  activation could be partially involved in the ameliorative effect in certain derivatives.

*The Journal of Antibiotics* (2009) 62, 365–369; doi:10.1038/ja.2009.43; published online 26 June 2009

**Keywords:** ascochlorin; AS-6; diabetes; MAC; PPAR- $\gamma$

## INTRODUCTION

There are two types of diabetes mellitus. Type I, or insulin-dependent diabetes mellitus, is characterized by a progressive loss of insulin-producing  $\beta$ -cells in the pancreas by an autoimmune mechanism, and the resulting insulin deficiency produces severe hyperglycemia.<sup>1</sup> Destruction of  $\beta$ -cells in type I diabetes is known to be caused by apoptosis induced through an oxidative reaction initiated by nitric oxide generated in  $\beta$ -cells.<sup>2–4</sup> Type II diabetes is developed through insulin resistance and the subsequent insufficiency of  $\beta$ -cell compensation.<sup>5</sup> Although the mechanism causing insulin resistance is not clearly understood, the involvement of a nuclear hormone receptor, peroxisome proliferator-activated receptor- $\gamma$  (PPAR- $\gamma$ ), is suggested. PPAR- $\gamma$  has a crucial function in the differentiation of adipocytes, and agonists of PPAR- $\gamma$  induce a differentiation of preadipocyte cell lines and ameliorate type II diabetes by improving insulin resistance.<sup>6</sup> PPAR- $\gamma$  is activated by thiazolidinediones, originally synthesized as a drug to treat hyperlipidemia and insulin resistance. These compounds bind to PPAR- $\gamma$  with high affinity and enhance the differentiation of preadipocyte cells into mature adipocytes.

Ascochlorin is a prenylphenol antibiotic, originally isolated as an antiviral agent produced by an incomplete fungus, *Ascochyta visiae*.<sup>7,8</sup>

Ascochlorin and its derivatives exhibit a large variety of physiological activities, including hypolipidemic activity,<sup>9,10</sup> suppression of hypertension,<sup>11</sup> amelioration of type I and II diabetes,<sup>12,13</sup> immunomodulation<sup>14,15</sup> and antitumor activity through the phagocyte-mediated activation of innate immunity.<sup>15,16</sup> In addition, ascochlorin and ascofuranone suppress tumor invasion *in vitro* and selectively suppress AP-1 activity in human renal carcinoma cells, as well as its downstream targets, such as matrix metalloproteinase-9, through suppression of the ERK1/2 signaling pathway.<sup>17,18</sup> 4-*O*-Methyl-ascochlorin (MAC), a methylated derivative of ascochlorin, induces apoptosis in a variety of leukemia cell lines through a mechanism that is distinct from conventional apoptosis.<sup>19</sup> Ascochlorin selectively kills estrogen receptor (ER)-negative breast cancer cells, partly through the induction of apoptosis.<sup>20</sup> A proteome analysis of ascochlorin-treated human osteosarcoma cells shows a decrease in the expression of several genes in the mitogen-activated protein kinase (MAPK)-signaling cascade, including epidermal growth factor receptor and ERK-1/2.<sup>21</sup> Ascochlorin and ascofuranone moderate oxidative phosphorylation by inhibiting ubiquinone-dependent electron transport in isolated mitochondria,<sup>22–24</sup> and it is suggested that the antiviral activity of ascochlorin and the macrophage activation of

<sup>1</sup>Radiation Safety Research Center, Central Research Institute of Electric Power Industry, 2-11-1 Iwado Kita, Komae-shi, Tokyo, Japan; <sup>2</sup>Department of Biotechnology, Institute of Research and Innovation, 1201 Takada, Kashiwa, Chiba, Japan; <sup>3</sup>Faculty of Pharmaceutical Sciences, Tokyo University of Science, 2641 Yamazaki Noda-shi, Chiba, Japan and <sup>4</sup>NRL Pharma Inc., KSP, 3-2-1 Sakado, Takatsu-ku, Kawasaki, Japan

Correspondence: Dr J Magae, Nuclear Technology Research Laboratory, Radiation Safety Research Center, Central Research Institute of Electric Power Industry, 2-11-1 Iwado Kita, Komae-shi, Tokyo 201-8511, Japan.

E-mail: jmagae@sannet.ne.jp

Received 19 December 2008; revised 18 May 2009; accepted 19 May 2009; published online 26 June 2009

ascofuranone result from this inhibitory activity on mitochondrial respiration.<sup>22,23,25</sup>

These compounds also modulate the activity of nuclear hormone receptors. Ascochlorin activates human ER, suggesting that mechanisms other than those involving the respiratory chain contribute to their physiological activities. Some derivatives, including 4-*O*-carboxymethyl-ascochlorin (AS-6), activate PPAR- $\gamma$  and induce a differentiation of preadipocytes.<sup>26,27</sup> AS-6 inhibits tumor necrosis factor- $\alpha$ -stimulated nuclear factor- $\kappa$ B activity and the inflammatory molecular expression of rat vascular smooth muscle cells in a manner dependent on PPAR- $\gamma$  activation.<sup>28</sup> In this paper, we compare the relationship between PPAR- $\gamma$  activation and the ameliorative effect on type II diabetic *db/db* mice lacking the leptin receptor. Our results suggest that the amelioration of type II diabetes by AS-6 is consistent with a mechanism of PPAR- $\gamma$  activation, whereas MAC may act by a mechanism that is independent of PPAR- $\gamma$ .

## MATERIALS AND METHODS

### Mice

Eight-week-old male *db/db* mice and age-matched normal male littermates (*db/m*) were purchased from Sankyo Lab Service Inc. (Tokyo, Japan). The mice were given a diet of commercial food pellets and tap water *ad libitum*. Animal studies were conducted in the animal facility of the Institute of Research and Innovation under approved protocols in accordance with institutional guidelines for laboratory animal care.

### Chemicals

AS-6 and MAC were obtained from Chugai Pharmaceutical Co. (Tokyo, Japan). Pioglitazone was obtained from Takeda Pharmaceutical Co. (Tokyo, Japan). The compounds were dissolved in dimethylsulfoxide at 10 mg ml<sup>-1</sup> as stock solutions and appropriately diluted with medium for addition to the culture medium. For *in vivo* administration, mice were fed a pellet diet containing one of the drugs *ad libitum*.

### Cell culture

U2OS, a human osteosarcoma, was provided by C-L Wu (MGH Cancer Center, Charlestown, MA, USA). Cells were cultured in Dulbecco's modified Eagle's medium supplemented with 5% fetal bovine serum at 37 °C in a humidified incubator under 10% CO<sub>2</sub> atmosphere.

### Plasmids

Expression vectors of the transactivation domain of PPAR- $\gamma$  fused with a Gal4-DNA-binding domain,<sup>29</sup> and the luciferase reporter plasmid containing a

Gal4-binding site upstream of SV-40 basic promoter<sup>30</sup> were kind gifts from S Kato (Institute of Molecular and Cellular Bioscience, University of Tokyo, Tokyo, Japan) and S Inamoto (Institute of Research and Innovation, Kashiwa, Japan). pCMV- $\beta$ -galactosidase was provided by NH Heintz (Department of Pathology, University of Vermont, Burlington, VT, USA).

### Proliferation assay

U2OS cells (1 × 10<sup>4</sup> cells) were cultured with drugs for 24 h in microplate wells, and [<sup>3</sup>H]thymidine (0.5  $\mu$ Ci/well) was added 4 h before harvesting.<sup>27</sup> Incorporated radioactivity was determined by a liquid scintillation counter.

### Reporter assay

U2OS cells (1 × 10<sup>6</sup> cells in a 10 cm dish) were transfected with pCMV- $\beta$ -Gal (4  $\mu$ g), an expression vector of the Gal4-fused PPAR- $\gamma$  (2  $\mu$ g), and a corresponding reporter plasmid (4  $\mu$ g) using a liposome-based transfection kit (Fugene, Roche Diagnostics, Tokyo, Japan) as described previously.<sup>26,27</sup> Cells were cultured for 24 h. Luciferase activity (Roche Diagnostics) and  $\beta$ -galactosidase activity (Promega, Madison, WI, USA) in the cell lysates were determined with commercial assay kits.

### Biochemical analysis of plasma

Plasma samples were obtained from blood samples containing 10 U ml<sup>-1</sup> heparin sulfate. Total cholesterol (Kyowa Medex, Tokyo, Japan) and glucose (GL-5, Kainos, Tokyo, Japan) in the samples were measured with a commercial assay kit. Insulin (Morinaga, Yokohama, Japan) and leptin (R&D Systems, Minneapolis, MN, USA) were measured by an enzyme-linked immunosorbent assay with a commercial assay kit according to the manufacturer's instructions.

### Statistical analysis

The results of animal experiments were statistically analyzed with a two-tailed *t*-test, judging the significance by a *P*-value less than 0.05.

## RESULTS

### Activation of PPAR- $\gamma$ by AS-6 but not by MAC

4-*O*-Methyl-ascochlorin (MAC) and 4-*O*-carboxymethyl-ascochlorin (AS-6) are prototypes of the ascochlorin derivatives that we have synthesized (Figure 1a). MAC has hypolipidemic activity,<sup>9,10</sup> whereas AS-6 ameliorates diabetes *in vivo*.<sup>12,13</sup> MAC inhibits cell growth, induces apoptosis and activates no nuclear receptors except PXR, whereas AS-6 is less toxic and selectively activates PPAR- $\gamma$ .<sup>27</sup> The agonistic activity of these two compounds on PPAR- $\gamma$  was compared in U2OS cells transfected with the expression plasmid for PPAR- $\gamma$  fused with the Gal4-DNA-binding domain, together with the luciferase reporter plasmid containing a Gal4-binding site in the promoter

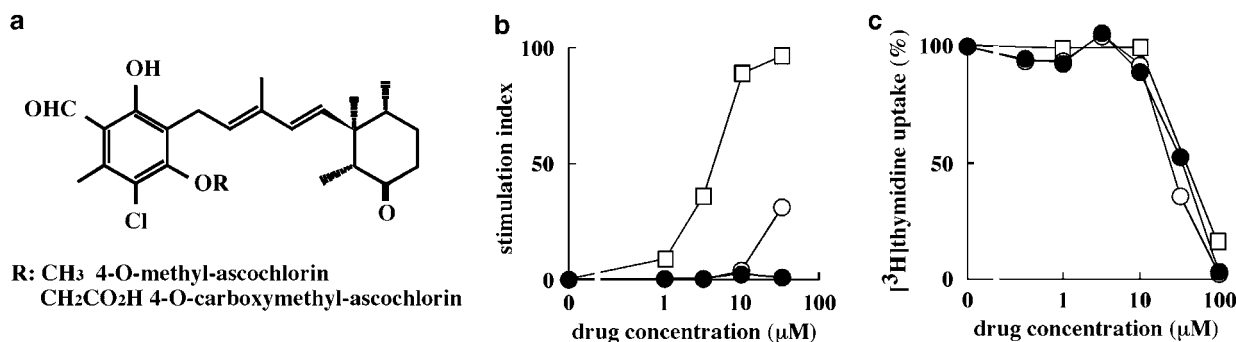


**Figure 1** Differential activation of PPAR- $\gamma$  by AS-6 and MAC. (a) The structure of AS-6 and MAC. (b) U2OS cells transfected with expression plasmids for Gal4-fused PPAR- $\gamma$   $\beta$ -galactosidase and a luciferase-reporter plasmid for Gal4 were cultured in the presence of the drug for 24 h. Luciferase activity normalized with  $\beta$ -galactosidase activity was determined. Each point represents the average stimulation index compared with non-stimulated controls in independent triplicate experiments. (c) U2OS cells were cultured in the presence of the drug for 24 h. Cell proliferation was determined by [<sup>3</sup>H] thymidine uptake over 4 h at the termination of culture. Each point represents an average percent uptake compared with non-stimulated controls in independent triplicate experiments. AS-6, open circles; MAC, filled circles; pioglitazone, open squares.

region. AS-6 at 30  $\mu\text{M}$  increased luciferase activity 30-fold 24 h after transfection, whereas MAC had no agonistic activity in this reporter system (Figure 1b). One of the thiazolidinedione compounds, pioglitazone, activates PPAR- $\gamma$  at concentrations above 1  $\mu\text{M}$ , and produced more than a 100-fold activation at 30  $\mu\text{M}$ . In contrast, the three compounds comparably suppressed cell proliferation as measured by [ $^3\text{H}$ ] thymidine incorporation 24 h after addition of the drug (Figure 1c). The drugs had only a negligible effect on cell proliferation at a concentration below 10  $\mu\text{M}$ , and completely suppressed cell [ $^3\text{H}$ ] thymidine incorporation at 100  $\mu\text{M}$ .

### Amelioration of type II diabetes in *db/db* mice

To evaluate the ameliorative effects of AS-6 and MAC, 8-week-old *db/db* mice were fed a 0.2–0.4% drug-containing diet for five consecutive days, and blood glucose levels were determined after overnight fasting. In *db/db* mice, blood glucose levels were elevated to a level three times that of age-matched normal *db/m* mice (Figure 2a). Administration of AS-6 and MAC significantly reduced elevated glucose levels. This effect was more pronounced in mice fed a MAC-containing diet. Mice fed a diet containing 0.8% AS-6, 0.4% MAC or 0.8% MAC showed glucose levels lower than normal. Administration of pioglitazone also

reduced blood glucose levels to normal. Polydipsia is one of the characteristics of diabetes patients, and *db/db* mice consumed much more drinking water than did normal mice (Figure 2b). The administration of AS-6 and MAC, as well as that of pioglitazone, reduced polydipsia. *db/db* mice also consumed more food than did normal mice, and food consumption was decreased in mice fed a drug-containing diet (Figure 2c). Mice consumed 50% less in the 0.8%-AS-6 group and in the 0.4 and 0.8%-MAC groups, compared with control *db/db* mice.

*db/db* mice are obese as well as diabetic, and their body weight (36.9  $\pm$  1.0) is much heavier than that of age-matched normal mice (21.8  $\pm$  0.2), although weight gain during the 5-day experiment was not significantly different between normal and *db/db* mice (Figure 2d). Weight gain during the experiment period was significantly reduced in 0.4 and 0.8% AS-6-fed mice and in all the MAC-treated mice. In contrast, weight gain was significantly increased in mice fed the 0.2% AS-6-containing diet or the 0.1% pioglitazone-containing diet, suggesting that activation of PPAR- $\gamma$  increases body weight, whereas blood glucose levels are reduced to normal. A lower dose of MAC (0.1%) did not increase weight gain and had no significant effect on blood glucose (data not shown). The administration of a diet containing more than 1% MAC or AS-6 killed the animals. Blood levels of

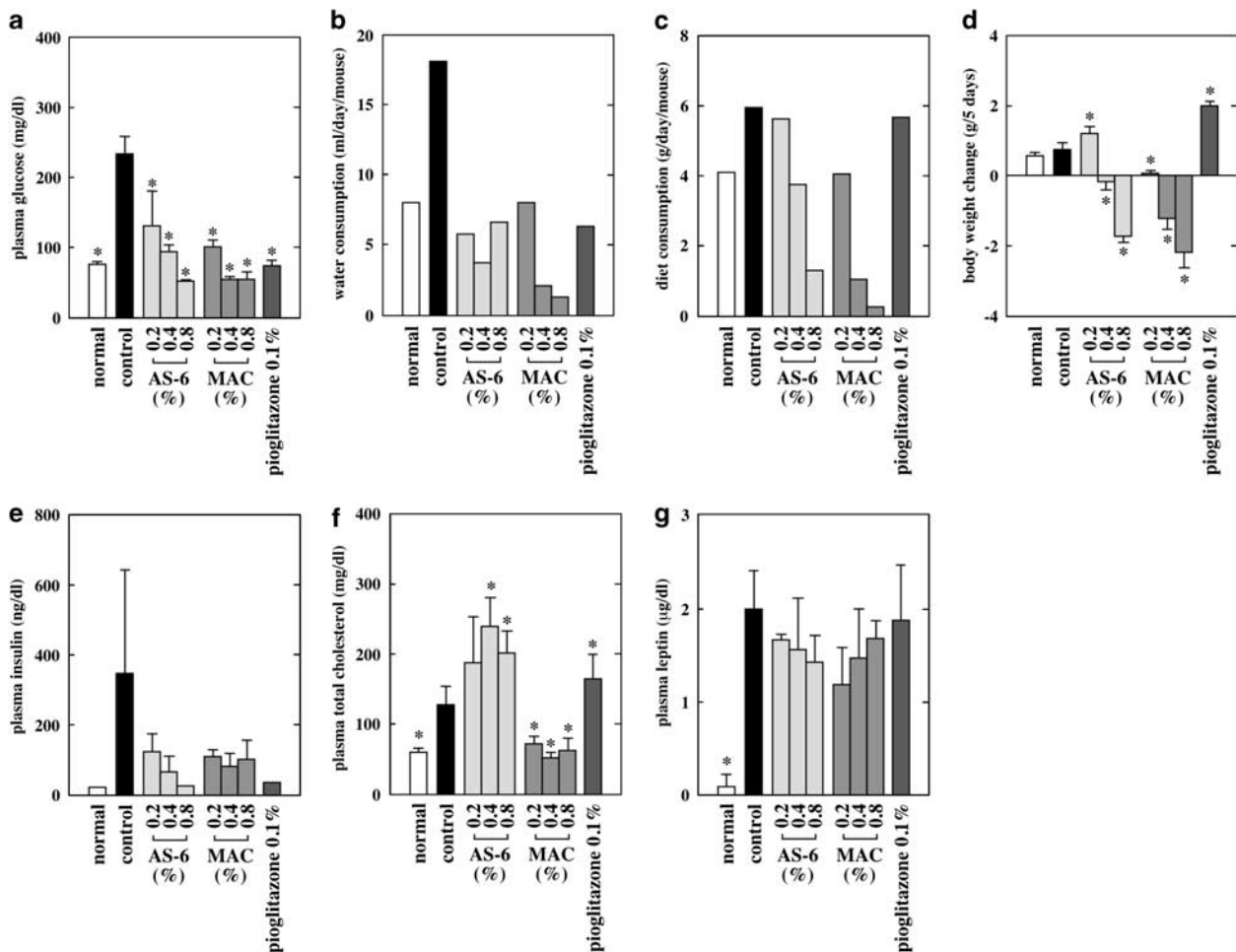


**Figure 2** *In vivo* ameliorative effects of AS-6 and MAC on type II diabetes in *db/db* mice. *Db/db* mice (three mice/group in each cage) were starved overnight, and then fed an AS-6 or MAC-containing diet for 5 days. After overnight fasting, plasma was isolated from heparin-treated blood samples, and concentrations of glucose (a), insulin (e), total cholesterol (f) and leptin (g) were determined. Water (b) and food consumption (c) in each group were recorded during the experiment. Body weights were compared before and after the experiment after overnight fasting (d). Each value for panels a, d–g represents the mean  $\pm$  s.d. \*Statistically significant compared with control group ( $P < 0.05$ ).

insulin and leptin are dramatically increased in *db/db* mice compared with those in normal mice (Figures 2e and f), which is characteristic of type II diabetes in *db/db* mice genetically lacking leptin receptors.<sup>29</sup> AS-6 and MAC, as well as pioglitazone, reduced leptin and insulin levels in blood, although, because of the variation among mice, these differences were not statistically significant.

#### Modulation of blood cholesterol in *db/db* mice

Ascochlorin derivatives affect lipid metabolism in mice. To confirm the hypocholesterolemic effects of AS-6 and MAC, blood cholesterol levels in *db/db* mice were measured. We found significantly higher cholesterol concentrations in *db/db* mice ( $123.8 \pm 27.1$  mg per 100 ml) compared with that in normal mice ( $58.4 \pm 6.6$  mg per 100 ml) (Figure 2g). Administration of AS-6 significantly increased the cholesterol levels up to more than 200 mg per 100 ml. In contrast, the administration of MAC significantly reduced cholesterol levels to below 100 mg per 100 ml, the level comparable with that in normal mice. Pioglitazone, similar to AS-6, significantly increased blood cholesterol levels, suggesting that the activation of PPAR- $\gamma$  increases blood cholesterol in type II diabetic model mice.

#### DISCUSSION

Since we isolated ascochlorin from fungal broth in 1968, we have studied the modulation of carbohydrate and lipid metabolism by ascochlorin and its derivatives.<sup>9–13</sup> AS-6 is one of the derivatives in which we found an amelioration of diabetes.<sup>12,13</sup> Treatment with AS-6 dramatically suppresses polydipsia, polyuria and glucosuria in *db/db* mice,<sup>13</sup> type II diabetes mice lacking leptin receptors.<sup>31</sup> The pancreatic islets isolated from AS-6-treated *db/db* mice release much more insulin in response to glucose loading. The combined treatment with insulin and AS-6 synergistically decreases serum glucose. Moreover, AS-6, similar to thiazolidinediones, which ameliorate type II diabetes through the improvement of insulin resistance,<sup>6</sup> activates PPAR- $\gamma$  and induces a differentiation of preadipocyte cell lines.<sup>26</sup> These results suggest that AS-6 restores sensitivity and responsiveness to insulin in *db/db* mice through the activation of PPAR- $\gamma$ . Agonistic activity on PPAR- $\gamma$  is not associated with all the derivatives we studied.<sup>27</sup> MAC is a derivative with much weaker agonistic activity than AS-6. Thus, it is of interest to compare the *in vivo* efficacy of AS-6 and MAC on type II diabetes. In this study, we found that MAC and AS-6 have comparable ameliorative activity on type II diabetes in *db/db* mice. They similarly reduced hyperglycemia, hyperinsulinemia and polydipsia, comparable with pioglitazone, in spite of the negligible PPAR- $\gamma$  agonistic activity of MAC *in vitro*. Treatment with pioglitazone significantly increases body weight and plasma cholesterol. Treatment with a lower dose of AS-6 (diet containing 0.2% AS-6) also increased body weight and plasma cholesterol. In contrast, MAC reduces weight gain and plasma cholesterol. These results suggest that MAC ameliorates type II diabetes in a manner independent of PPAR- $\gamma$ , whereas AS-6 does so through mechanisms dependent on and independent of PPAR- $\gamma$ . Consistent with these results, AS-6 is also effective in treating streptozotocin-induced type I diabetes, caused by insulin deficiency resulting from drug-mediated  $\beta$ -cell destruction.<sup>12</sup>

Several possibilities could be proposed for the mechanism of PPAR- $\gamma$ -independent amelioration of type II diabetes mediated by ascochlorin derivatives. The most distinguishing characteristic of MAC among ascochlorin derivatives *in vitro* is apoptosis induction.<sup>19</sup> It is reported that many regulators of apoptosis have an important function in energy metabolism. For instance, a proapoptotic Bcl-2 family member, Bad, associates with glucokinase in mitochondria, and a dysfunction of the protein impairs glucose clearance in glucose

tolerance tests.<sup>32</sup> Survival kinases Akt and Pim also regulate cellular metabolism, in part, through a phosphatidylinositol-3-kinase/mammalian target of rapamycin-dependent mechanism.<sup>33</sup> Although type II diabetes is characterized by insulin resistance,<sup>5</sup> the ability of pancreatic islets to secrete insulin is gradually decreased as the disease progresses, because the islets degenerate as a result of the toxic effects of reactive oxygen species.<sup>34,35</sup> Thus, antioxidants reduce blood glucose levels, improve glucose clearance and increase insulin secretion in response to glucose loading.<sup>35</sup> A mitochondrial NADH reductase, apoptosis-inducing factor, released from mitochondria during the apoptotic process leading to caspase-independent apoptosis, serves as a free radical scavenger to prevent apoptosis in cerebellar granule cells.<sup>36</sup> It is also possible that ascochlorin derivatives directly participate in a cellular oxidative reaction because they react with the electron transport chain in mitochondria.<sup>23–25</sup>

Finally, we could not exclude the trivial possibility that a suppression of food intake might reduce hyperglycemia and glucosuria, because higher doses of MAC and AS-6 significantly reduced body weight, whereas a low dose of AS-6 and pioglitazone rather increased weight gain. Although the administration of AS-6 and MAC by mixing in the diet could not determine the exact doses, we could not detect significant efficacy by direct administration methods. Oral administration of AS-6 or MAC up to  $1 \text{ g kg}^{-1}$  using a gastric feeding needle failed to demonstrate a significant ameliorative effect on diabetes as well as toxicity, presumably because of their bioavailability. The intraperitoneal administration of AS-6 and MAC every other day showed no significant efficacy on diabetes at  $25 \text{ mg kg}^{-1}$ , and caused toxic death at  $50 \text{ mg/kg}$ . An improvement of toxicity and bioavailability through chemical structure modification or through the drug delivery method is absolutely necessary to develop AS-6 and MAC as clinical drugs for the treatment of diabetes patients.

#### ACKNOWLEDGEMENTS

This study was in part supported by grants from the New Energy and Industrial Technology Development Organization (NEDO).

- 1 Yoon, J. W., Jun, H. S. & Santamaria, P. Cellular and molecular mechanisms for the initiation and progression of  $\beta$  cell destruction resulting from the collaboration between macrophages and T cells. *Autoimmunity* **27**, 109–122 (1998).
- 2 O'Brien, A., Harmon, B. V., Cameron, D. P. & Allan, D. J. Apoptosis is the mode of  $\beta$ -cell death responsible for the development of IDDM in the nonobese diabetic mouse. *Diabetes* **46**, 750–757 (1997).
- 3 Kurrer, M. O., Pakala, S. V., Hanson, H. L. & Katz, D. J.  $\beta$ -cell apoptosis in T cell-mediated autoimmune diabetes. *Proc. Natl Acad. Sci. USA* **94**, 213–218 (1997).
- 4 Corbett, J. A., Swetland, M. A., Wang, J. L., Lancaster, Jr. J. R. & McDaniel, M. L. Nitric oxide mediates cytokine-induced inhibition of insulin secretion by human islets of Langerhans. *Proc. Natl Acad. Sci. USA* **90**, 1713–1735 (1993).
- 5 DeFronzo, R. A. Pathogenesis of type 2 diabetes: metabolic and molecular implications for identifying diabetes genes. *Diabetes Rev.* **5**, 177–269 (1997).
- 6 Rosen, E. D., Walkey, C. J., Puigserver, P. & Spiegelman, B. M. Transcriptional regulation of adipogenesis. *Genes Dev.* **14**, 1293–1307 (2000).
- 7 Tamura, G., Suzuki, S., Takatsuki, A., Ando, K. & Arima, K. Ascochlorin, a new antibiotic, found by the paper-disc agar-diffusion method. I. Isolation, biological and chemical properties of ascochlorin. (Studies on antiviral and antitumor antibiotics. I). *J. Antibiot.* **21**, 539–544 (1968).
- 8 Nawata, Y., Ando, K., Tamura, G., Arima, K. & Iitake, Y. The molecular structure of ascochlorin. *J. Antibiot.* **2**, 511–512 (1969).
- 9 Hosokawa, T., Sawada, M., Ando, K. & Tamura, G. Enhanced excretion of fecal neutralsterols and the hypercholesterolemic properties of 4-O-methylascochlorin. *Agric. Biol. Chem.* **44**, 2461–2468 (1980).
- 10 Hosokawa, T., Sawada, M., Ando, K. & Tamura, G. Alteration of cholesterol metabolism by 4-O-methylascochlorin in rats. *Lipids* **16**, 433–438 (1981).
- 11 Hosokawa, T., Okutomi, T., Sawada, M., Ando, K. & Tamura, G. Unusual concentration of urine and prevention of polydipsia by fungal prenylphenols in DOCA hypertensive rats. *Eur. J. Pharmacol.* **69**, 429–438 (1981).

- 12 Hosokawa, T., Ando, K. & Tamura, G. An ascochlorin derivative, AS-6 potentiates insulin action in streptozotocin diabetic mice and rats. *Agric. Biol. Chem.* **46**, 775–781 (1982).
- 13 Hosokawa, T., Ando, K. & Tamura, G. An ascochlorin derivative, AS-6, reduces insulin resistance in the genetically obese diabetic mice. *Diabetes* **34**, 267–274 (1982).
- 14 Magae, J. *et al.* *In vitro* effects of an antitumor antibiotic, ascofuranone, on the murine immune system. *Cancer Res.* **46**, 1073–1078 (1986).
- 15 Magae, J. *et al.* Antitumor and antimetastatic activity of an antibiotic, ascofuranone and activation of phagocytes. *J. Antibiot.* **40**, 959–965 (1988).
- 16 Magae, J., Hosokawa, T., Ando, K., Nagai, K. & Tamura, G. Antitumor protective property of an isoprenoid antibiotic, ascofuranone. *J. Antibiot.* **35**, 1547–1552 (1982).
- 17 Hong, S. H. *et al.* Ascochlorin inhibits matrixmetalloproteinase-9 expression by suppressing AP-1 mediated-gene expression through the ERK1/2 signaling pathway: inhibitory effects of ascochlorin on the invasion of renal carcinoma cells. *J. Biol. Chem.* **280**, 25202–25209 (2005).
- 18 Cho, H. J. *et al.* Ascofuranone suppresses PMA-mediated matrix metalloproteinase-9 gene activation through the Ras/Raf/MEK/ERK- and Ap1-dependent mechanisms. *Carcinogenesis* **28**, 1104–1110 (2007).
- 19 Tsuruga, M. Characterization of 4-*O*-methyl-ascochlorin-induced apoptosis in comparison with typical apoptotic inducers in human leukemia cell lines. *Apoptosis*, **9**, 429–435 (2004).
- 20 Sakaguchi, K. *et al.* Selective cytotoxicity of ascochlorin in ER-negative human breast cancer cell lines. *Biochem. Biophys. Res. Commun.* **329**, 46–50 (2005).
- 21 Kang, J. H. *et al.* Proteome analysis of responses to ascochlorin in a human osteocarcinoma cell line by 2-D gel electrophoresis and MALDI-TOF MS. *J. Proteome Res.* **5**, 2620–2631 (2006).
- 22 Takatsuki, A., Tamura, G. & Arima, K. Antiviral and antitumor antibiotics. XIV. Effects of ascochlorin and other respiration inhibitors on multiplication of Newcastle disease virus in cultured cells. *Appl. Microbiol.* **17**, 825–829 (1969).
- 23 Magae, J. *et al.* Effects of microbial products on glucose consumption and morphology of macrophages. *Biosci. Biotechnol. Biosci.* **57**, 1628–1631 (1993).
- 24 Minagawa, N., Meguro, K., Sakajo, S. & Yoshimoto, A. Effects of ascofuranone on the mitochondria isolated from *Hansenulaanomala*. *Biosci. Biotechnol. Biochem.* **58**, 1334–1335 (1994).
- 25 Ashikaga, T. *et al.* Selective induction of interleukin-1 production and tumor killing activity of macrophages through apoptosis by the inhibition of oxidative respiration. *Biosci. Biotechnol. Biochem.* **62**, 1115–1121 (1998).
- 26 Togashi, M. *et al.* PPAR $\gamma$  activation and adipocyte differentiation induced by AS-6, a prenylphenol antidiabetic antibiotic. *J. Antibiot.* **55**, 417–422 (2002).
- 27 Togashi, M. *et al.* Ascochlorin derivatives as ligands for nuclear hormone receptors. *J. Med. Chem.* **46**, 4113–4123 (2003).
- 28 Kang, J. H. *et al.* Ascochlorin suppresses oxLDL-induced MMP-9 expression by inhibiting the MEK/ERK signaling pathway in human THP-1 macrophages. *J. Cell Biochem.* **102**, 506–514 (2007).
- 29 Yanase, T. *et al.* Differential expression of PPAR $\gamma_1$  and  $\gamma_2$  isoforms in human adipose tissue. *Biochem. Biophys. Res. Commun.* **233**, 320–324 (1997).
- 30 Harding, H. P. & Lazar, M. A. The monomer-binding orphan receptor Rev-Erb represses transcription as a dimer on a novel direct repeat. *Mol. Cell Biol.* **15**, 4791–4802 (1995).
- 31 Chen, H. *et al.* Evidence that the diabetes gene encodes the leptin receptor: Identification of a mutation in the leptin receptor gene in *db/db* mice. *Cell* **84**, 491–495 (1996).
- 32 Danial, N. N. *et al.* BAD and glucokinase reside in a mitochondrial complex that integrates glycolysis and apoptosis. *Nature* **424**, 952–956 (2003).
- 33 Amaravadi, R. & Thompson, C. B. The survival kinases Akt and Pim as potential pharmacological targets. *J. Clin. Invest.* **115**, 2618–2624 (2005).
- 34 Kaneto, H. *et al.* Reducing sugars trigger oxidative modification and apoptosis in pancreatic  $\beta$ -cells by provoking oxidative stress through the glycation reaction. *Biochem. J.* **320**, 855–863 (1996).
- 35 Kaneto, H. *et al.* Beneficial effects of antioxidants in diabetes. Possible protection of pancreatic  $\beta$ -cells against glucose toxicity. *Diabetes* **48**, 2398–2406 (1999).
- 36 Klein, J. A. *et al.* The harlequin mouse mutation downregulates apoptosis-inducing factor. *Nature* **419**, 367–374 (2002).

ORIGINAL ARTICLE

# Enzymatic synthesis of bis-5-alkylresorcinols by resorcinol-producing type III polyketide synthases

Akimasa Miyanaga and Sueharu Horinouchi

No enzyme systems responsible for the biosynthesis of structurally and biosynthetically intriguing bis-5-alkylresorcinols produced by plants have been identified. Herein, we show that bacterial, fungal and plant alkylresorcinol-producing type III polyketide synthases (PKSs), such as *ArsB* in the Gram-negative bacterium *Azotobacter vinelandii*, *ORAS* in the fungus *Neurospora crassa* and *ARAS2* in the rice plant *Oryza sativa*, can synthesize bis-5-alkylresorcinol from alkanedioic acid *N*-acetylcysteamine dithioester as a starter substrate and from malonyl-CoA as an extender substrate by two-step conversion. Plants presumably use a type III PKS for the biosynthesis of bis-5-alkylresorcinols.

*The Journal of Antibiotics* (2009) 62, 371–376; doi:10.1038/ja.2009.44; published online 26 June 2009

**Keywords:** bis-5-alkylresorcinol; enzymatic synthesis; polyketide synthase

## INTRODUCTION

Type III polyketide synthases (PKSs) are structurally simple enzymes that catalyze the synthesis of aromatic polyketides in bacteria, fungi and plants.<sup>1</sup> Type III PKSs catalyze iterative decarboxylative condensations of an extender substrate such as malonyl-CoA with a starter substrate such as acyl-CoA, and subsequently cyclize the resultant polyketide chain to yield various bioactive natural compounds with great structural diversity. This structural diversity of polyketide scaffolds is governed mainly by the selectivity of starter and extender substrates, the number of condensation reactions and the mode of ring closure of the resultant polyketide chains. One class of the products of type III PKSs includes alkylresorcinols that consist of polar dihydroxybenzene rings and hydrophobic alkyl chains, and exhibit a wide variety of biological and biochemical activities.<sup>2–6</sup> For example, *ArsB*, a bacterial type III PKS from *Azotobacter vinelandii*, catalyzes three condensations of malonyl-CoA with a long-chain acyl starter substrate and subsequently cyclizes the resultant tetraketide intermediate by aldol condensation to yield alkylresorcinol.<sup>3,4</sup> *ORAS*, a fungal type III PKS from *Neurospora crassa*, synthesizes tetraketide and pentaketide alkylresorcylic acids from a long-chain acyl starter substrate such as stearoyl-CoA.<sup>5</sup> *ARAS2* (*Oryza sativa* genome DB os10g08620, alkylresorcylic acid synthase 2), a plant type III PKS from the rice plant *O. sativa*, also produces a tetraketide alkylresorcylic acid from a long-chain acyl starter substrate, as does *ORAS* (our unpublished data). The alkylresorcylic acids produced by *ORAS* and *ARAS2* are immediately converted into alkylresorcinols by non-enzymatic decarboxylation.

Bis-5-alkylresorcinol, having a dihydroxybenzene ring at both terminal ends of an alkyl chain, has a relatively uncommon chemical structure (Figure 1a). The alkyl chain length of the bis-5-alkylresorcinols so far

isolated, for instance, from *Hakea trifurcata*,<sup>7</sup> *Oncostemon bojeranum*,<sup>8</sup> *Panopsis rubescens*<sup>9</sup> and the rye *Secale cereale*,<sup>10</sup> ranges from C14 to C22. Some of the bis-5-alkylresorcinols contain one or two double bonds in their alkyl chains. Bis-5-alkylresorcinols were shown to be capable of both mediating Cu<sup>2+</sup>-dependent DNA cleavage and potentiating the action of bleomycin through the inhibition of DNA polymerase  $\beta$ .<sup>11</sup> It seems plausible that these two activities could function synergistically to potentiate the destruction of cancer cells. A transient inhibition of DNA polymerase  $\beta$ , concomitant with anti-tumor therapy, improves the effectiveness of DNA-damaging anti-tumor agents. Although the chemical synthesis method has been developed because of the important biological activities of bis-5-alkylresorcinols,<sup>12</sup> enzyme systems responsible for their biosynthesis have not yet been identified. As mentioned above, our recent studies of type III PKSs showed that a dihydroxybenzene ring of alkylresorcinols is derived from polyketide intermediate chains. We thus hypothesized that a type III PKS could synthesize bis-5-alkylresorcinols. If so, as all the PKSs so far found in plants belong to the type III PKS family, bis-5-alkylresorcinols in plants must also be synthesized by a type III PKS(s). In this case, two reactions by a type III PKS(s) are required for the formation of two hydroxybenzene rings in bis-5-alkylresorcinol, as depicted in Figure 1b. In this proposed pathway, the acyl substrate used in the second ring formation is uncommon. It was obscure whether type III PKSs could accept long-chain acyl thioesters harboring an aromatic ring in the alkyl tail as a starter substrate in the second reaction. In this report, we describe that *ArsB*, *ARAS2* and *ORAS*, all belonging to the type III PKS family, show the ability to synthesize bis-5-alkylresorcinol from alkanedioic acid *N*-acetylcysteamine (NAC) dithioester as a starter substrate and from malonyl-CoA as an extender substrate.

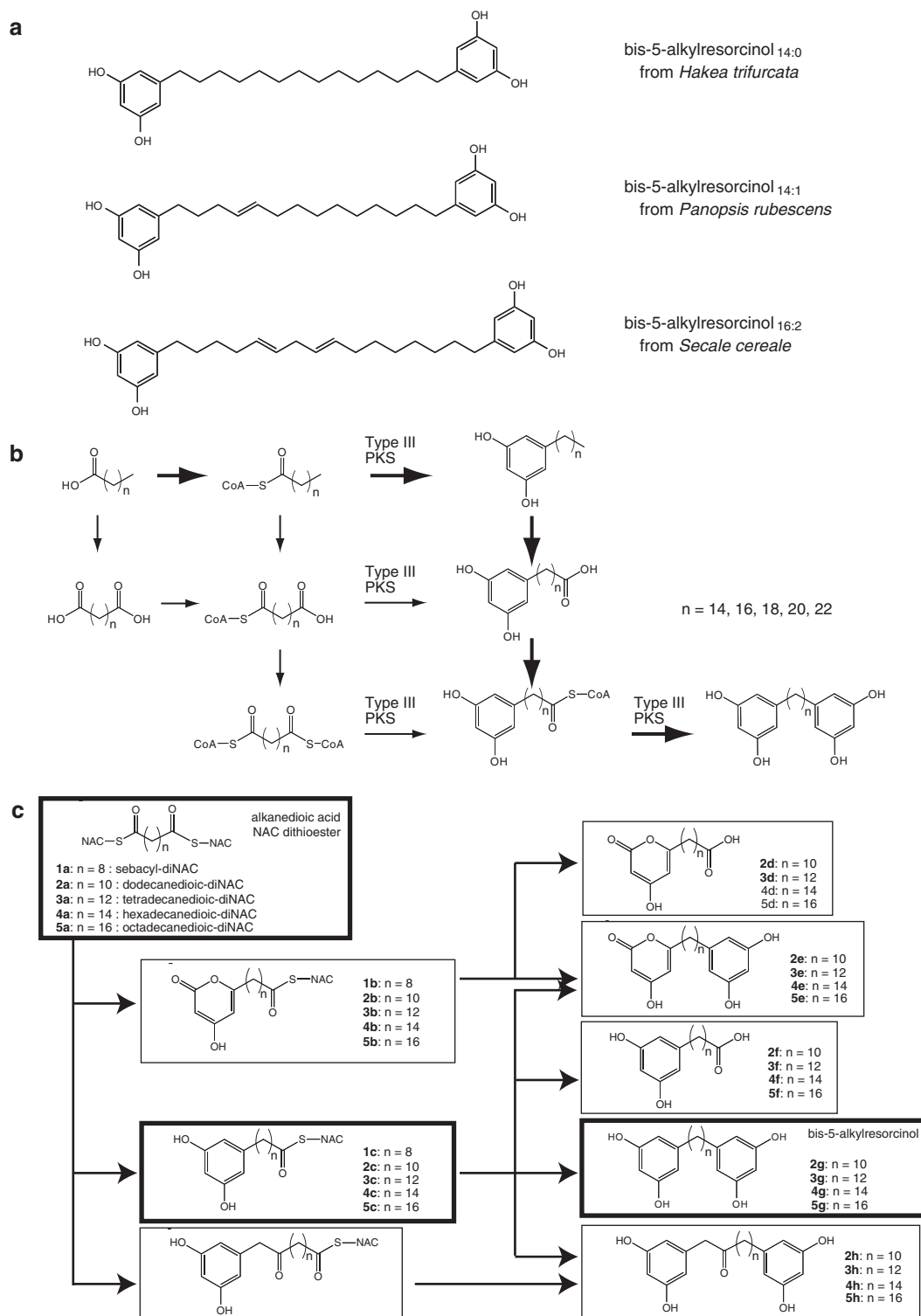


**Figure 1** Bis-5-alkylresorcinol synthesis. **(a)** A variety of natural bis-5-alkylresorcinols. **(b)** A proposed biosynthetic pathway of bis-5-alkylresorcinol in plants. **(c)** A proposed synthetic route of bis-5-alkylresorcinols and by-products by type III polyketide synthases (PKSs) from alkanedioic acid NAC (*N*-acetylcysteamine) dithioester substrates *in vitro*. A part of the proposed synthetic route of bis-5-alkylresorcinols by type III PKSs is highlighted by using thicker squares.

## MATERIALS AND METHODS

### Materials

The carboxylic acids used were purchased from Tokyo Chemical Industry (Tokyo, Japan) and from Apollo Scientific Limited (Bredbury,

UK). The NAC compounds used in this study were chemically synthesized from their corresponding carboxylic acids according to a published method.<sup>13</sup> Recombinant ArsB, ARAS2 and ORAS were prepared, as described.<sup>3,5</sup>



### Reaction of type III PKS with NAC compound

Recombinant type III PKS (2.0  $\mu\text{M}$ ) was incubated at 30 °C for 6 h with 50  $\mu\text{M}$  NAC compound, 100  $\mu\text{M}$  malonyl-CoA, 20 mM HEPES-Na (pH 7.5), 150 mM NaCl and 10% (w/v) glycerol in a total volume of 200  $\mu\text{l}$ . After incubation at 30 °C for 6 h, the reactions were quenched by the addition of 20  $\mu\text{l}$  of 6 M HCl. The products were extracted with 400  $\mu\text{l}$  of ethyl acetate, and the organic layer was evaporated to dryness. The residual material was dissolved in methanol for HPLC, liquid chromatography-atmospheric pressure chemical ionization mass spectrometry (LC-APCI/MS) and radio-TLC analyses. HPLC and LC-APCI/MS analyses were carried out using an esquire high-capacity trap plus system (Bruker Daltonics, Bremen, Germany) and a Hitachi LaChrom ELITE system (Hitachi, Tokyo, Japan), respectively, on the apparatus equipped with a Pegasil-B C4 reversed-phase column (4 $\times$ 250 mm; Senshu Scientific, Tokyo, Japan). The products were eluted with 55 or 70% acetonitrile in water containing 0.1% trifluoroacetic acid as an eluent at a flow rate of 1 ml min<sup>-1</sup>. For radio-TLC analysis, a silica-gel 60 WF<sub>254</sub> TLC plate (Merck, Darmstadt, Germany) was developed in benzene/acetone/acetic acid (75:25:1, v/v/v) and the <sup>14</sup>C-labeled compounds derived from the substrate [2-<sup>14</sup>C]malonyl-CoA were detected using a Fujifilm BAS-MS imaging plate (Fujifilm, Tokyo, Japan). The identification of <sup>14</sup>C-labeled signals on TLC was confirmed by the co-migration of radioactivity with each product purified by HPLC.

### <sup>1</sup>H NMR spectral data of synthetic compounds

Sebacyl-diNAC (**1a**): H NMR (500 MHz, CDCl<sub>3</sub>)  $\delta$  5.85 (2H, br), 3.44 (4H, dd,  $J=12.5$ , 6 Hz), 3.03 (4H, t,  $J=6$  Hz), 2.58 (4H, t,  $J=7.5$  Hz), 1.97 (6H, s), 1.66 (4H, t,  $J=7.5$  Hz), 1.27 (8H, m).

Dodecanedioyl-diNAC (**2a**): H NMR (500 MHz, CDCl<sub>3</sub>)  $\delta$  5.86 (2H, br), 3.44 (4H, dd,  $J=12.5$ , 6.5 Hz), 3.03 (4H, t,  $J=6.5$  Hz), 2.58 (4H, t,  $J=7.5$  Hz), 1.97 (6H, s), 1.66 (4H, t,  $J=7.5$  Hz), 1.28 (12H, m).

Tetradecanedioyl-diNAC (**3a**): H NMR (500 MHz, CDCl<sub>3</sub>)  $\delta$  5.84 (2H, br), 3.44 (4H, dd,  $J=12.5$ , 6.5 Hz), 3.03 (4H, t,  $J=6.5$  Hz), 2.58 (4H, t,  $J=8$  Hz), 1.97 (6H, s), 1.66 (4H, t,  $J=7.5$  Hz), 1.26 (16H, m).

Hexadecanedioyl-diNAC (**4a**): H NMR (500 MHz, CDCl<sub>3</sub>)  $\delta$  5.85 (2H, br), 3.44 (4H, dd,  $J=12.5$ , 6 Hz), 3.03 (4H, t,  $J=6$  Hz), 2.58 (4H, t,  $J=7.5$  Hz), 1.98 (6H, s), 1.66 (4H, t,  $J=7.5$  Hz), 1.26 (20H, m).

1,3-Dihydroxy-5-(14'-(3'',5''-dihydroxyphenyl)tetradecenyl)benzene (**4g**): H NMR (500 MHz, THF-*d*<sub>8</sub>)  $\delta$  7.79 (4H, s), 6.03 (4H, d,  $J=2$  Hz), 5.97 (2H, t,  $J=2$  Hz), 2.41 (4H, t,  $J=8$  Hz), 1.60 (4H, br), 1.29 (20H, m).

Octadecanedioyl-diNAC (**5a**): H NMR (500 MHz, CDCl<sub>3</sub>)  $\delta$  5.83 (2H, s), 3.45 (4H, dd,  $J=12.5$ , 6 Hz), 3.03 (4H, t,  $J=6.5$  Hz), 2.58 (4H, t,  $J=7.5$  Hz), 1.98 (6H, s), 1.66 (4H, t,  $J=7.5$  Hz), 1.26 (20H, m).

15-Phenylpentadecanoyl-NAC (**6c**): H NMR (500 MHz, CDCl<sub>3</sub>)  $\delta$  7.28 (2H, t,  $J=7.5$  Hz), 7.18 (3H, m), 3.44 (2H, dd,  $J=12.5$ , 6 Hz), 3.03 (2H, t,  $J=6$  Hz), 2.60 (2H, t), 2.58 (2H, t), 1.98 (3H, s), 1.66 (2H, t,  $J=7.5$  Hz), 1.61 (2H, t,  $J=7.5$  Hz), 1.26 (20H, m).

5-(14'-(3'',5''-Dihydroxyphenyl)tetradecenyl)benzene (**6g**): H NMR (500 MHz, THF-*d*<sub>8</sub>)  $\delta$  7.78 (2H, s), 7.20 (2H, t,  $J=7.5$  Hz), 7.14 (2H, d,  $J=7$  Hz), 7.10 (H, t,  $J=7$  Hz), 6.03 (2H, d,  $J=2$  Hz), 5.97 (H, t,  $J=2$  Hz), 2.58 (2H, t,  $J=8$  Hz), 2.41 (2H, t,  $J=8$  Hz), 1.60 (4H, m), 1.29 (20H, m).

### Spectrometric data

Sebacyl-diNAC (**1a**): HPLC (45% acetonitrile):  $R_t=9.0$ , LC-APCI/MS (positive): MS,  $m/z$  405 [M+H]<sup>+</sup>, UV:  $\lambda_{\text{max}}$  231 nm.

Dodecanedioyl-diNAC (**2a**): HPLC (45% acetonitrile):  $R_t=12.5$ , LC-APCI/MS (positive): MS,  $m/z$  433 [M+H]<sup>+</sup>, UV:  $\lambda_{\text{max}}$  231 nm.

Tetradecanedioyl-diNAC (**3a**): HPLC (50% acetonitrile):  $R_t=13.0$ , LC-APCI/MS (positive): MS,  $m/z$  461 [M+H]<sup>+</sup>, UV:  $\lambda_{\text{max}}$  231 nm.

Hexadecanedioyl-diNAC (**4a**): HPLC (55% acetonitrile):  $R_t=13.4$ , LC-APCI/MS (positive): MS,  $m/z$  489 [M+H]<sup>+</sup>, UV:  $\lambda_{\text{max}}$  231 nm.

Compound **4c**: HPLC (55% acetonitrile):  $R_t=11.7$ , LC-APCI/MS (positive): MS,  $m/z$  452 [M+H]<sup>+</sup>.

Compound **4d**: HPLC (55% acetonitrile):  $R_t=7.2$ , LC-APCI/MS (negative): MS,  $m/z$  351 [M-H]<sup>-</sup>, UV:  $\lambda_{\text{max}}$  285 nm.

Compound **4e**: HPLC (55% acetonitrile):  $R_t=8.9$ , LC-APCI/MS (negative): MS,  $m/z$  415 [M-H]<sup>-</sup>, UV:  $\lambda_{\text{max}}$  282 nm.

Compound **4f**: HPLC (55% acetonitrile):  $R_t=8.3$ , LC-APCI/MS (negative): MS,  $m/z$  349 [M-H]<sup>-</sup>, MS/MS (precursor ion at  $m/z$  349),  $m/z$  331, 287, UV:  $\lambda_{\text{max}}$  274 nm.

1,3-Dihydroxy-5-(14'-(3'',5''-dihydroxyphenyl)tetradecenyl)benzene (**4g**): HPLC (55% acetonitrile):  $R_t=9.9$ , LC-APCI/MS (negative): MS,  $m/z$  413 [M-H]<sup>-</sup>, MS/MS (precursor ion at  $m/z$  413),  $m/z$  369, UV:  $\lambda_{\text{max}}$  274 nm.

Compound **4h**: HPLC (55% acetonitrile):  $R_t=7.8$ , LC-APCI/MS (negative): MS,  $m/z$  455 [M-H]<sup>-</sup>, UV:  $\lambda_{\text{max}}$  274 nm.

Tetradecanedioyl-diNAC (**5a**): HPLC (60% acetonitrile):  $R_t=13.6$ , LC-APCI/MS (positive): MS,  $m/z$  517 [M+H]<sup>+</sup>, UV:  $\lambda_{\text{max}}$  231 nm.

15-Phenylpentadecanoyl-NAC (**6c**): HPLC (70% acetonitrile):  $R_t=15.9$ , LC-APCI/MS (positive): MS,  $m/z$  420 [M+H]<sup>+</sup>, UV:  $\lambda_{\text{max}}$  231 nm.

5-(14'-(3'',5''-Dihydroxyphenyl)tetradecenyl)benzene (**6g**): HPLC (70% acetonitrile):  $R_t=11.8$ , LC-APCI/MS (negative): MS,  $m/z$  381 [M-H]<sup>-</sup>, MS/MS (precursor ion at  $m/z$  381),  $m/z$  339, UV:  $\lambda_{\text{max}}$  274 nm.

## RESULTS

### Reaction of ArsB with alkanedioic acid NAC dithioesters

To investigate whether a type III PKS has the ability to synthesize bis-5-alkylresorcinol, we synthesized hexadecanedioyl-diNAC (**4a**) as an analog of hexadecanedioyl-diCoA, which is one of the candidates for the initial substrate. When ArsB was incubated with **4a** and malonyl-CoA, two compounds in a major peak **4g** and a minor peak **4e** were detected in HPLC analysis (Figure 2b). Neither of the two compounds was detected in the control experiments performed with a boiled enzyme (Figure 2a). The molecular mass of **4g** was 414, on the basis of the [M-H]<sup>-</sup> ion at  $m/z$  413 on LC-APCI/MS analysis. To determine the chemical structure of **4g** by <sup>1</sup>H NMR spectroscopy, we obtained **4g** (0.3 mg, 7% yield) from a large-scale enzyme reaction. As a result, **4g** was identified as 1,3-dihydroxy-5-(14'-(3'',5''-dihydroxyphenyl)tetradecenyl)benzene by comparing its <sup>1</sup>H NMR spectrum with that of the synthetic compound in the previous report.<sup>12</sup> A minor peak **4e** was predicted to be a by-product, which possessed both a resorcinol and a pyrone group, on the basis of LC-APCI/MS analysis.

As shown in Figure 1c, in this reaction, ArsB might first convert one of the two NAC groups of **4a** into a resorcinol group, yielding an intermediate (**4c**). ArsB might subsequently accept **4c** as a substrate in the second reaction and convert the remaining NAC group of **4c** into a resorcinol group, yielding bis-5-alkylresorcinol (**4g**). To clarify this prediction, we examined the course of the production of **4c** and **4g** from **4a**. During the early stage of the reaction with ArsB, for about 5–10 min after the reaction initiation, **4c** peak was detected by the LC-APCI/MS analysis, concomitant with the reduction in the amount of **4a** (Figures 2e–g), suggesting that **4a** was converted to **4c**. Thereafter, the **4g** peak was gradually increased, concomitant with the reduction in the amount of **4c**, suggesting that **4c** was converted into **4g**. Such a two-step process in the production of **4g** hampered us in determining the kinetic parameters of ArsB. The **4g** production by ArsB is similar to the curcuminoid production by CUS (curcuminoid synthase) from *O. sativa*<sup>14</sup> in terms of the two-step conversion. However, the mechanism of curcuminoid synthesis is different from that of bis-5-alkylresorcinol synthesis. CUS uses same starter substrates and two different extender substrates in the curcuminoid synthesis, whereas ArsB uses two different starter substrates and the same extender substrate in the bis-5-alkylresorcinol synthesis.

To investigate whether ArsB is able to accept an acyl thioester harboring an aromatic ring, we synthesized 15-phenylpentadecanoyl-NAC (**6c**) as a substrate analog in the second reaction. When ArsB was incubated with **6c** and malonyl-CoA, a single compound (**6g**) was produced (Figures 3 and 4). This compound was predicted as

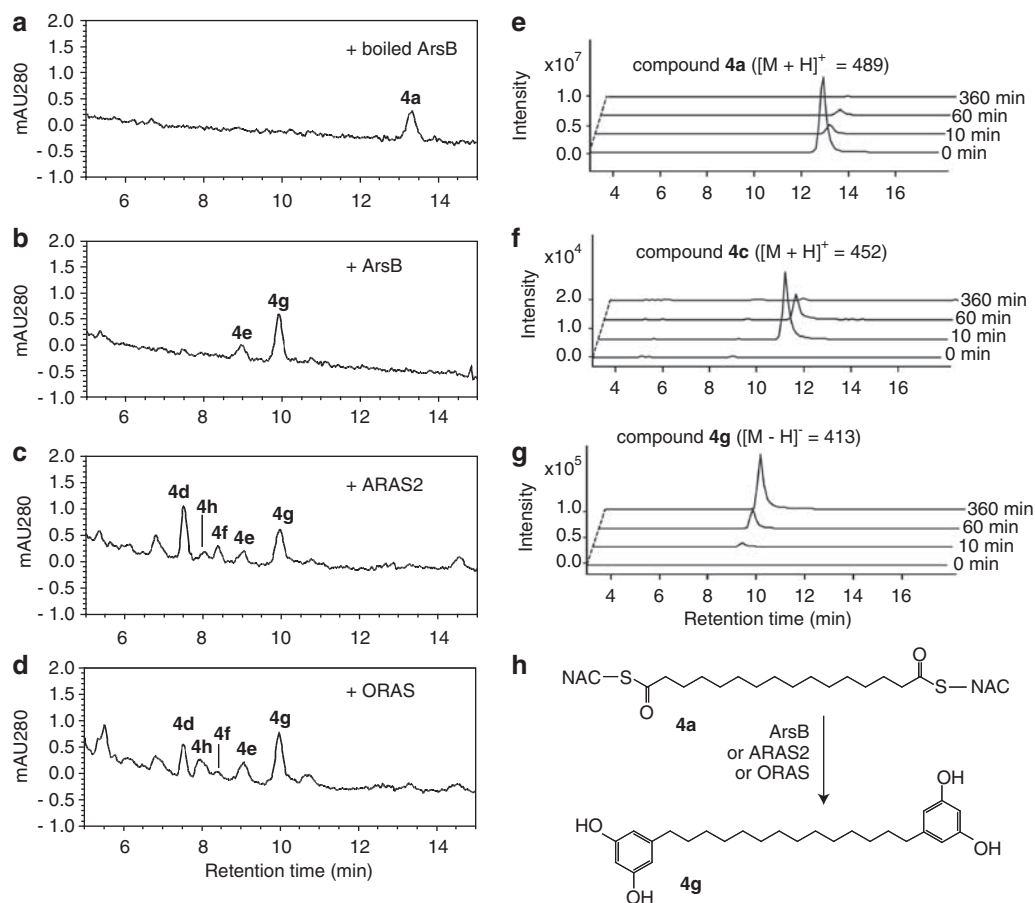


**Figure 2** Chromatography analysis of the *in vitro* products of type III polyketide synthases (PKSs). (a, b, c and d) HPLC chromatograms of the *in vitro* reactions of type III PKSs with **4a** and malonyl-CoA. The reaction mixture contained boiled ArsB as a negative control (a), ArsB (b), ARAS2 (c) and ORAS (d). (e, f and g) Selected extracted ion LC-APCI/MS chromatograms of the *in vitro* reaction of ArsB with **4a** and malonyl-CoA at four time points. These chromatograms were prepared at  $m/z$  489  $[M+H]^+$  (e),  $m/z$  452  $[M+H]^+$  (f) and  $m/z$  413  $[M-H]^-$  (g). The conversion of **4a** to **4g** catalyzed by these enzymes is shown (h).

5-(14'-(3'',5''-dihydroxyphenyl)tetradecenyl)benzene on the basis of LC-APCI/MS analysis. These observations clearly showed that ArsB could accept the acyl substrate possessing an aromatic ring at the alkyl tail as a substrate.

Substrate specificity of ArsB was determined by incubating four different, synthesized alkanedioic acid NAC dithioesters (**1a**, **2a**, **3a** and **5a**) possessing various lengths of alkyl chains with ArsB and malonyl-CoA. As a result, the radio-TLC, HPLC and LC-APCI/MS analyses of the resultant products revealed a broad range of bis-5-alkylresorcinol productivities of ArsB. ArsB accepted dodecanedioyl-diNAC (**2a**), tetradecanedioyl-diNAC (**3a**) and octadecanedioyl-diNAC (**5a**) as substrates and gave bis-5-alkylresorcinol compounds (**2g**, **3g** and **5g**), as observed in the reaction of ArsB with **4a** (Figure 4). In the reaction with **2a** and **3a**, the intermediate compounds (**2c** and **3c**) were simultaneously produced. ArsB also accepted sebacyl-diNAC (**1a**) as a substrate, but gave only an intermediate compound (**1c**) (Figure 4). In the reaction of ArsB with **1a**, only one of the two NAC groups in **1a** was converted into a resorcinol and the other NAC group was retained, probably because ArsB could not carry out the second reaction. ArsB was thus revealed to exhibit broad substrate specificity for alkyl-diNAC substrates. These results show that ArsB can synthesize bis-5-alkylresorcinol.

#### Reaction of other type III PKSs with alkanedioic acid NAC dithioesters

We assayed other resorcinol-producing type III PKSs, such as ARAS2 and ORAS, by using **4a** and malonyl-CoA as substrates. As expected, both enzymes synthesized **4g**, as observed in the reaction of ArsB (Figures 2c, d and 4). However, the production of **4g** by these enzymes was less effective than that by ArsB. This may be because of the production of by-products in significant amounts. The production of a by-product **4e** was observed in both reactions, as in the ArsB reaction. Moreover, the production of other by-products (**4d**, **4f** and **4h**) was detected. Peak **4d** was predicted to be a compound that possessed both a pyrone and a carboxyl group on the basis of LC-APCI/MS analysis. This carboxyl group may be produced by cleavage of the thioester bond between a carboxylic acid and NAC. Similarly, peak **4f** was predicted to be a compound that possessed both a resorcinol and a carboxyl group. Peak **4h** was predicted to be a compound that possessed both a resorcinol and a 2'-oxoresorcinol group on the basis of LC-APCI/MS analysis. ArsB almost completely produces alkylresorcinols from long-chain acyl substrate,<sup>3</sup> whereas ARAS2 and ORAS produce significant amounts of alkylpyrones, in addition to alkylresorcylic acids and alkylresorcinols.<sup>5</sup> This property of ARAS2 and ORAS may cause a low productivity of **4g** and a

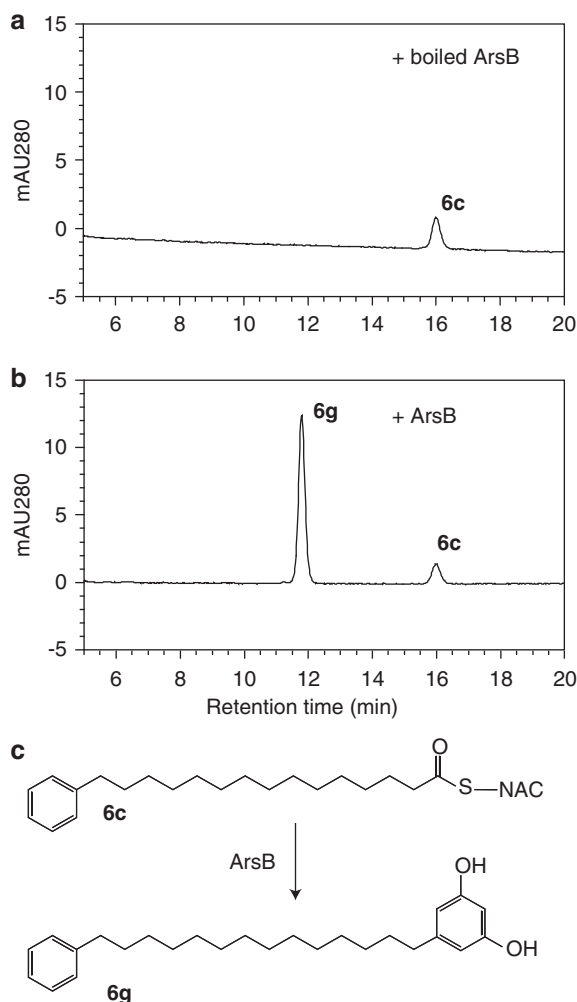


**Figure 3** HPLC chromatograms of *in vitro* reactions of ArsB with **6c** and malonyl-CoA. The reaction mixture contained boiled ArsB as a negative control (**a**) and ArsB (**b**). The conversion of **6c** to **6g** catalyzed by ArsB is shown (**c**).

by-product production in significant amounts. ARAS2 and ORAS were shown to produce alkylresorcylic acid from acyl-CoA.<sup>5</sup> This fact permits us to speculate that ARAS2 and ORAS also synthesize resorcylic acid compounds as a direct product in this reaction. However, we could detect no resorcylic acid compound. This may be caused by the low productivity. Almost all of the resorcylic compounds produced by ARAS2 and ORAS in this reaction might have been converted into resorcinol compounds by non-enzymatic decarboxylation before the accumulation of resorcylic compounds. ARAS2 and ORAS also accepted **2a**, **3a** and **5a** as a substrate and gave bis-5-alkylresorcinol compounds (**2g**, **3g** and **5g**) (data not shown). This substrate specificity is similar to that of ArsB. In addition, ARAS2 and ORAS accepted **6c** as a substrate. When they were incubated with **6c** and malonyl-CoA, **6g** was mainly produced, although a by-product possessing a pyrone moiety was also produced (data not shown). This shows that ARAS2 and ORAS, similar to ArsB, can accept an acyl thioester harboring an aromatic ring as a substrate. These results show that ARAS2, a plant enzyme, and ORAS, a fungal enzyme, can synthesize bis-5-alkylresorcinol, as does ArsB, a bacterial enzyme.

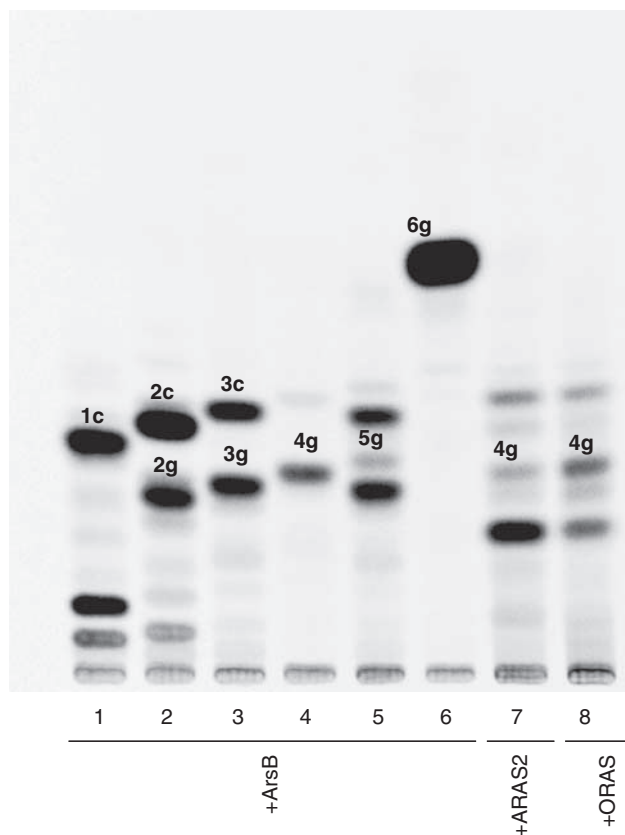


**Figure 4** Radio-TLC analysis of products synthesized by type III polyketide synthases (PKSs) from various starter substrates and malonyl-CoA. The type III PKSs used were ArsB (lanes 1–6), ARAS2 (lane 7) and ORAS (lane 8). The starter substrates used were **1a** (lane 1), **2a** (lane 2), **3a** (lane 3), **4a** (lanes 4, 7 and 8), **5a** (lane 5) and **6c** (lane 6).

## DISCUSSION

No type III PKS reactions against long-chain acyl thioesters harboring a bulkier substituent moiety at the alkyl tail have been reported. Our present data suggest that alkylresorcinol-producing type III PKSs can generally accept such unusual acyl thioesters as starter substrates. The crystal structures of type III PKSs revealed that some type III PKSs have an acyl-binding tunnel that accommodates a long acyl chain, extending from the active site to the surface of the protein.<sup>15,16</sup> On the other hand, other type III PKSs such as chalcone synthases have no acyl-binding tunnel. The acyl-binding tunnel may be characteristic of all type III PKSs that use a long-chain acyl-CoA ester as a starter substrate. However, this tunnel seems to be too narrow for acyl substrates possessing bulkier substituents to accommodate whole molecules because of steric hindrance. This conflicts with our result that three type III PKSs could accept such acyl substrates. How do they accept such unusual acyl substrates? One speculation is that the alkyl chain of substrates bound in the acyl-binding tunnel is long enough to penetrate into the surface of the protein and the bulky aromatic group extrudes outside of the protein. However, this speculation can probably not be applied to type III PKSs. For example, ORAS perfectly envelopes an entire molecule of eicosanoic acid in its acyl-binding tunnel and the hydrocarbon tail of eicosanoic acid does not reach the surface of ORAS, as revealed by the X-ray crystallography of an ORAS–eicosanoic acid complex.<sup>16</sup> PKS18 was also reported to hold a myristic acid molecule perfectly in its acyl-binding tunnel.<sup>17</sup> Thus,

the alkyl chain of substrate must be accommodated in the tunnel and must not penetrate into the surface of type III PKS.

Another speculation is that, during the reaction, some type III PKSs change the conformation of their acyl-binding tunnel so as to accommodate aromatic moiety. This hypothesis is supported by the crystal structures of ORAS. ORAS was reported to rearrange its conformation to accommodate eicosanoic acid into the acyl-binding tunnel on the basis of a comparison of the structures of the unliganded ORAS and an ORAS–eicosanoic acid complex.<sup>16</sup> Some type III PKSs may thus acquire broad substrate specificity owing to the flexibility of the acyl-binding tunnel region. A short-chain acyl substrate **1a** was not converted into bis-5-alkylresorcinol, although mono-alkylresorcinol intermediate **1c** was produced. This observation suggests that type III PKSs cannot accommodate the aromatic ring attached to short-chain acyl intermediates, such as **1c**, in the acyl-binding tunnel.

Given that some type III PKSs, including a plant type III PKS, ARAS2, can synthesize bis-5-alkylresorcinols, we suppose that plants use a type III PKS for their biosynthesis. However, no type III PKS enzymes involved in the biosynthesis of bis-5-alkylresorcinol in plants have been isolated or predicted. The rye was reported to contain two type III PKS genes.<sup>17</sup> These type III PKSs might be involved in the biosynthesis of bis-5-alkylresorcinols, although they are rather similar to chalcone synthases but not to alkylresorcinol-producing-type PKSs. We assume that alkylresorcinol-producing-type PKSs are involved in their biosynthesis in the rye plant, although they have not yet been identified.

In addition, the other part of the biosynthesis of bis-5-alkylresorcinol remains unclear. At least two enzymes, an oxidase and a CoA-ligase, are presumably necessary for the biosynthesis of bis-5-alkylresorcinol, other than the PKS reaction. One or more oxidases may have a function in the conversion of the methyl group at the alkyl tail into a carboxyl group, and CoA-ligase may have a function in the ligation of CoA to the resultant carboxyl group. A number of possible bis-5-alkylresorcinol biosynthetic pathways including these enzymes are illustrated in Figure 1b. The most possible pathway is that bis-5-alkylresorcinols are synthesized by alkylresorcinols, which are known to be distributed widely in plants.<sup>2</sup> In this pathway, alkylresorcinols are first produced from acyl-CoAs. Next, the  $\omega$ -carbon of the alkyl chain of alkylresorcinols is oxidized, and the CoA is attached to the newly formed carboxyl group. Finally the resultant unusual acyl-CoA esters are converted into bis-5-alkylresorcinols by a type III PKS. The reaction in the final step is supported by our *in vitro* study that type III PKSs accepted unusual acyl thioesters as a substrate. Our present findings show that a type III PKS can produce a wide variety of bis-5-alkylresorcinol, the alkyl chain lengths of which are over C10. However, the alkyl chain lengths of bis-5-alkylresorcinols isolated from plants are limited to over C14. The step of producing substrates for

type III PKSs may be controlled by the substrate specificity of the putative oxidase and CoA-ligase. Bis-5-alkylresorcinol has not been isolated from bacteria, fungi and rice plant. This may be caused by the lack of oxidase and ligase involved in the biosynthesis of bis-5-alkylresorcinol in those organisms. Although further analysis is absolutely necessary to elucidate the biosynthetic pathway of bis-5-alkylresorcinol in plants, we believe that a type III PKS is responsible for the final step in which it converts acyl-CoA esters into bis-5-alkylresorcinols.

## ACKNOWLEDGEMENTS

This work was supported by a research grant from the New Energy and Industrial Technology Development Organization of Japan and a Grant-in-Aid for Scientific Research on Priority Area 'Applied Genomics' from Monkasho.

- 1 Austin, M. B. & Noel, J. P. The chalcone synthase superfamily of type III polyketide synthases. *Nat. Prod. Rep.* **20**, 79–110 (2003).
- 2 Kozubek, A. & Tyman, J. H. Resorcinolic lipids, the natural non-isoprenoid phenolic amphiphiles and their biological activity. *Chem. Rev.* **99**, 1–26 (1999).
- 3 Funa, N., Ozawa, H., Hirata, A. & Horinouchi, S. Phenolic lipid synthesis by type III polyketide synthases is essential for cyst formation in *Azotobacter vinelandii*. *Proc. Natl. Acad. Sci. USA* **103**, 6356–6361 (2006).
- 4 Miyanaga, A., Funa, N., Awakawa, T. & Horinouchi, S. Direct transfer of starter substrates from type I fatty acid synthase to type III polyketide synthases in phenolic lipid synthesis. *Proc. Natl. Acad. Sci. USA* **105**, 871–876 (2008).
- 5 Funa, N., Awakawa, T. & Horinouchi, S. Pentaketide resorcylic acid synthesis by type III polyketide synthase from *Neurospora crassa*. *J. Biol. Chem.* **282**, 14476–14481 (2007).
- 6 Funabashi, M., Funa, N. & Horinouchi, S. Phenolic lipids synthesized by type III polyketide synthase confer penicillin resistance on *Streptomyces griseus*. *J. Biol. Chem.* **283**, 13983–13991 (2008).
- 7 Lytollis, W. *et al.* 5-Alkylresorcinols from *Hakea trifurcata* that cleave DNA. *J. Am. Chem. Soc.* **117**, 12683–12690 (1995).
- 8 Chaturvedula, V. S. *et al.* New cytotoxic bis-5-alkylresorcinol derivatives from the leaves of *Oncostemon bojerianum* from the Madagascar rainforest. *J. Nat. Prod.* **65**, 1627–1632 (2002).
- 9 Deng, J. Z., Starck, S. R. & Hecht, S. M. Bis-5-alkylresorcinols from *Panopsis rubescens* that inhibit DNA polymerase  $\beta$ . *J. Nat. Prod.* **62**, 477–480 (1999).
- 10 Suzuki, Y., Esumi, Y. & Yamaguchi, I. Structures of 5-alkylresorcinol-related analogues in rye. *Phytochemistry* **52**, 281–289 (1999).
- 11 Starck, S. R., Deng, J. Z. & Hecht, S. M. Naturally occurring alkylresorcinols that mediate DNA damage and inhibit its repair. *Biochemistry* **39**, 2413–2419 (2000).
- 12 Fürstner, A. & Seidel, G. Shortcut syntheses of naturally occurring 5-alkylresorcinols with DNA-cleaving properties. *J. Org. Chem.* **62**, 2332–2336 (1997).
- 13 Gilbert, I. H. *et al.* Synthesis of  $\beta$ -keto and  $\alpha,\beta$ -unsaturated *N*-acetylcysteamine thioesters. *Bioorg. Med. Chem. Lett.* **5**, 1587–1590 (1995).
- 14 Katsuyama, Y., Matsuzawa, M., Funa, N. & Horinouchi, S. *In vitro* synthesis of curcuminoids by type III polyketide synthase from *Oryza sativa*. *J. Biol. Chem.* **282**, 37702–37709 (2007).
- 15 Sankaranarayanan, R. *et al.* A novel tunnel in mycobacterial type III polyketide synthase reveals the structural basis for generating diverse metabolites. *Nat. Struct. Mol. Biol.* **11**, 894–900 (2004).
- 16 Rubin-Pitel, S. B. *et al.* Distinct structural elements dictate the specificity of the type III pentaketide synthase from *Neurospora crassa*. *Chem. Biol.* **15**, 1079–1090 (2008).
- 17 Haussühl, K., Rohde, W. & Weissenböck, G. Expression of chalcone synthase genes in coleoptiles and primary leaves of *Secale cereale* L. after induction by UV radiation: evidence for a UV-protective role of the coleoptile. *Bot. Acta.* **109**, 229–238 (1996).

## ORIGINAL ARTICLE

# Evaluation of solid (disc diffusion)- and liquid (turbidity)-phase antibiogram methods for clinical isolates of diarrheagenic *E. coli* and correlation with efflux

Alagiachidambaram Alagumaruthanayagam<sup>1</sup>, Asalapuram R Pavankumar<sup>1</sup>, Thangammal K Vasanthamallika<sup>2,3</sup> and Krishnan Sankaran<sup>1</sup>

Multiple drug resistance (MDR) in bacteria causes higher mortality and morbidity, complicates treatment and increases health-care outlay. With no new-generation antibiotics in sight, its rapid spread through the environment poses grave danger. Therefore, rapid detection to identify effective antibiotics and to prevent their indiscriminate use is imperative. However, the widely used clinical method for antibiogram, the Kirby–Bauer disc-diffusion method (DDM), requires 2–3 days, has inherent shortcomings of solid-phase assays and is not suitable for high-throughput operations. In our research on MDR associated with childhood diarrhea, we determined the antibiogram of 73 clinical diarrheagenic *Escherichia coli* strains using both the DDM and the more reliable liquid turbidity method (LTM) performed in 96-microwell plates. The results were further correlated with a dye-exclusion efflux assay using fluorescein diacetate. Although LTM is apparently superior in saving critical time, suitability to high-throughput operations and reliability, we found that the serious shortcomings of DDM could be effectively countered by just doubling the dosage of antibiotics currently used in discs or by using two discs in place of one. With 48 of the 49 MDR strains being positive for efflux and the 12 strains ‘susceptible’ to all the antibiotics being negative, the efflux assay could be useful as an integral component of the antibiogram test or for additional confirmation. The presence of 65% of MDR strains among diarrheagenic *E. coli* is a matter of serious concern, although most of them could be treated with either Gentamycin or Amikacin, as is the practice by experience.

*The Journal of Antibiotics* (2009) 62, 377–384; doi:10.1038/ja.2009.45

**Keywords:** antibiogram; antibiotics; efflux; fluorescence; Kirby–Bauer disc-diffusion method; liquid turbidity method; multidrug-resistant *E. coli*.

## INTRODUCTION

Multiple drug resistance (MDR) in bacteria is increasingly and widely reported. Even common pathogens such as *Salmonella* spp. are developing resistance to multiple antibiotics and are complicating treatment procedures.<sup>1</sup> Globally, the morbidity and mortality rates due to MDR in bacteria affect billions of people, and the expenditure incurred exceeds \$19 billion in the United States and the United Kingdom annually.<sup>2</sup> It contributes to 10–31% of mortality in hospitals.<sup>3</sup>

Antibiotic resistance is caused by enzymatic inactivation (for example,  $\beta$ -lactamases), or by the mutation of target (for example, gyrases) or by active efflux,<sup>4–6</sup> which is an important diagnostic target providing nonspecific resistance to multiple antibiotics.<sup>7</sup> Genetic transfer of resistance among microbes in the environment<sup>8,9</sup> calls for the prudent use of antibiotics<sup>10</sup> with reliable antibiograms. In

spite of limitations, such as formation of concentration gradients in solid-phase assays and the delay of 2–3 days for obtaining results, the Kirby–Bauer disc-diffusion method (DDM) is the only widely used clinical method. Other techniques such as colorimetric, fluorimetric or flow cytometric methods and PCR are unsuitable because of cost, labor or skill.<sup>11</sup> Such limitations force clinicians to select improper antibiotics for early diagnosis and treatment. In this regard, the microculture method that is performed routinely in 96-well plates for screening microbes and their metabolites is more appealing.

In our study on childhood diarrheagenic pathogens, it is observed that MDR strains are normally associated with severe cases, and we are concerned about the loss of critical time in selecting effective antibiotics.

<sup>1</sup>Centre for Biotechnology, Anna University, Chennai, Tamilnadu, India and <sup>2</sup>Department of Pediatrics, Institute of Child Health and Hospital for Children, Chennai, Tamilnadu, India

<sup>3</sup>Current address: Division of Pediatrics, Madras Medical Mission, Chennai, Tamilnadu, India

Correspondence: Professor K Sankaran, Centre for Biotechnology, Anna University, Sardar Patel Road, Chennai 600025, Tamilnadu, India.

E mails: ksankran@yahoo.com or ksankran@annauniv.edu

Received 2 April 2009; revised 19 May 2009; accepted 21 May 2009

**Table 1** Antibiotics used and their respective doses

Antibiotics	Kirby–Bauer disc-diffusion method (dose in µg)	Liquid turbidity method (dose in µg)
Amikacin	30/60 <sup>a</sup>	2
Gentamycin	10/20 <sup>a</sup>	2
Kanamycin	30/60 <sup>a</sup>	6
Nalidixic acid	30	3
Ampicillin	10	20
Ceftazidime	30/60 <sup>a</sup>	2/4 <sup>a</sup>
Cephotaxime	30/60 <sup>a</sup>	4/8 <sup>a</sup>

<sup>a</sup>Double the dose used for investigation—see Results and Discussion sections.

In particular *Escherichia coli*, an emerging pathogen with a variety of virulent attributes, contributes to 20–30% of childhood mortality globally.<sup>12,13</sup> In this study, we determined the antibiograms (against commonly prescribed antibiotics for diarrhea) of 73 clinical isolates of *E. coli* using both DDM and the microplate-based liquid turbidity method (LTM). This comparative study is also meant to address the limitations of DDM over LTM and find possible simple solutions to enhance its reliability. Correlation of the MDR phenotype with the efflux of fluorescein diacetate (FDA) in line with their known association was carried out to probe the utility of efflux assays in the early detection of MDR. This study has provided a reliable estimate of MDR among childhood diarrheagenic *E. coli*, which is an important emerging pathogen.

## MATERIALS AND METHODS

### Instruments and standard procedure used

OD of bacterial cultures was measured using Multiscan (Thermo Bioanalysis Company, LabSystems Oy, Vantee, Finland). Intensity of fluorescence was measured in the form of relative fluorescence units (RFUs) using Fluroscan (Thermo Bioanalysis Company). Drug susceptibility was determined using the Kirby–Bauer DDM by measuring the zone of clearance.

The selected antibiotics comprised three groups, namely aminoglycosides (Amikacin, Kanamycin and Gentamycin); penicillins (Ceftazidime, Cephotaxime and Ampicillin) and quinolones (Nalidixic acid). The antibiotic-impregnated discs with a uniform disc diameter of 8 mm for DDM were procured from Himedia Laboratories (Mumbai, Maharashtra, India). Antibiotics used in LTM were procured from the following different indigenous suppliers: Amikacin (Aristo Pharma, Mumbai, India), Gentamycin (Fulford Pharma, Mumbai, India), Kanamycin (Macleods Pharma, Mumbai, India), Ampicillin (Ranbaxy Pharma, Gurgaon, India), Cephotaxime (Lupin Labs, Mumbai, India), Ceftazidime (GlaxoSmithKline, Mumbai, India) and Nalidixic acid (Ranbaxy Pharma). The doses of different antibiotics in LTM were calculated according to the following formula<sup>14</sup>

$$W = (1000/P) * V * C$$

where *W* is the weight of antibiotic to be dissolved in *V*, the volume required; *P*, potency of the antibiotic base; and *C*, final concentration of solution. Table 1 represents the final doses of antibiotics used in both the methods. Half-lives of all antibiotics except Nalidixic acid (6 h) and Cephotaxime (0.9 h) are in the range of 2–3 h. FDA (Molecular Probes, Invitrogen, Eugene, OR, USA) was used to detect efflux activity.

### Collection and identification of clinical diarrheagenic *E. coli* isolates

*Escherichia coli* strains were isolated from stool samples of children, who were hospitalized because of acute or persistent diarrhea at the Institute of Child Health and Hospital for Children (ICH and HC, Chennai, Tamilnadu, India). *E. coli* strains were identified by conducting standard biochemical tests such as IMViC (Indole, Methyl Red, Voges-Proskauer and Citrate)<sup>15</sup> and were confirmed by PCR.<sup>16</sup>

### Preparation of Luria Bertani broth and Mueller–Hinton agar plates

Luria Bertani (LB) broth and Mueller–Hinton agar (MHA, Himedia) plates were used to perform antibiograms of LTM and DDM, respectively. LB was prepared by dissolving 10 g of Tryptone (Himedia), 5 g of yeast extract (Himedia) and 10 g of sodium chloride (Merck, Mumbai, India) in one liter of distilled water, and the pH was adjusted to 7.2 with 1 M sodium hydroxide (Merck). MHA plates were prepared by dissolving 38 g of MHA in one liter of distilled water, sterilized and cooled to ~45 °C, and 20 ml of the molten agar was poured into pre-sterilized petri plates. The plates were checked for sterility by incubating them at 37 °C for 6–7 h before experimentation.<sup>14,17</sup>

### Kirby–Bauer DDM

Approximately 10<sup>8</sup> cells (1 OD corresponding to 10<sup>9</sup> cells/ml<sup>8</sup>) of *E. coli* were spread-plated on the above-prepared MHA plates. Antibiotic discs were placed in duplicates and incubated at 37 °C for 16–18 h for zone formation. Zones of inhibition measured as mean diameter were categorized as ‘susceptible’ (S), ‘intermediary’ (I) and ‘resistant’ (R) according to Clinical and Laboratory Standards Institute (CLSI) standards.<sup>19</sup> DDM with double the dose of antibiotic concentration was performed by stacking two discs (instead of one) on MHA plates. We resorted to increase the doses of the antibiotics retaining the same CLSI standards for the zone of clearance.

### Liquid turbidity method

Approximately 10<sup>5</sup> cells were cultured by shaking at 170 r.p.m. at 37 °C in 200 µl of LB with calculated amounts of antibiotics (in duplicates) contained in each well of a 96-well microtiter plate (Laxbro Bio-Medical Aids, Pune, India) (Table 1). The turbidity measured at hourly time intervals for 8 h was plotted and compared with control (without antibiotic). On the basis of OD at 595 nm (measured using Multiscan, Thermo Bioanalysis Company), the strains were categorized with respect to their susceptibility as ≤0.05, ‘susceptible;’ 0.05–0.15, ‘intermediate;’ ≥0.15, ‘resistant.’ Figure 1 shows the distinct growth pattern for the ‘resistant’ and ‘intermediate’ types for a set of representative strains. The clinical isolates found ‘resistant’ to three or more antibiotics were scored as MDR phenotypes.<sup>14</sup>

### Detection of efflux using FDA

Fluorescein diacetate is a known marker used to study bacterial viability.<sup>20,21</sup> The dye was added to the medium at a concentration of 50 µM just 30 min before harvesting the cells, to avoid interference due to a spontaneous hydrolysis of the dye by the medium.<sup>22</sup> Viable ‘resistant’ bacteria are able to convert the passively transported dye from non-fluorescent form (FDA) to its charged acid form, fluorescein, and efflux it actively using a pump mechanism. Therefore, fluorescence in the medium indicates the operation of efflux mechanism and hence viability. Fluorescence in the spent medium obtained after centrifugation (6000 g, 1 min) was measured using a fluorimeter (Fluroscan, Thermo Bioanalysis Company) in a microtiter plate<sup>23</sup> and then correlated with the antibiogram results of LTM.

## RESULTS

For a clinically relevant investigation, the efficacy of the popular clinical antibiogram method (DDM) was compared with that of the turbidity measurement method (normally used in research) among drug-resistant diarrheagenic *E. coli*, which is an emerging threat in pediatric care. This knowledge could be useful in the management of pediatric diarrhea due to MDR strains. Among the 73 strains used in this study, 69 were isolated from children with persistent diarrhea, 3 strains (*E. coli* A5, *E. coli* B5 and *E. coli* C2) were reference strains and 1 was the laboratory strain *E. coli* (DH5α).

### Lack of correlation in antibiogram results between DDM and LTM

The degree of antibiotic susceptibility of these isolates to the first-line antibiotics was determined using both DDM and LTM and scored as ‘susceptible,’ ‘intermediate’ and ‘resistant’ (Table 2). A fair correlation between the two methods can be observed in all ‘S’ and ‘R’ categories

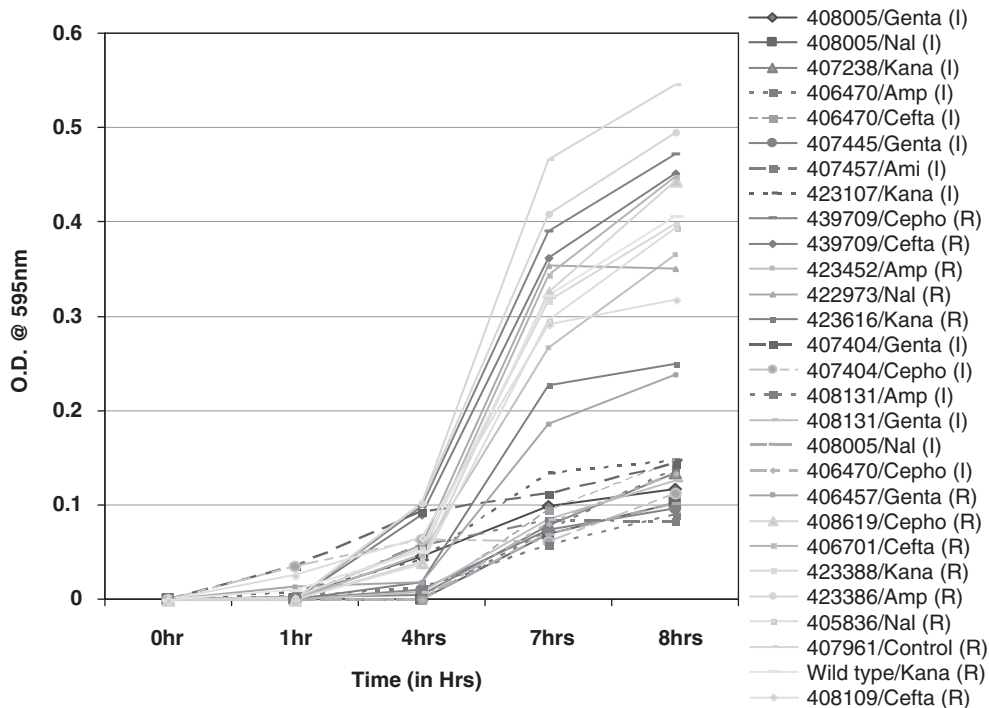


**Figure 1** The graph shows a distinct difference in growth between 'Intermediates' (O.D. 0.05–0.15) and 'Resistant' ( $\geq 0.15$ ) strains.

of Nalidixic acid, Amikacin and Ceftazidime; in particular, the last-mentioned drug showed the best correlation; The 'intermediary' in these cases were correlating poorly, probably because of the subjectivity in manual measurement in DDM. Generally, DDM tended to score less 'S' types compared with LTM. In contrast, the 'R' types were present more in DDM and less in LTM. DDM scored more 'intermediary' for Amikacin, Kanamycin and Cephotoxime, and less for others, in comparison with LTM.

The number of strains identified by DDM as 'susceptible' to Ampicillin, Ceftazidime and Cephotoxime, all belonging to the same penicillin group was quite variable, and in the 'intermediary' category, the number was particularly high for Cephotoxime. LTM, on the other hand, showed similar numbers for the whole group in all the categories. A better correlation was observed between both the methods only in the 'R' category. In the group of aminoglycosidic antibiotics, only six strains, in the case of Kanamycin, and nearly half of the strains in the case of Amikacin and Gentamycin were found to be 'susceptible' by DDM, whereas LTM showed uniformly high scores (80–90%) in this category. DDM scored about a third of the strains to be 'resistant,' whereas, in contrast, either none or only a few were scored by LTM. To rule out the possibility that the quality of commercial antibiotic disc could affect the results, we even used homemade discs that contained the specified amount of antibiotics from the same stock used for LTM. We did not find any significant difference in the results (data not shown).

#### Physicochemical and stability factors of antibiotics affect DDM results

To account for the above-mentioned contrasting behavior and to identify a better method, especially in view of the limitations of solid-phase assays compared with liquid-phase assays, we have compiled in Table 3 various properties of the antibiotics<sup>24,25</sup> that could plausibly affect the zone of clearance in DDM. The contrasting 'S' scores in the case of Kanamycin by DDM (6/73) and LTM (63/73) could be

**Table 2 Antibiotic susceptibility: comparison of disc-diffusion method (DDM) and liquid turbidity method (LTM)**

Susceptibility Antibiotics	S (Nos.)		I (Nos.)		R (Nos.)	
	DDM	LTM	DDM	LTM	DDM	LTM
Amikacin	35	72	18	01	20	00
Gentamycin	39	60	08	11	26	02
Kanamycin	06	63	35	03	32	07
Nalidixic acid	10	14	04	10	59	49
Ampicillin	14	22	04	10	55	41
Ceftazidime	30	25	03	12	40	36
Cephotoxime	08	32	25	10	40	31

Abbreviations: I, intermediate; R, resistance; S, Susceptible.  
Nos. represents the number of strains.

attributed to the higher minimal inhibitory concentration ratios (MIC) ( $8 \mu\text{g ml}^{-1}$ ) of the antibiotic requiring higher concentrations in the killing zone. Hence, most of the strains would have been distributed either as 'I' or 'R' in DDM. In another instance, it is well known that DH5 $\alpha$  is 'susceptible' to all antibiotics other than Nalidixic acid, but the zone of clearance for Ceftazidime under our experimental condition was found to be 14 mm, indicating that it was 'resistant.' This anomaly may be attributable to its higher molecular weight (637) and sparingly soluble nature, both limiting drug diffusion. Instead of adjusting for all these complex factors that affect the antibiotic availability to form proper zones of clearance, we resorted to increasing the doses of the antibiotics retaining the same CLSI standards for the zone of clearance.

As can be seen in Table 4, doubling the dose by stacking two discs increased the number of strains 'susceptible' to aminoglycosides. All the 73 strains were now found to be 'susceptible' to Amikacin compared with 35 originally; 69 were 'susceptible' for Gentamycin compared with 39 before. For Kanamycin, the numbers increased

**Table 3** Properties of different antibiotics that could influence antibiogram

Properties Antibiotics	Molecular formula	Molecular weight	Solubility in water	MIC (in $\mu\text{g ml}^{-1}$ )	Observed zone of clearance for DH5 $\alpha$ (in mm)	Half-life (in hours)	Factors influencing the zone of clearance
Amikacin	C <sub>22</sub> H <sub>43</sub> N <sub>5</sub> O <sub>13</sub>	781.75	Freely soluble	10	19	2-3	Higher molecular weight, high solubility, high MIC
Gentamycin	C <sub>21</sub> H <sub>43</sub> N <sub>5</sub> O <sub>7</sub>	477	Freely soluble	1	20	2-3	High solubility, low MIC
Kanamycin	C <sub>18</sub> H <sub>36</sub> N <sub>4</sub> O <sub>11</sub>	484	Freely soluble	8	23	2-4	High solubility, moderate MIC
Nalidixic acid	C <sub>12</sub> H <sub>12</sub> N <sub>2</sub> O <sub>3</sub>	232.24	Sparingly soluble	5	11	6-7	Low molecular weight, low solubility, moderate MIC, higher half life
Ampicillin	C <sub>16</sub> H <sub>18</sub> N <sub>3</sub> O <sub>4</sub> S	371.39	Freely soluble	22	24	2	High solubility, high MIC
Ceftazidime	C <sub>22</sub> H <sub>22</sub> N <sub>6</sub> O <sub>7</sub> S <sub>2</sub>	636.65	Sparingly soluble	1	14	1.4-2	Higher molecular weight, low solubility, low MIC
Cephataxime	C <sub>16</sub> H <sub>16</sub> N <sub>6</sub> O <sub>7</sub> S <sub>2</sub>	477.44	Freely soluble	4	19	0.9-1.7	High solubility, low-moderate MIC, lower half-life

The MIC values are against Gram-negative bacteria, in general *E. coli* spp. and the reported half-life is the time of plasma elimination in humans. The values are adopted from British Pharmacopoeia<sup>24</sup> and United States Pharmacopoeia.<sup>25</sup>

from a mere 6 for a single dose to 50 with a corresponding shift from 'I' and 'R' phenotypes. In the case of Cephataxime of the cephalosporin group, doubling the dose brought many from the 'I' and 'R' categories into 'S' (from 8 to 49). This is perhaps justified by the labile nature of the drug with a lower half-life (Table 3) and therefore, the increased dose could have compensated the loss of potency. For the same reason, doubling the concentration of Cephataxime in LTM, drastically reduced the 'R' types (from 31 to 13) with a corresponding increase in 'I' (3) and 'S' (15) types. In the case of Ceftazidime, a related member in the group with better half-life, doubling the dose did not alter the numbers significantly. Among 36 'resistant' phenotypes only 4 turned out to be 'susceptible' and 2 were 'intermediate,' the rest remained as 'resistant' forms.

#### MDR phenotype detection by antibiogram methods and efflux matched well

A novel adaptation of bacteria to counter antibiotic pressure is in using an efflux pump to effectively throw out the antibiotic. In Table 5, the antibiogram of individual strains by both the methods (DDM and LTM modified for the dosage) and their efflux activity has been shown. The efflux activity, as indicated by the zero or low background RFU value, was clearly absent in 'susceptible' cases. However, the absolute RFU, did not clearly indicate the level of resistance, either 'I' or 'R'. There were cases of 'resistant' phenotypes with moderate RFU and 'intermediary' with high RFU. Without correlating the RFU quantities with 'I' or 'R' phenotypes, anything above the background level of fluorescence was considered efflux positive. Table 6 shows that several strains were 'resistant' to  $\geq 3$  antibiotics, the common two being Nalidixic acid and Ampicillin, normally avoided in the treatment of diarrhea.

There was a good correlation between the efflux and MDR phenotypes seen in LTM, as summarized in Table 6; 'intermediary' was also considered as 'resistant' for compilation. To detect the efflux in strains that were 'susceptible' to all antibiotics, we had to grow them in the absence of antibiotics and the strains were found to be efflux negative. The results of efflux and antibiogram reflect the documented association of efflux with MDR phenotypes. The fluorescence-based efflux detection could be a good addition to the tools for antibiogram. In total, 13 strains were found to be 'resistant' to only one or two antibiotics, mostly to Nalidixic acid and Ampicillin, but they were efflux positive. This perhaps indicates that the dye efflux might be occurring through a pump system not involved in antibiotic efflux.<sup>21-23</sup> The only case of MDR positive but efflux negative, as seen in strain 407457 (Table 5), could possibly contain an enzymatic degradation mechanism for  $\beta$ -lactamases with a broader specificity.<sup>4,5</sup>

**Table 4** Susceptible, intermediary and resistant types based on double the dose of antibiotics in DDM compared with the results of DDM single dose and LTM

Antibiotics	Double disc/single disc (LTM)		
	Susceptible (S)	Intermediate (I)	Resistant (R)
Amikacin	73/35 (72)	00/18 (01)	00/20 (00)
Gentamycin	69/39 (60)	03/08 (11)	01/26 (02)
Kanamycin	50/06 (63)	06/35 (03)	17/32 (07)
Ceftazidime	31/30 (29/25)	09/03 (14/12)	33/40 (30/36)
Cephataxime	49/08 (47/32)	18/25 (13/10)	06/40 (13/31)

Abbreviations: DDM, disc-diffusion method; LTM, liquid turbidity method. The values in parentheses show the score by LTM, which, in the case of Cephataxime and Ceftazidime, had double the antibiotic dose; the first number corresponds to double dose.

#### DISCUSSION

In current clinical practice in India, diarrhea, which is refractory to oral rehydration therapy, is treated using first-line antibiotics, such as cotrimoxazole, or cephalosporins, such as cephalexin, cefazolin and Nalidixic acid, in outpatients. Third-generation cephalosporins such as cefoperazone, Ceftazidime or cefixime are used to treat severe forms of diarrhea. More potent drugs such as cancomycin, methicillin, imipenem are used when diarrhea is associated with other systemic infections, according to the severity of disease.<sup>13</sup> In spite of the prevalence of MDR strains associated with various infectious diseases including diarrhea, there is no effective clinical tool other than the time-consuming DDM to quickly determine the antibiogram of a pathogen in order to initiate the correct antibiotic therapy or apply early course correction. A lack of correlation between antibiogram results of 73 strains obtained by DDM and LTM prompted us to take-up this study to evaluate superior methods, as it affects the efficacy of treatment. Furthermore, the saving of precious treatment time by adapting to quicker LTM compared with DDM, as well as inherent limitations of solid-phase assays compared with those of liquid-phase assays encouraged us to investigate the former for clinical utility. As the MDR phenotype is increasingly contributed by a broad-spectrum efflux mechanism, we have also incorporated an FDA-based viability assay in LTM for detecting efflux.

#### Double the antibiotic dose improves the performance of DDM

Overall, it was found that DDM was biased toward 'R' type and scored fewer 'S' types. This is perhaps attributable to various physicochemical properties<sup>24,25</sup> of these antibiotics such as molecular weight, water solubility, MIC, half-life etc., in determining the zone of clearance.



**Table 5** Compilation of the results of 73 *E. coli* strains with respect to the methods of determining antibiogram (DDM and LTM modified for the dosage)

Strain	Amikacin			Gentamycin			Kanamycin			Nalidixic acid			Ampicillin			Ceftazidime			Cephotaxime		
	DDM	LTM	Efflux in RFU	DDM	LTM	Efflux in RFU	DDM	LTM	Efflux in RFU	DDM	LTM	Efflux in RFU	DDM	LTM	Efflux in RFU	DDM	LTM	Efflux in RFU	DDM	LTM	Efflux in RFU
DH5 $\alpha$	S	S	12	S	S	15	S	S	12	R	R	165	S	S	10	S	S	0	S	S	12
A5	S	S	12	I	S	12	S	R	90	S	R	34	R	R	94	S	R	160	S	R	155
C2	S	S	7	S	S	4	S	S	12	R	R	99	R	R	98	S	S	32	S	S	6
LMA	S	S	8	S	S	5	S	S	6	R	R	27	S	S	10	S	S	13	S	S	1
406006	S	S	7	S	S	6	R	S	3	S	S	12	I	S	9	S	I	85	I	S	9
405964	S	S	0	I	I	26	R	I	47	R	I	67	R	R	47	S	S	1	I	S	0
407445	S	S	2	S	I	14	S	S	0	R	R	44	R	I	16	S	S	3	I	S	1
407457	S	I	0	S	I	12	R	I	0	R	R	7	R	I	16	S	I	4	I	I	2
407404	S	S	0	S	I	17	S	S	0	R	R	41	R	I	11	S	I	7	S	I	5
441067	S	S	0	S	S	0	S	S	0	R	S	4	R	S	2	S	S	2	S	S	0
408005	S	S	0	S	I	18	S	S	0	R	I	62	R	I	9	S	S	0	S	S	0
421132	S	S	0	S	I	0	I	S	0	R	R	47	R	R	41	I	S	32	S	R	28
439709	S	S	0	S	S	0	I	S	0	R	R	52	R	R	44	R	R	48	S	R	47
429624	S	S	0	S	S	0	S	S	0	R	R	55	R	R	36	R	R	41	S	R	34
407851	S	S	0	S	S	0	S	S	0	R	R	42	R	R	41	R	R	100	S	R	90
422061	S	S	0	S	S	0	S	S	0	R	R	58	S	S	0	I	S	0	I	S	0
407961	S	S	0	S	S	0	S	S	0	R	R	55	S	S	0	S	S	0	S	S	0
408131	S	S	0	S	I	0	S	S	0	R	I	59	I	S	11	S	S	0	S	S	0
423452	S	S	0	I	S	0	R	S	0	R	R	32	R	R	25	R	R	27	I	R	24
441144	S	S	0	S	S	0	R	S	0	R	R	33	R	R	18	I	S	21	I	R	17
408619	S	S	0	S	S	0	R	S	0	R	R	42	S	R	36	R	R	37	I	R	36
406964	S	S	0	S	S	0	S	S	0	R	S	23	S	S	4	I	S	7	S	S	2
406433	S	S	0	S	I	17	S	S	0	R	R	48	R	I	42	S	S	0	S	S	0
423793	S	S	0	S	S	0	S	S	0	R	R	62	S	I	5	S	I	7	S	I	0
408314	S	S	0	S	S	0	S	S	0	I	S	10	R	R	58	S	S	0	S	S	0
440835	S	S	0	S	S	0	R	S	0	R	I	45	R	R	30	R	R	29	S	R	30
406701	S	S	0	S	S	0	S	S	0	R	R	38	R	R	45	R	R	38	S	R	38
426749	S	S	0	S	S	0	S	S	3	R	S	12	S	S	6	S	S	3	S	S	5
422644	S	S	0	S	S	0	S	S	2	R	R	41	R	R	28	R	R	60	S	R	33
422790	S	S	0	S	S	0	S	S	0	R	R	68	R	R	18	R	I	22	I	R	12
422800	S	S	0	S	S	0	S	S	0	R	R	58	R	R	11	I	S	14	S	R	20
422861	S	S	0	S	S	0	S	S	0	R	R	49	R	R	18	R	R	26	S	R	19
422973	S	S	0	S	S	0	S	S	0	R	I	22	R	I	5	R	I	16	S	I	10
405836	S	S	0	S	I	45	S	S	0	R	R	84	R	R	64	R	I	20	S	R	22
404407	S	S	0	S	S	0	S	S	0	S	S	23	R	I	106	S	S	2	R	S	0
433983	S	S	0	S	R	17	I	S	3	R	R	79	R	R	89	R	R	87	S	R	86
407459	S	S	0	S	I	17	S	R	5	R	R	118	R	R	105	R	R	123	S	R	125
406470	S	S	0	S	S	0	S	I	0	I	R	35	R	I	8	R	I	11	I	I	6
408420	S	S	3	S	S	3	S	S	2	R	R	35	R	S	9	S	S	5	S	R	125
423107	S	S	0	S	S	0	S	I	24	R	R	77	S	S	5	S	S	0	S	I	6
423383	S	S	0	S	S	0	S	S	0	I	S	17	S	S	0	S	S	0	S	S	2
423386	S	S	0	S	I	22	I	S	2	R	R	80	R	R	74	R	R	77	R	S	0

Table 5 Continued

Strain	Amikacin			Gentamycin			Kanamycin			Nalidixic acid			Ampicillin			Ceftazidime			Cephotaxime		
	DDM	LTM	Efflux in RFU	DDM	LTM	Efflux in RFU	DDM	LTM	Efflux in RFU	DDM	LTM	Efflux in RFU	DDM	LTM	Efflux in RFU	DDM	LTM	Efflux in RFU	DDM	LTM	Efflux in RFU
423427	S	S	<b>2</b>	S	S	<b>3</b>	S	S	<b>17</b>	R	R	<b>61</b>	R	R	<b>46</b>	R	R	<b>132</b>	S	S	<b>0</b>
423354	S	S	<b>0</b>	S	S	<b>0</b>	S	S	<b>1</b>	R	R	<b>62</b>	R	R	<b>41</b>	R	R	<b>43</b>	R	R	<b>78</b>
423314	S	S	<b>2</b>	S	S	<b>0</b>	I	S	<b>5</b>	R	R	<b>46</b>	R	R	<b>45</b>	R	R	<b>39</b>	S	R	<b>38</b>
423587	S	S	<b>0</b>	S	S	<b>0</b>	R	S	<b>0</b>	R	R	<b>46</b>	R	R	<b>39</b>	R	R	<b>36</b>	S	R	<b>35</b>
423798	S	S	<b>0</b>	S	S	<b>0</b>	R	S	<b>1</b>	R	R	<b>40</b>	R	R	<b>34</b>	R	R	<b>38</b>	R	R	<b>30</b>
423616	S	S	<b>0</b>	S	S	<b>0</b>	S	R	<b>20</b>	R	R	<b>62</b>	S	S	<b>1</b>	S	S	<b>0</b>	R	R	<b>30</b>
402746	S	S	<b>0</b>	S	S	<b>2</b>	S	S	<b>0</b>	R	I	<b>67</b>	S	S	<b>5</b>	I	I	<b>132</b>	S	R	<b>30</b>
408027	S	S	<b>0</b>	S	S	<b>0</b>	S	S	<b>0</b>	S	S	<b>12</b>	I	S	<b>1</b>	S	S	<b>5</b>	S	S	<b>0</b>
408109	S	S	<b>0</b>	S	S	<b>0</b>	S	S	<b>0</b>	R	R	<b>62</b>	R	R	<b>41</b>	R	R	<b>50</b>	S	S	<b>0</b>
423892	S	S	<b>7</b>	S	S	<b>8</b>	S	S	<b>5</b>	I	R	<b>130</b>	R	S	<b>12</b>	R	R	<b>343</b>	S	S	<b>2</b>
423864	S	S	<b>0</b>	S	S	<b>0</b>	R	S	<b>0</b>	S	S	<b>15</b>	S	S	<b>0</b>	S	S	<b>2</b>	I	R	<b>43</b>
423394	S	S	<b>10</b>	S	S	<b>8</b>	S	S	<b>13</b>	I	R	<b>108</b>	R	S	<b>12</b>	R	R	<b>354</b>	S	S	<b>35</b>
408619	S	S	<b>0</b>	S	S	<b>0</b>	S	S	<b>0</b>	S	S	<b>7</b>	I	S	<b>3</b>	S	S	<b>7</b>	S	S	<b>0</b>
406319	S	S	<b>0</b>	S	S	<b>0</b>	S	S	<b>0</b>	R	I	<b>12</b>	R	I	<b>5</b>	R	R	<b>269</b>	S	S	<b>32</b>
423212	S	S	<b>0</b>	S	S	<b>0</b>	S	S	<b>0</b>	R	I	<b>19</b>	R	R	<b>20</b>	R	R	<b>20</b>	S	S	<b>5</b>
423383	S	S	<b>0</b>	S	S	<b>0</b>	I	S	<b>0</b>	S	S	<b>13</b>	S	S	<b>0</b>	S	S	<b>0</b>	S	I	<b>4</b>
423396	S	S	<b>0</b>	S	S	<b>0</b>	S	S	<b>0</b>	S	S	<b>14</b>	S	S	<b>0</b>	S	S	<b>0</b>	S	S	<b>0</b>
423402	S	S	<b>0</b>	S	S	<b>0</b>	S	S	<b>0</b>	R	R	<b>58</b>	R	S	<b>2</b>	I	S	<b>0</b>	S	S	<b>0</b>
407238	S	S	<b>0</b>	S	S	<b>3</b>	R	I	<b>5</b>	R	R	<b>37</b>	R	R	<b>50</b>	R	R	<b>60</b>	I	S	<b>0</b>
406012	S	S	<b>0</b>	S	S	<b>0</b>	S	S	<b>0</b>	R	R	<b>44</b>	R	R	<b>35</b>	R	R	<b>42</b>	I	S	<b>0</b>
407783	S	S	<b>0</b>	S	S	<b>0</b>	S	S	<b>0</b>	R	R	<b>62</b>	R	R	<b>25</b>	R	R	<b>33</b>	S	R	<b>13</b>
408109	S	S	<b>0</b>	R	S	<b>0</b>	R	S	<b>0</b>	R	R	<b>50</b>	R	R	<b>28</b>	R	R	<b>35</b>	I	R	<b>39</b>
407998	S	S	<b>0</b>	S	S	<b>0</b>	R	S	<b>0</b>	R	R	<b>44</b>	R	R	<b>28</b>	R	R	<b>38</b>	S	R	<b>28</b>
423388	S	S	<b>0</b>	S	S	<b>0</b>	S	R	<b>25</b>	R	S	<b>10</b>	R	R	<b>32</b>	S	S	<b>9</b>	S	R	<b>17</b>
433864	S	S	<b>0</b>	S	S	<b>0</b>	S	S	<b>1</b>	R	R	<b>10</b>	R	R	<b>22</b>	I	S	<b>20</b>	I	R	<b>35</b>
441220	S	S	<b>0</b>	S	S	<b>0</b>	S	R	<b>19</b>	R	I	<b>10</b>	R	R	<b>24</b>	I	I	<b>15</b>	S	S	<b>0</b>
406457	S	S	<b>0</b>	S	R	<b>14</b>	S	S	<b>0</b>	R	R	<b>32</b>	R	R	<b>28</b>	R	R	<b>38</b>	S	R	<b>25</b>
406484	S	S	<b>0</b>	S	S	<b>1</b>	S	S	<b>0</b>	R	I	<b>22</b>	R	S	<b>3</b>	R	I	<b>7</b>	S	I	<b>7</b>
EPEC1	S	S	<b>0</b>	S	S	<b>0</b>	R	R	<b>25</b>	S	S	<b>3</b>	R	R	<b>24</b>	S	S	<b>12</b>	R	R	<b>36</b>
EPEC2	S	S	<b>0</b>	S	S	<b>0</b>	I	R	<b>20</b>	S	S	<b>2</b>	R	R	<b>24</b>	S	S	<b>7</b>	I	S	<b>3</b>
403396	S	S	<b>9</b>	S	S	<b>7</b>	S	S	<b>14</b>	R	R	<b>82</b>	R	R	<b>90</b>	S	I	<b>92</b>	S	I	<b>83</b>

Abbreviations: DDM, disc-diffusion method; *E. coli*, *Escherichia coli*; LTM, liquid turbidity method. Bold values indicate effluxing ability of the bacteria.

**Table 6 Correlation between MDR and efflux**

Phenotype	MDR positive		MDR-negative/efflux positive	
	Efflux positive	Efflux negative	All susceptible	Resistant to any one or two antibiotics
LTM/efflux	49/48	49/1	12/12	12/12

LTM, liquid turbidity method.

MDR positive—resistant to three or more antibiotics in LTM; Efflux positive—relative fluorescence unit (RFU) &gt; 15.

For different antibiotics, the zone of clearance for 'R' ranges from 12 to 14 mm across the disc. This leaves only 2–3 mm annular width in the clearance zone and, at this lower scale, the errors in reading could be very high, especially given the smallest reading in a ruler to be 1 mm. Fairly uniform cutoff of 12–14 mm for different antibiotics used in this study seems to be artifactual, given the wide variations in solubility (from being freely soluble to sparingly soluble), molecular size (232–760) and MIC (1–22).<sup>24,25</sup> Although MHA is popular for DDM, parameters such as pH (that influences the potency of antibiotics such as aminoglycosides, quinolones, tetracyclines and macrolides), moisture content of the media, concentration of thymine or thymidine and variation in divalent cations have been reported to result in variable or unusual zone of clearances (in antibiotics such as aminoglycosides and tetracyclines) leading to false evaluations during laboratory screening.<sup>26</sup> In this regard, the LTM is superior, as antibiotics will be uniformly distributed and for the antibodies with a similar half-life, the MIC will truly reflect their efficacy. Modifications in the dosage for DDM may also be warranted because of the nature of clinical isolates, which, even though are *E. coli*, may have differently adapted to harsher conditions in the host and environment when compared with the laboratory strains used for determining the dosage on the disc. Our reasoning was substantiated by the fact that, when we doubled the antibiotic dose to counter the above limitations, we found that the results matched well with those obtained using LTM. Therefore, in the absence of an evaluation of the contributions of these interferences and the properties of antibiotics affecting the zone of clearance, instead of complicated optimization for DDM, the simple adaptation of using two discs or doubling the dose on a disc could be the easiest way to compensate for the anomalies.

#### Efflux assay coupled with LTM is a desirable diagnostic method

The adaptation of efflux by bacteria obviates the need to develop unique resistance mechanisms for individual antibiotics and facilitates resistance to group-specific or to a wide spectrum of antibiotics.<sup>6,7</sup> Therefore, the identification of even 'intermediary' types becomes important in choosing the right antibiotic. Certain subjectivity in the DDM could vitiate this estimate, as can be seen from this study. The capability of quantitative measurement using LTM provides a better handle to identify such 'intermediary' cases with increased confidence. To enhance the scope of such a possibility, we tested the use of a well-documented marker dye, FDA, to detect efflux phenotype during the determination of antibiogram.<sup>21,23</sup> Accordingly, the fluorescence resulting from the uptake of non-fluorescent FDA and efflux as fluorescein by viable and growing cells indicates efflux pump-dependent resistance. This observation correlated well with the antibiogram results obtained from the modified DDM and LTM methods.

#### Potential of LTM as a clinical tool for antibiogram determination

In conclusion, LTM, a potential tool for tackling diseases caused by MDR pathogens, can be performed within 7–8 h as against 2–3 days for DDM. It is also easily performed in 96-well microtiter plates,

routinely used in clinical practice and in MIC determination.<sup>19</sup> Inclusion of the efflux test by a convenient and established fluorescent method, as used in this study, will not only substantiate the MDR phenotype but will also indicate the mechanism involved. The occurrences of some false positives are possible, if the efflux pumps or efficiency for the dye and the drug are different. The LTM can be easily adopted in clinical laboratories, including peripheral hospitals. It is also economical from the view of labor, use of antibiotics and media, as well as waste generated. Being suitable for high-throughput format, it is highly compatible for instrumentation in surveillance and epidemiology. A significant outcome of this study is the fact that, in accordance with the recent observation and reports of clinicians, *E. coli* isolates were in fact 'resistant' to multiple antibiotics, especially to third-generation cephalosporins (~65%), but antibiotics such as Gentamycin and Amikacin are still effective.

#### ACKNOWLEDGEMENTS

We acknowledge Dr Jayanthi, Dr Saradha Suresh, Dr Md Meeran and Dr Umadevi of the Institute of Child Health and Hospital for Children (ICH and HC), Chennai, India for their support in sample collection and discussions. We thank Dr Rolf Reissbordt for contributing reference EPEC strains. We gratefully acknowledge the financial support from the Department of Science and Technology, India under their Technology Development Programme, UGC under DRS as well as the Centre with Potential for Excellence Programme and European Union-sponsored Each Child project.

- McCormick, J. B. Epidemiology of emerging/re-emerging antimicrobial-resistant bacterial pathogens. *Curr. Opin. Microb.* **1**, 125–129 (1998).
- US-FDA website: <http://www.fda.gov/oc/2008/antimicrobials> (13 December 2008, date last accessed).
- Giske, C. G., Dominique, L., Cars, M. O. & Carmeli, Y. Clinical and economic impact of common multidrug-resistant Gram-negative Bacilli. *Antimicrob. Agents Chemother.* **52**, 813–821 (2008).
- Bradford, P. A. Extended spectrum  $\beta$ -Lactamases in 21st century: characterization, epidemiology, and detection of this important resistance threat. *Clin. Microbiol. Rev.* **14**, 933–951 (2001).
- Nikaido, H. Multi-drug efflux in bacteria as a basis of resistance. *Abstr. Intersci. Conf. Antimicrob. Agents Chemother., Intersci. Conf. Antimicrob. Agents Chemother.* **39**, 26–29 (1999).
- Pitout, J. D. D., Nordmann, P., Laupland, K. B. & Poirel, L. Emergence of Enterobacteriaceae producing extended-spectrum  $\beta$ -lactamases (ESBLs) in the community. *J. Antimicrob. Chemother.* **56**, 52–59 (2005).
- Livermore, D. M. Bacterial resistance: origins, epidemiology, and impact. *Clin. Infect. Dis.* **36**, S11–S23 (2003).
- Burrus, V., Pavlovic, G., Decaris, B. & Guedon, G. Conjugative transposons: the tip of the iceberg. *Mol. Microbiol.* **46**, 601–610 (2002).
- McDermott, P. F., Walker, R. D. & White, D. G. Antimicrobials: modes of action and mechanisms of resistance. *Int. J. Toxicol.* **22**, 135–143 (2003).
- Travers, K. & Barza, M. Morbidity infections caused by antimicrobial resistant bacteria. *Clin. Infect. Dis.* **34**(Suppl. 3S), 131–134 (2002).
- Tellefson, L., Fedorka-Cray, P. J. & Angulo, F. J. Public health aspects of resistance monitoring in the USA. *Acta. Vet. Scand. Suppl.* **92**, 67–75 (1999).
- Pavankumar, A. R. & Sankaran, K. The need and new tools for surveillance of *Escherichia coli* pathogens. *Food Technol. Biotechnol.* **46**, 125–145 (2008).
- WHO Fact Sheet 2005. <http://www.oneworldhealth.org> (13 December 2008, date last accessed).

- 14 Mayer, R. M. & Koshi, G. *Manual of Diagnostic Procedures in Medical Microbiology and Immunology/Serology*, Revised edn 70–75 (Faculty, Christian Medical College and Hospital, Vellore, India, 2001).
- 15 James, G. C. & Natalie, S. *Microbiology, A Laboratory Manual*, 3rd edn (Benjamin/Cummings Publishing Company, Redwood City, CA, USA, 2005).
- 16 Kong, R. Y. C., So, C. L., Law, W. F. & Wu, R. S. S. A sensitive and versatile multiplex PCR system for rapid detection of enterotoxigenic, enterohaemorrhagic and enteropathogenic strains of *Escherichia coli*. *Mar. Pollut. Bull.* **38**, 1207–1215 (1999).
- 17 Lalitha, M. K. *et al.* E-test as an alternative to conventional MIC determination for surveillance of drug resistant *S. pneumoniae*. *Indian J. Med. Res.* **106**, 500–503 (1997).
- 18 Segal, I. H. *Biochemical Calculations*, 2nd edn (John Wiley & Sons Inc., Singapore, 1994).
- 19 Clinical and Laboratory Standards Institute. *Performance Standards for Antimicrobial Susceptibility Testing: Fifteenth Informational Supplement M100-S15* (CLSI, Wayne, PA, 2006).
- 20 Breeuwer, P., Jean-Louis, D. & Bunschoten, N. Characterization of uptake and hydrolysis of fluorescein diacetate and carboxyfluorescein diacetate by intracellular esterases in *Saccharomyces cerevisiae*, which result in accumulation of fluorescent product. *App. Environ. Microbiol.* **61**, 1614–1619 (1995).
- 21 Lindhagen, E., Nygren, P. & Larsson, R. The fluorometric microculture cytotoxicity assay. *Nat. Protoc.* **3**, 1364–1369 (2008).
- 22 Clarke, J. M., Gillings, M. R., Altavilla, N. & Beattie, A. J. Potential problems with fluorescein diacetate assays of cell viability when testing natural products for antimicrobial activity. *J. Microbiol. Meth.* **46**, 261–267 (2001).
- 23 Helen, I., Zgurskaya, H. I. & Nikaido, H. Multi-drug resistance mechanisms: drug efflux across two membranes. *Mol. Microb.* **37**, 219–225 (2000).
- 24 British Pharmacopoeia TSO associated publications UK (2004).
- 25 United States Pharmacopoeia. Rockville, MD, USA (2002).
- 26 National Committee for Clinical Laboratory Standards. *Performance Standards for Antimicrobial Testing: Twelfth Informational Supplement* (NCCLS, Wayne, PA, USA, 2003).

## ORIGINAL ARTICLE

# NovQ is a prenyltransferase capable of catalyzing the addition of a dimethylallyl group to both phenylpropanoids and flavonoids

Taro Ozaki<sup>1</sup>, Satoshi Mishima<sup>2</sup>, Makoto Nishiyama<sup>1</sup> and Tomohisa Kuzuyama<sup>1</sup>

NovQ is a member of a recently identified CloQ/NphB class of prenyltransferases. Although NphB has been well characterized as a prenyltransferase with flexibility against aromatic substrates, few studies have been carried out on characterization of NovQ. Hence, in this study, we investigate the kinetics, substrate specificity and regioselectivity of NovQ. The corresponding *novQ* gene was cloned from *Streptomyces niveus*, which produces an aminocoumarin antibiotic, novobiocin. Recombinant NovQ was overexpressed in *Escherichia coli* and purified to homogeneity. The purified enzyme was a soluble monomeric 40-kDa protein that catalyzed the transfer of a dimethylallyl group to 4-hydroxyphenylpyruvate (4-HPP) independently of divalent cations to yield 3-dimethylallyl-4-HPP, an intermediate of novobiocin. Steady-state kinetic constants for NovQ with the two substrates, 4-HPP and dimethylallyl diphosphate, were also calculated. In addition to the prenylation of 4-HPP, NovQ catalyzed carbon-carbon-based and carbon-oxygen-based prenylations of a diverse collection of phenylpropanoids, flavonoids and dihydroxynaphthalenes. Despite its catalytic promiscuity, the NovQ-catalyzed prenylation occurred in a regioselective manner. NovQ is the first reported prenyltransferase capable of catalyzing the transfer of a dimethylallyl group to both phenylpropanoids, such as *p*-coumaric acid and caffeic acid, and the B-ring of flavonoids. This study shows that NovQ can serve as a useful biocatalyst for the synthesis of prenylated phenylpropanoids and prenylated flavonoids.

*The Journal of Antibiotics* (2009) 62, 385–392; doi:10.1038/ja.2009.48; published online 26 June 2009

**Keywords:** chemoenzymatic synthesis; prenylated phenylpropanoids; prenylated flavonoids; prenylation; prenyltransferase; *Streptomyces*; substrate specificity

## INTRODUCTION

Natural products with one or more prenyl groups have been isolated predominantly from higher plants. These compounds, originating from multiple natural product classes, such as flavonoids, phenylpropanoids and polyketides, often possess anti-microbial, anti-oxidant, anti-inflammatory, anti-viral or anti-cancer activities.<sup>1–4</sup> For example, prenylated phenylpropanoids, drupanin, artepillin C and baccharin, which are *p*-coumaric acid derivatives with one or two prenyl groups, have been shown to induce an apoptotic event in human leukemia cell line HL60 and colon cancer cell line SW480.<sup>5</sup> Moreover, it has been reported that the oral administration of these prenylated phenylpropanoids to mice allografted with sarcoma S-180 causes a significant reduction in tumor growth.<sup>6</sup> In contrast, *p*-coumaric acid, which is non-prenylated, does not show these anti-cancer activities. Thus, given their enhanced and distinct activities, prenylated flavonoids and phenylpropanoids show promise as lead compounds for the development of nutraceuticals in plants and as new pharmacological agents for the treatment of human diseases.<sup>1–4</sup> However, as prenylated compounds often exist at trace levels in natural sources, they are seldom amenable to cost-effective synthesis.

Biocatalysts with relaxed substrate specificity displaying regioselectivity in prenyl group transfer can serve as an alternative production platform for prenylated compounds. Recently, we identified a newly described functional class of prenyltransferases, NphB and SCO7190 in *Streptomyces* strains.<sup>7</sup> These prenyltransferases accept a diverse collection of hydroxyl-containing aromatic substrates, such as flavonoids, to yield the corresponding prenylated products.<sup>8</sup>

Two prenyltransferases belonging to the same class as NphB, CloQ and NovQ have been identified. Both CloQ, isolated from *Streptomyces roseochromogenes*,<sup>9</sup> and NovQ, from *S. spheroides*,<sup>10</sup> are involved in the biosynthesis of the aminocoumarin antibiotics clorobiocin and novobiocin, respectively. They share 84% amino acid sequence identity. Purified recombinant CloQ catalyzes the formation of 3-dimethylallyl-4-HPP, a common intermediate of the aminocoumarin antibiotics, from 4-hydroxyphenylpyruvate (4-HPP) and dimethylallyl diphosphate (DMAPP) independently of divalent cations (Figure 1).<sup>9</sup> However, the enzymatic function of NovQ has not been fully elucidated and few studies have been carried out on substrate specificities of the CloQ/NovQ class of enzymes.

<sup>1</sup>Biotechnology Research Center, The University of Tokyo, Bunkyo-ku, Tokyo, Japan and <sup>2</sup>Nagaragawa Research Center, API Co., Ltd., Nagara, Gifu, Japan  
Correspondence: Dr T Kuzuyama, Biotechnology Research Center, The University of Tokyo, 1-1-1 Yayoi, Bunkyo-ku, Tokyo 113-8657, Japan.  
E-mail: utkuz@mail.ecc.u-tokyo.ac.jp

Received 20 April 2009; revised 2 June 2009; accepted 3 June 2009; published online 26 June 2009

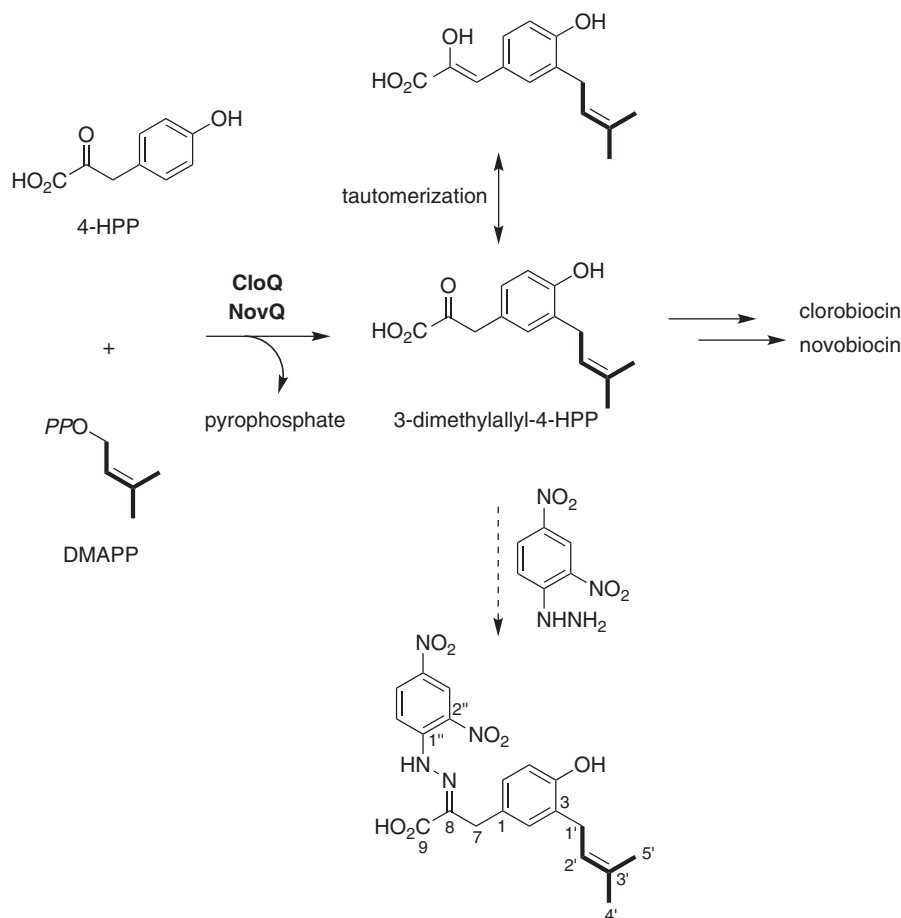


**Figure 1** CloQ- and NovQ-catalyzed reaction in clorobiocin and novobiocin biosyntheses. The dashed line represents a derivatization reaction with 2,4-dinitrophenylhydrazine.

Here, we report the cloning of the *novQ* gene from another novobiocin-producing *Streptomyces* strain, *S. niveus* 16259,<sup>11</sup> and the kinetics and relaxed substrate specificity of the purified recombinant NovQ enzyme. NovQ catalyzes carbon-carbon-based and carbon-oxygen-based prenylations of a diverse collection of phenylpropanoids, flavonoids and dihydroxynaphthalenes (DHNs). Despite its catalytic promiscuity, NovQ-catalyzed prenylation occurs in a regio-specific manner. This is the first report showing that the bacterial enzyme NovQ can be used as a biocatalyst for the synthesis of both prenylated phenylpropanoids and prenylated flavonoids.

## RESULTS

### Expression and purification of recombinant NovQ protein

The *novQ* gene from *S. niveus* 16259 was overexpressed in *E. coli* as an N-terminal His<sub>8</sub>-tagged protein, and the recombinant protein was purified to apparent homogeneity (Figure 2). The molecular mass of NovQ was estimated to be 40 kDa by SDS-polyacrylamide gel electrophoresis (Figure 2) and by gel filtration chromatography, suggesting that NovQ is likely a monomer.

### Identification of the reaction product of NovQ

We next attempted to detect the formation of 3-dimethylallyl-4-HPP by the action of NovQ on 4-HPP and DMAPP. Initial efforts to directly detect the formation of 3-dimethylallyl-4-HPP were carried out using HPLC, but the results were inconclusive. This was thought to be because of an equilibrium between the keto and enol forms of

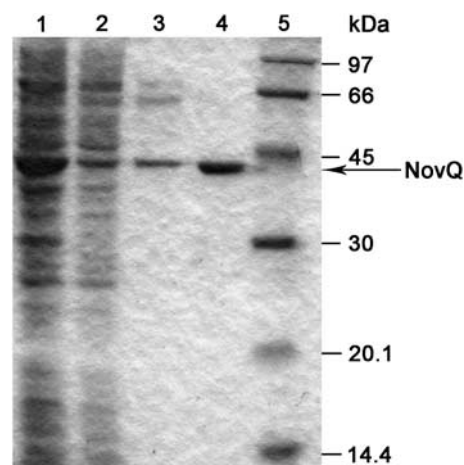


**Figure 2** Expression and purification of the recombinant NovQ enzyme. A total of 12% SDS-polyacrylamide gel electrophoresis of the enzyme. Lanes: 1, total protein after the induction; 2, soluble protein after the induction; 3, fraction eluted with 250 mM imidazole from a Ni-NTA Superflow column; 4, purified enzyme after gel filtration chromatography and 5, low molecular mass markers.

3-dimethylallyl-4-HPP synthesized by NovQ. Therefore, we decided to derivatize the NovQ reaction product with 2,4-dinitrophenylhydrazine to yield a dinitrophenylhydrazone, because 2,4-dinitrophenylhydrazine

is often used to detect compounds, such as 4-HPP with a keto group. After derivatization, a major dinitrophenylhydrazone derivative was purified by HPLC and identified as 3-dimethylallyl-4-HPP-dinitrophenylhydrazone from the HR-MS,  $^1\text{H}$  NMR and  $^{13}\text{C}$  NMR spectral data, unequivocally showing that the NovQ cloned in this study catalyzes the addition of a dimethylallyl group to 4-HPP to yield 3-dimethylallyl-4-HPP (Figure 1).

#### Steady-state kinetic studies of NovQ

For steady-state kinetic studies of NovQ, we used a spectrophotometric NovQ prenyltransferase assay using a coupled system with a pyrophosphate reagent, because the NovQ prenyltransferase forms a pyrophosphate anion co-product during catalysis (Figure 1). This assay quantifies product formation by the concomitant oxidation of NADH. From initial velocity measurements, we determined that the NovQ reaction followed Michaelis–Menten kinetics. Apparent  $K_m$  values were determined to be  $33.3 \pm 4.7 \mu\text{M}$  for 4-HPP and  $15.1 \pm 1.9 \mu\text{M}$  for DMAPP at fixed saturating concentrations of DMAPP (1 mM) and 4-HPP (1 mM), respectively (Supplementary Table S1). The turnover number of the reaction was  $5.0 \pm 0.1 \text{ min}^{-1}$ .

#### Substrate specificity of NovQ

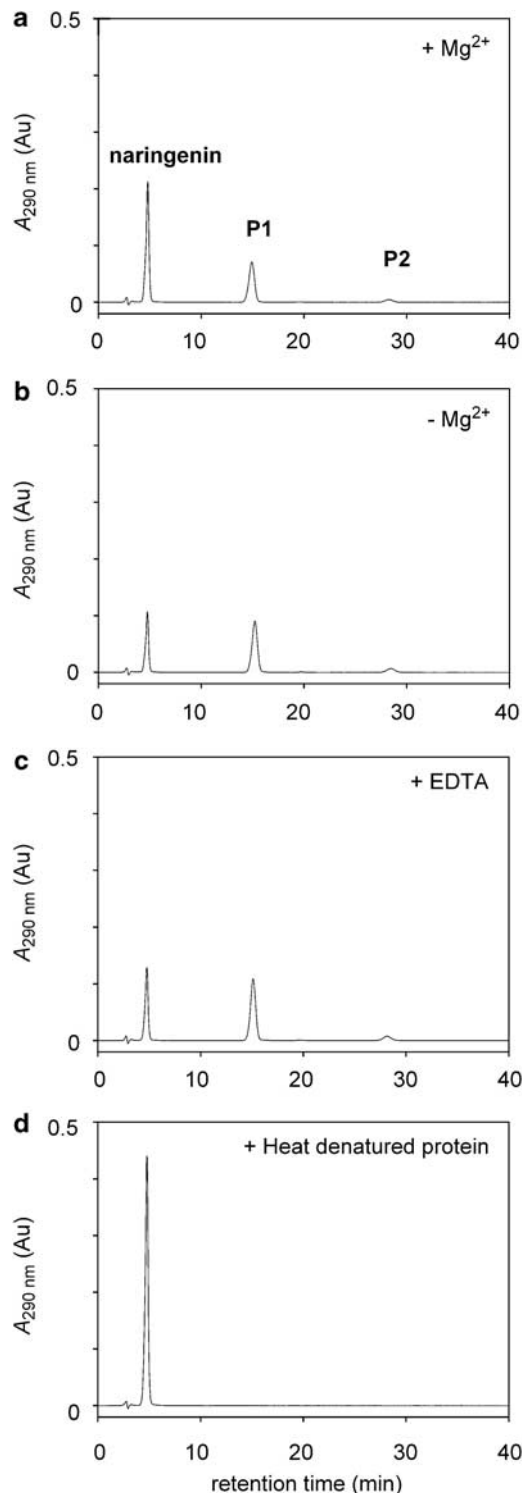
Next, we examined the substrate specificity of NovQ. We focused on the following prenyl acceptors: phenylpropanoids, including *p*-coumaric acid and caffeic acid; the plant polyketides, including resveratrol and olivetol; the (iso)flavonoid sub-class, including naringenin, apigenin, daidzein and genistein; and DHNs, including 1,3-DHN, 1,6-DHN and 2,7-DHN. We first incubated NovQ with naringenin in the presence of DMAPP ( $C_5$ ) or geranyl diphosphate ( $C_{10}$ ). The resultant prenyltransferase activity of NovQ was detected only in the presence of DMAPP. Therefore, in the further experiments, each substrate was incubated with NovQ in the presence of DMAPP. All substrates, except for olivetol and 1,3-DHN, underwent facile prenylation, yielding between one and three products. The prenylation activity was independent of divalent cations, such as  $\text{Mg}^{2+}$ . Even in the presence of 5 mM EDTA, NovQ possessed full enzymatic activity (Figure 3). Thus, we concluded that NovQ, similar to CloQ,<sup>9</sup> is a magnesium-independent prenyltransferase (Supplementary Table S1).

NovQ-catalyzed reaction products were purified by preparative HPLC, and their structures were elucidated primarily by comparison of the  $^1\text{H}$  NMR spectra of the isolated products with their corresponding substrates. Most reaction products contained a dimethylallyl group in the *ortho* position with respect to a neighboring hydroxy moiety. In addition to this carbon–carbon-based prenylation, NovQ catalyzed carbon–oxygen-based prenylation in some cases.

**Phenylpropanoids.** With two phenylpropanoids, *p*-coumaric acid and caffeic acid, NovQ catalyzed the prenylation of a hydroxy group, leading to the formation of an *O*-prenyl linkage (Table 1). Interestingly, NovQ appended two dimethylallyl groups to caffeic acid to yield 3-*O*,4-*O*-di-(dimethylallyl) caffeic acid. In addition to this *O*-prenylation, NovQ prenylated the C-3 of *p*-coumaric acid to yield drupanin (3-dimethylallyl coumaric acid).

**Plant polyketides.** Of the two plant polyketides tested, resveratrol and olivetol, NovQ used only resveratrol as a substrate, prenylating it at C-3' (Table 1).

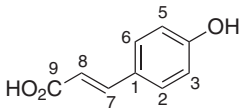
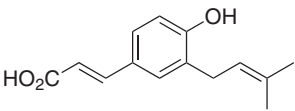
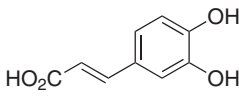
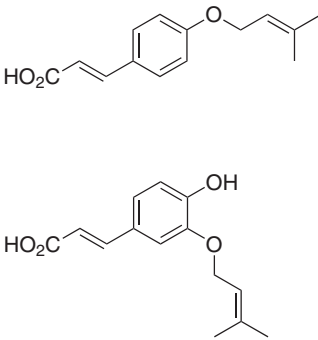
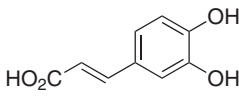
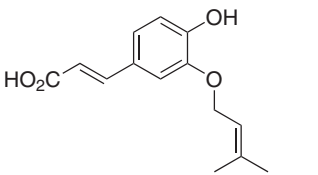
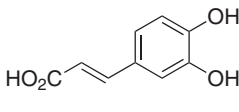
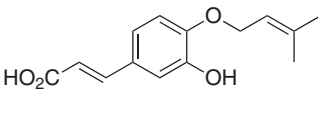
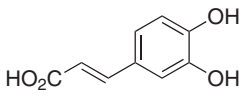
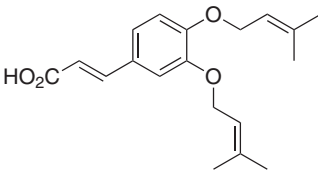
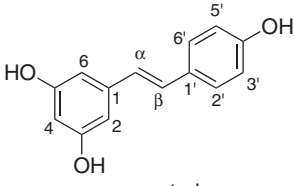
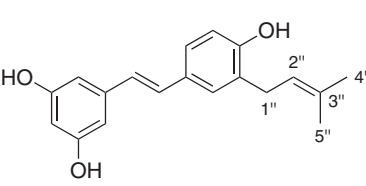
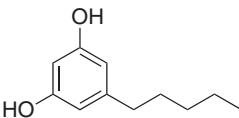
**Flavonoids.** NovQ prenylated all flavonoids tested as substrates (Table 2). Incubation with naringenin and genistein yielded two



**Figure 3** HPLC analysis of prenylated products formed from naringenin by the action of NovQ. After incubation for 1 h with NovQ (a) in the presence of 2.5 mM  $\text{Mg}^{2+}$ , (b) in the absence of  $\text{Mg}^{2+}$  or (c) in the presence of 5 mM EDTA. (d) After incubation for 1 h with heat-denatured NovQ. **P1**, 3'-dimethylallyl naringenin; **P2**, 4'-*O*-dimethylallyl naringenin.

products with a dimethylallyl group at C-3' or *O*-4' in the B-ring. In contrast, C-3' specific prenylation in the B-ring occurred with apigenin and daidzein.

**Table 1** Prenylated phenylpropanoids and plant polyketides synthesized by NovQ

Substrate	Product	Yield (%)
 <p><i>p</i>-coumaric acid</p>		16.8
 <p>caffeic acid</p>		34.4
 <p>caffeic acid</p>		17.3
 <p>caffeic acid</p>		26.1
 <p>caffeic acid</p>		20.0
 <p>resveratrol</p>		12.3
 <p>olivetol</p>	N.P.	-

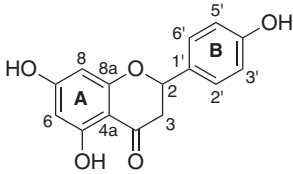
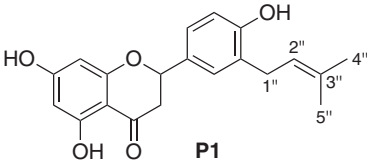
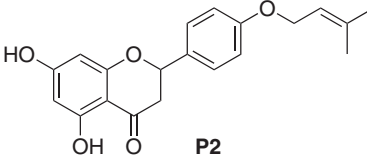
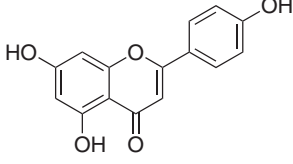
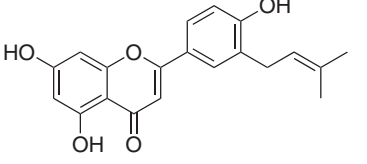
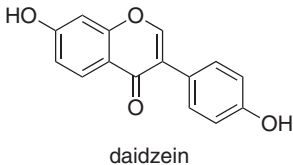
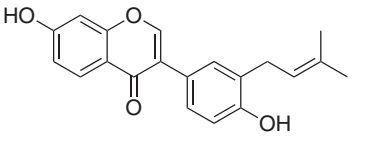
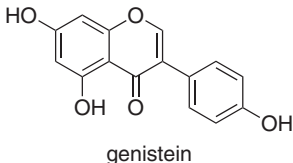
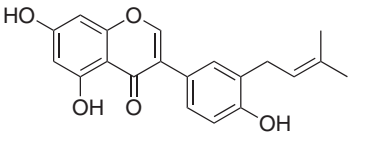
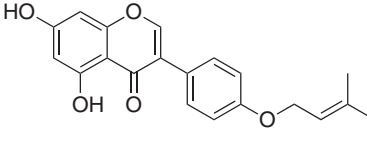
Abbreviation: N.P., no products.

*Dihydroxynaphthalenes.* NovQ accepted 1,6-DHN and 2,7-DHN as substrates to yield three and one products, respectively, but it did not accept 1,3-DHN (Table 3). The main product of 1,6-DHN was 1-*O*-dimethylallyl-1,6-DHN. Other products were prenylated at C-4 or C-2 of 1,6-DHN. Interestingly, NovQ catalyzed attachment of the C-3' carbon of the dimethylallyl group to 1,6-DHN. Reaction with 2,7-DHN yielded only 1-dimethylallyl-2,7-DHN.

In addition, we determined the yields of prenylated products formed after a 24-h incubation with NovQ. Naringenin was most highly converted to its prenylated derivatives, with a yield of 98.3%. On the other hand, the yield of the prenylated products of the other substrates ranged from 2.5 to 63.4%. The ratio of C-prenylated and O-prenylated products was dependent on substrates. For example, the major product in the presence of the naringenin substrate was



**Table 2** Prenylated flavonoids synthesized by NovQ

Substrate	Product	Yield (%)
 naringenin	 P1	87.2
	 P2	11.1
 apigenin		7.6
 daidzein		2.5
 genistein		2.3
		5.3

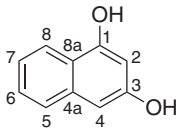
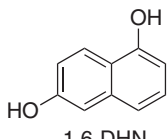
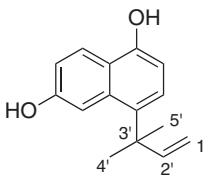
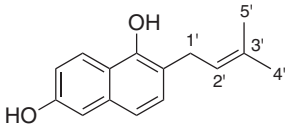
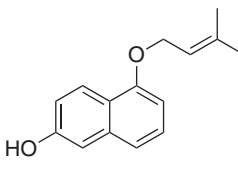
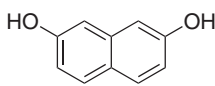
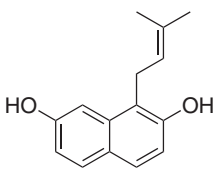
C-prenylated, whereas *O*-prenylated forms were the major products of genistein, *p*-coumaric acid and 1,6-DHN. With caffeic acid, only *O*-prenylated products were synthesized at a high yield (63.4%).

## DISCUSSION

In this study, we examined the kinetics and substrate specificity of the NovQ gene, which was cloned from a novobiocin-producing *S. niveus* 16259. The recombinant NovQ enzyme showed enzymatic properties similar to those of the previously characterized CloQ,<sup>9</sup> as summarized in Supplementary Table S1, probably reflecting the high sequence identity (84%) between these enzymes.

To date, CloQ/NovQ enzymes have been considered prenyltransferases that are highly specific to 4-HPP.<sup>9,10</sup> The recombinant CloQ enzyme did not accept related aromatic compounds, such as 4-hydroxybenzoic acid, 4-hydroxybenzaldehyde, and *L*-tyrosine, as substrates,<sup>9</sup> and nor did a partially purified NovQ enzyme from *S. spheroides* NCIMB 11891 accept *p*-coumaric acid or 4-hydroxybenzoic acid as substrates.<sup>10</sup> These results had prevented us from thoroughly elucidating the substrate specificity of the CloQ/NovQ enzymes, although these enzymes are potential biocatalysts for the production of diverse prenylated compounds. However, in this study, we clearly showed for the first time that NovQ also accepts a diverse

Table 3 Prenylated DHNs synthesized by NovQ

Substrate	Product	Yield (%)
 1,3-DHN	N.P.	-
 1,6-DHN		1.5
		6.4
		49.8
 2,7-DHN		31.0

Abbreviations: DHNs, dihydroxynaphthalenes; N.P., no products.

collection of hydroxy-containing aromatic substrates, such as phenylpropanoids, flavonoids and DHNs, to yield the corresponding prenylated products. It is noted that NovQ showed substrate specificities and regio-specificities that were substantially different from those of NphB.<sup>8</sup> For example, NovQ catalyzed the prenylation of phenylpropanoids, such as *p*-coumaric acid and caffeic acid (Table 1), neither of which is prenylated by NphB.<sup>8</sup> In addition, NovQ appended a dimethylallyl group to the B-ring of flavonoids (Table 2), whereas NphB appends a geranyl group to the A-ring of flavonoids.<sup>8</sup> These differences may be ascribed to the low sequence identity (19%) between NovQ and NphB. On the other hand, the substrate specificity of CloQ is probably similar to that of NovQ, because of the high sequence identity of these enzymes.

We recently solved an architecturally new crystal structure of NphB.<sup>7</sup> Keller *et al.*<sup>12</sup> reported the crystallization and preliminary X-ray analysis of CloQ. Thus, the potential of employing these biocatalysts using structure-based enzyme engineering provides a convenient starting point for exploring novel prenylation chemistry and the bioactivity of aromatic compounds.<sup>13–15</sup> In addition, such rationally based engineering of NphB and CloQ/NovQ will provide another powerful synthetic tool with which to expand the diversity

and bioactivities of many synthetic and natural compounds through enzyme-directed regiospecific prenylation.

## EXPERIMENTAL SECTION

### Cloning of the *novQ* gene from *S. niveus* 16259

On the basis of the nucleotide sequences 80 bp upstream and 58 bp downstream of the *novQ* gene previously cloned from *S. spheroides* NCIMB 11891 (accession no. AF170880),<sup>9</sup> oligonucleotide primers pNOVQN1 (5'-GAACGATCACGATCGACCG-3') and pNOVQC1 (5'-TCGAACACCGGCGGCTGACG-3') were synthesized (Operon Biotechnologies, Tokyo, Japan). These primers were used to amplify the DNA fragment containing the *novQ* gene from the *S. niveus* 16259<sup>11</sup> genome by PCR. The PCR-amplified 1.1-kb DNA fragment was cloned into a pT7Blue vector (Takara Bio, Tokyo, Japan) to give pT7BnovQ. Sequence analysis of the 1.1-kb DNA fragment revealed one complete open reading frame that is completely identical to that of the *novQ* gene from *S. spheroides* NCIMB 11891.<sup>9</sup>

### Construction of an expression plasmid for the *novQ* gene

PCR amplification using pT7BnovQ and oligonucleotides for ligation into the *E. coli* expression vector pHis8<sup>16</sup> was carried out with the forward primer 5'-GGGGGGCCATGGACCCGCACTCCCAGATGAATC-3' (*Nco*I site underlined) and the reverse primer 5'-GGGGGGGATCCATCGGGCACCTC

CGGTG-3' (*Bam*HI site underlined) (Operon Biotechnologies) to generate pHis8novQ. The pHis8novQ construct was transformed into *E. coli* BL21(DE3), and the *novQ* gene was overexpressed as previously described.<sup>16</sup>

### Recombinant NovQ purification

For protein extraction, cells were suspended in lysis buffer (50 mM Tris-HCl (pH 8.0), 500 mM NaCl, 20 mM imidazole, 20% (w/v) glycerol and 1% Tween 20). The cell suspensions were sonicated with a Branson Sonifier 250 (Emerson Japan, Tokyo, Japan). To separate the cellular debris from the soluble protein, the lysate was centrifuged at 17 000 rpm at 4 °C for 20 min. NovQ was purified from the resulting supernatant with a Ni-NTA Superflow resin (Qiagen, Tokyo, Japan). After washing with wash buffer containing 50 mM Tris-HCl (pH 8.0), 500 mM NaCl, 20% (w/v) glycerol and 20 mM imidazole, NovQ was eluted using the same buffer containing 250 mM imidazole. After elution, NovQ was dialyzed against 75 mM Tris-HCl (pH 7.5) buffer containing 100 mM NaCl to remove glycerol and imidazole.

### Molecular weight analysis

The molecular weight of His<sub>8</sub>-NovQ was determined by gel filtration chromatography on a HiLoad 26/60 Superdex 75pg column (GE Healthcare Bio-Sciences, Tokyo, Japan) that had been equilibrated with 75 mM Tris-HCl buffer (pH 7.5) containing 100 mM NaCl. The column was calibrated with a Gel Filtration Calibration Kit LMW (GE Healthcare Bio-Sciences) that included conalbumin (75 kDa), ovalbumin (43 kDa), carbonic anhydrase (29 kDa), ribonuclease A (13.7 kDa) and aprotinin (6.5 kDa). The proteins were eluted with 75 mM Tris-HCl (pH 7.5) containing 100 mM NaCl.

### Conditions for enzymatic reactions

All NovQ assays were carried out in 75 mM Tris-HCl (pH 7.5) containing 2.5 mM MgCl<sub>2</sub>, 0.25 mM aromatic substrate, 0.5 mM DMAPP and 1 mg ml<sup>-1</sup> NovQ, in a total volume of 300 µl. The reaction mixtures were incubated at 30 °C for 24 h. After incubation, the reaction mixtures were freeze-dried, and the residues were dissolved in 100 µl of methanol. The reaction products were analyzed by HPLC equipped with an MD-2010 Plus photodiode array (JASCO, Tokyo, Japan) with PEGASIL ODS (4.6 × 250 mm, Senshu Scientific, Tokyo, Japan) using an isocratic elution of 70% methanol with 0.1% acetate or a linear gradient (30 min) of 50–100% methanol with 0.1% acetate. The yield of each product was defined as the ratio of the peak area of the prenylated product to the sum of those of the remaining substrate and all prenylated products.

### Steady-state kinetic parameters

A spectrophotometric NovQ prenyltransferase assay using a coupled system with a pyrophosphate reagent (Sigma-Aldrich Japan, Tokyo, Japan) was used for steady-state kinetic studies of NovQ, because the NovQ prenyltransferase forms a pyrophosphate anion co-product during catalysis (Figure 1). Prenyltransferase activity was assayed in 75 mM Tris-HCl (pH 7.5) containing 2.5 mM MgCl<sub>2</sub>, 4-HPP, DMAPP and 267 µl of the pyrophosphate reagent in a total volume of 800 µl. When the concentration of DMAPP was fixed at 1 mM, the concentrations of 4-HPP were varied at 25, 50, 100 and 500 µM. With a fixed concentration of 1 mM 4-HPP, the concentrations of DMAPP were varied: 12.5, 25, 50 and 100 µM. After the reaction mixture containing no enzyme was incubated at 30 °C for 5 min, the reaction was started by adding 117 µg of NovQ. NovQ-dependent oxidation of NADH was monitored in a UV-1600PC spectrophotometer (Shimadzu, Kyoto, Japan) equipped with a cell holder CPS-240A (Shimadzu) adjusted at 30 °C. Initial velocities were determined from the slope of a plot of NADH consumption versus incubation time. The molar extinction coefficient ( $\epsilon$ ) of NADH at 340 nm was 6220. Steady-state kinetic parameters were calculated using the SigmaPlot 10.0 software and Enzyme Kinetics Module 1.3 (Systat Software, Point Richmond, CA, USA).

### Product analysis

Large-scale production of prenyl products was carried out in 75 mM Tris-HCl (pH 7.5) containing 2.5 mM MgCl<sub>2</sub>, 2.5 mM aromatic substrate, 5 mM DMAPP and 1 mg ml<sup>-1</sup> NovQ, in a total volume of 10 ml. The reaction mixtures were incubated overnight at 25 °C, and then extracted thrice with 10 ml ethyl acetate. When 4-HPP was used as a substrate, the reaction mixture was incubated at

30 °C for 1 h and then mixed with an equal volume of a 2,4-dinitrophenylhydrazine solution (0.25 mM in 2 M HCl) for derivatization. After 1 h of incubation with continuous stirring, the reaction mixture was extracted thrice with 10 ml of ethyl acetate. After drying over Na<sub>2</sub>SO<sub>4</sub>, the ethyl acetate extract was evaporated *in vacuo* and the residue was dissolved in 1 ml of methanol. Prenylated products were further purified by preparative HPLC with PEGASIL ODS (20 × 250 mm, Senshu Scientific) using an isocratic elution of 70% methanol containing 0.1% acetate. For the dinitrophenylhydrazine derivative, 80% methanol containing 0.1% trifluoroacetic acid was used. The structures of the reaction products were analyzed by their <sup>1</sup>H NMR, <sup>13</sup>C NMR and HMBC spectroscopic data (600 MHz, JEOL ECA-600, JEOL, Tokyo, Japan) and HR-MS data (JEOL JMS-T100LC, JEOL, Tokyo, Japan). MS analysis was performed using electrospray ionization (ESI) in negative ion mode.

### 3-dimethylallyl-4-HPP-dinitrophenylhydrazone

The above product was synthesized from 4-HPP and DMAPP by the recombinant NovQ and derivatized with 2,4-dinitrophenylhydrazine. HR-MS (ESI<sup>-</sup>) *m/z* 427.12249 (calcd for C<sub>20</sub>H<sub>19</sub>N<sub>4</sub>O<sub>7</sub><sup>-</sup> 427.12537). <sup>1</sup>H NMR (600 MHz, MeOH-*d*<sub>4</sub>)  $\delta$  1.63 (s, 3H, H-5'), 1.66 (s, 3H, H-4'), 3.20 (d, *J* = 7.5 Hz, 2H, H-2'), 3.98 (s, 2H, H-7), 5.24 (t, *J* = 7.6 Hz, 1H, H-2'), 6.66 (d, *J* = 8.2 Hz, 1H, H-5), 6.94 (d, *J* = 8.3 Hz, 1H, H-6), 7.01 (s, 1H, H-2), 8.20 (d, *J* = 9.6 Hz, 1H, H-6''), 8.40 (dd, *J* = 2.0, 9.6 Hz, 1H, H-5''), 8.98 (d, *J* = 2.0 Hz, 1H, H-2''). <sup>13</sup>C NMR (MeOH-*d*<sub>4</sub>)  $\delta$  14.9 (C-5'), 23.1 (C-4'), 26.2 (C-1'), 29.2 (C-7), 113.4 (C-5), 115.8 (C-6''), 120.7 (C-2'), 120.7 (C-3''), 122.9 (C-1), 124.9 (C-6), 127.1 (C-3), 127.9 (C-2), 128.1 (C-5''), 129.7 (C-2''), 130.4 (C-3'), 138.1 (C-4''), 142.4 (C-1''), 145.6 (C-8), 152.4 (C-4), 165.4 (C-9).

### Accession number

The nucleotide sequence of the 1.1-kb DNA fragment including the *novQ* gene from *S. niveus* 16259 has been deposited in the DDBJ/EMBL/GenBank nucleotide sequence databases under accession number AB496950.

### ACKNOWLEDGEMENTS

We thank Kazu-Michi Suzuki and Yayoi Tashiro (API) for assistance with the assignment of the NMR spectra of prenylated phenylpropanoids. This work was supported by an R & D project, 'Development of Fundamental Technologies for Production of High-value Materials using Transgenic Plants,' funded by the Ministry of Economy, Trade and Industry (METI) (to TK).

- 1 Di Pietro, A. *et al.* Modulation by flavonoids of cell multidrug resistance mediated by P-glycoprotein and related ABC transporters. *Cell Mol. Life Sci.* **59**, 307–322 (2002).
- 2 Ahn, M. R. *et al.* Suppression of tumor-induced angiogenesis by Brazilian propolis: major component artepillin C inhibits *in vitro* tube formation and endothelial cell proliferation. *Cancer Lett.* **252**, 235–243 (2007).
- 3 Paulino, N. *et al.* Anti-inflammatory effects of a bioavailable compound, Artepillin C, in Brazilian propolis. *Eur. J. Pharmacol.* **587**, 296–301 (2008).
- 4 Messerli, S. M. *et al.* Artepillin C (ARC) in Brazilian green propolis selectively blocks oncogenic PAK1 signaling and suppresses the growth of NF tumors in mice. *Phytother. Res.* **23**, 423–427 (2009).
- 5 Akao, Y. *et al.* Cell growth inhibitory effect of cinnamic acid derivatives from propolis on human tumor cell lines. *Biol. Pharm. Bull.* **26**, 1057–1059 (2003).
- 6 Mishima, S., Ono, Y., Araki, Y., Akao, Y. & Nozawa, Y. Two related cinnamic acid derivatives from Brazilian honey bee propolis, baccharin and drupanin, induce growth inhibition in allografted sarcoma S-180 in mice. *Biol. Pharm. Bull.* **28**, 1025–1030 (2005).
- 7 Kuzuyama, T., Noel, J. P. & Richard, S. B. Structural basis for the promiscuous biosynthetic prenylation of aromatic natural products. *Nature* **435**, 983–987 (2005).
- 8 Kumano, T., Richard, S. B., Noel, J. P., Nishiyama, M. & Kuzuyama, T. Chemoenzymatic syntheses of prenylated aromatic small molecules using *Streptomyces* prenyltransferases with relaxed substrate specificities. *Bioorg. Med. Chem.* **16**, 8117–8126 (2008).
- 9 Pojer, F. *et al.* CloQ, a prenyltransferase involved in clorobiocin biosynthesis. *Proc. Natl Acad. Sci. USA* **100**, 2316–2321 (2003).
- 10 Steffensky, M., Li, S. M., Vogler, B. & Heide, L. Novobiocin biosynthesis in *Streptomyces spheroides*: identification of a dimethylallyl diphosphate: 4-hydroxyphenylpyruvate dimethylallyltransferase. *FEMS Microbiol. Lett.* **169**, 69–74 (1998).
- 11 Orihara, N., Kuzuyama, T., Takahashi, S., Furihata, K. & Seto, H. Studies on the biosynthesis of terpenoid compounds produced by actinomycetes. 3. Biosynthesis of

- the isoprenoid side chain of novobiocin via the non-mevalonate pathway in *Streptomyces niveus*. *J. Antibiot.* **51**, 676–678 (1998).
- 12 Keller, S., Pojer, F., Heide, L. & Lawson, D. M. Crystallization and preliminary X-ray analysis of the aromatic prenyltransferase CloQ from the clorobiocin biosynthetic cluster of *Streptomyces roseochromogenes*. *Acta. Crystallogr. Sect. F. Struct. Biol. Cryst. Commun.* **62**, 1153–1155 (2006).
  - 13 Koehl, P. Relaxed specificity in aromatic prenyltransferases. *Nat. Chem. Biol.* **1**, 71–72 (2005).
  - 14 Tello, M., Kuzuyama, T., Heide, L., Noel, J. P. & Richard, S. B. The ABBA family of aromatic prenyltransferases: broadening natural product diversity. *Cell. Mol. Life Sci.* **65**, 1459–1463 (2008).
  - 15 Heide, L. Prenyl transfer to aromatic substrates: genetics and enzymology. *Curr. Opin. Chem. Biol.* **13**, 171–179 (2009).
  - 16 Jez, J. M., Ferrer, J. L., Bowman, M. E., Dixon, R. A. & Noel, J. P. Dissection of malonyl-coenzyme A decarboxylation from polyketide formation in the reaction mechanism of a plant polyketide synthase. *Biochemistry* **39**, 890–902 (2000).

Supplementary Information accompanies the paper on The Journal of Antibiotics website (<http://www.nature.com/ja>)

## NOTE

# JBIR-44, a new bromotyrosine compound from a marine sponge *Psammaplysilla purpurea*

Takeshi Fujiwara<sup>1</sup>, Ji-Hwan Hwang<sup>2</sup>, Akihiko Kanamoto<sup>3</sup>, Hiroshi Nagai<sup>1</sup>, Motoki Takagi<sup>4</sup> and Kazuo Shin-ya<sup>2</sup>

*The Journal of Antibiotics* (2009) 62, 393–395; doi:10.1038/ja.2009.49; published online 26 June 2009

**Keywords:** bromotyrosine; cytotoxic effect; marine sponge; *Psammaplysilla purpurea*; Verongida

Marine sponges of the order Verongida are characterized by their ability to synthesize brominated tyrosine derivatives, many of which possess potent anti-microbial and cytotoxic activities.<sup>1</sup> Purealin,<sup>2–4</sup> Lipopurealin A–E,<sup>5,6</sup> Purealidin A–S,<sup>6–11</sup> Psammaplysins A–B,<sup>12</sup> Purpuramine A–J,<sup>11,13</sup> Aplysamines 2–5<sup>14</sup> and Macrocytic peptides Bastadins<sup>15</sup> isolated from Verongida have been previously reported as brominated tyrosine derivatives. The diverse modification of these biosynthetically related compounds occurs in both the side chain and aromatic ring of the brominated tyrosine precursors. It has been reported that many brominated tyrosine derivatives were isolated from Verongida, *Psammaplysilla purpurea*;<sup>1,2,5–10,13–15</sup> therefore, *P. purpurea* is a potential resource for the chemical screening of novel compounds. We thus attempted to isolate new compounds from *P. purpurea*, and resulted in the isolation of a new compound designated as JBIR-44 (**1**) (Figure 1). In this paper, we report the isolation, structure elucidation and brief biological activity of **1**.

*P. purpurea* (class, Demospongiae; order, Verongida; family, Aplysinellidae) was collected at a depth of –25 m from Kinwan bay, Okinawa prefecture, Japan, in February 2007. *P. purpurea* (300 g, wet) was extracted with MeOH and, after concentration in vacuo, MeOH–H<sub>2</sub>O (3:7) was added to the aqueous concentrate. The MeOH–H<sub>2</sub>O solution (500 ml) was partitioned with EtOAc (three times). After drying over Na<sub>2</sub>SO<sub>4</sub>, the EtOAc layer was evaporated to dryness. The dried residue was subjected to normal-phase MPLC (Purif-Pack SI-60, Moritex, Tokyo, Japan) eluted with a Hexane–EtOAc (0–30% EtOAc) linear gradient system, followed by elution with a CHCl<sub>3</sub>–MeOH (0–90% MeOH) linear gradient system. The 10–30% MeOH elute fractions were further purified by reversed-phase HPLC using a PEGASIL ODS column (Senshu Pak, 20 i.d. × 150 mm, Senshu Scientific, Tokyo, Japan) with a H<sub>2</sub>O–MeOH (0–100% MeOH) linear gradient system containing 0.1% formic acid to yield JBIR-44 (**1**, 4.4 mg), together with four known compounds, purealidin

C (2.1 mg),<sup>6</sup> purpuramine F (1.8 mg),<sup>13</sup> araplysillin I (45.3 mg)<sup>16</sup> and aplysamine 4 (175 mg).<sup>14</sup>

Compound **1** was obtained as a colorless oil (UV (MeOH)  $\lambda_{\max}$  ( $\epsilon$ ) 283 (1700), 208 (17 600)). The electrospray ionization-mass spectrum (ESI-MS) displayed an isotopic cluster (640.9, 642.9, 644.9, 646.9, 648.9) that was consistent with the presence of four bromine atoms. Its molecular formula was established as C<sub>18</sub>H<sub>16</sub>Br<sub>4</sub>N<sub>2</sub>O<sub>4</sub> ( $m/z$  [M+H]<sup>+</sup> 640.7918, –0.4 mmu) by high-resolution ESI-MS. Compound **1** also displayed the IR spectrum [(KBr)  $\nu_{\max}$ ] at 3560, 3510, 3415, 1675 and 1630 cm<sup>-1</sup>.

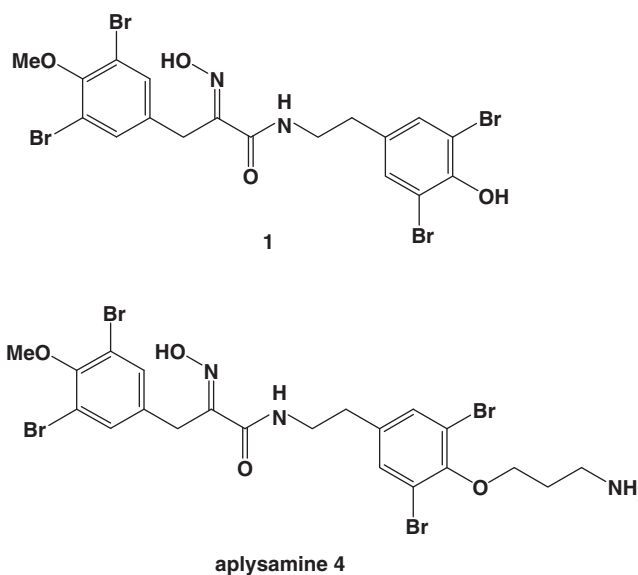


**Figure 1** Structures of **1** and aplysamine 4.

<sup>1</sup>Tokyo University of Marine Science and Technology, Minato-ku, Tokyo, Japan; <sup>2</sup>Biomedical Information Research Center (BIRC), National Institute of Advanced Industrial Science and Technology (AIST), Koto-ku, Tokyo, Japan; <sup>3</sup>OP Bio Factory Co., Ltd., Oroku, Naha, Okinawa, Japan and <sup>4</sup>Biomedical Information Research Center (BIRC), Japan Biological Informatics Consortium (JBIC), Koto-ku, Tokyo, Japan

Correspondence: K Shin-ya, Biomedical Information Research Center (BIRC), National Institute of Advanced Industrial Science and Technology (AIST), 2-42 Aomi, Koto-ku, Tokyo 135-0064, Japan.

E-mail: k-shinya@aist.go.jp or Dr M Takagi, Biomedical Information Research Center (BIRC), Japan Biological Informatics Consortium (JBIC), 2-42 Aomi, Koto-ku, Tokyo 135-0064, Japan.

E-mail: motoki-takagi@aist.go.jp

Received 21 April 2009; revised 12 May 2009; accepted 14 May 2009; published online 26 June 2009

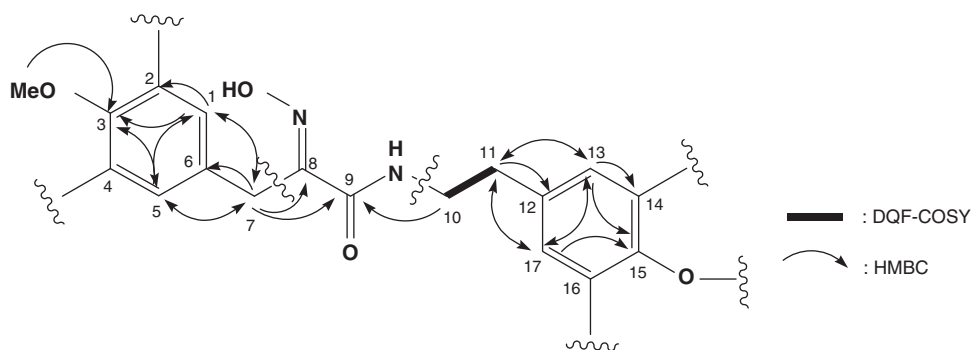


**Figure 2** Key correlations in DQF-COSY (bold line) and HMBC (arrow) spectra of **1**.

The structure of **1** was elucidated as follows: The  $^1\text{H}$  and  $^{13}\text{C}$  NMR spectral data for **1** are shown in Table 1 and the structural information on **1** was further obtained by a series of 2D NMR analyses, such as heteronuclear single-quantum coherence, heteronuclear multiple-bond correlation (HMBC) and double-quantum-filtered correlation (DQF-COSY) spectra (Figure 2). Analyses of  $^1\text{H}$ - $^{13}\text{C}$  long-range couplings in the HMBC spectrum revealed two partial structures. In the HMBC spectrum, aromatic protons 1/5-H ( $\delta_{\text{H}}$  7.52) strongly *m*-coupled with each other and with an aromatic carbon C-3 ( $\delta_{\text{C}}$  152.0), which in turn long-range coupled to a methoxy proton 3-OMe ( $\delta_{\text{H}}$  3.85,  $\delta_{\text{C}}$  61.0). A singlet methylene proton 7-H ( $\delta_{\text{H}}$  3.87) was long-range coupled to aromatic methine carbons C-1/5 ( $\delta_{\text{C}}$  134.4) and to an aromatic quaternary carbon C-6 ( $\delta_{\text{C}}$  137.3). Thus, the methylene carbon C-7 was deduced to be substituted at the position of C-6. The all assignment of this tetrasubstituted benzene ring moiety was established by  $^1\text{H}$ - $^{13}\text{C}$  long-range couplings as shown in Figure 2. These results revealed the presence of a 2,4-disubstituted-3-methoxyphenylene moiety as shown in Figure 2. In the same manner, long-range couplings observed in the HMBC spectrum and the  $^{13}\text{C}$  chemical shift at C-15 ( $\delta_{\text{C}}$  150.7) revealed a 4-oxygenated 1,3,4,5-tetrasubstituted benzene moiety. A methylene proton 11-H ( $\delta_{\text{H}}$  2.73), which was spin coupled to a methylene proton 10-H ( $\delta_{\text{H}}$  3.45), was  $^1\text{H}$ - $^{13}\text{C}$  long-range coupled to aromatic methine carbons C-13/17 ( $\delta_{\text{C}}$  133.6) and to an aromatic quaternary carbon C-12 ( $\delta_{\text{C}}$  134.6).  $^1\text{H}$ - $^{13}\text{C}$  long-range couplings from the methylene proton 10-H to an amide carbonyl carbon C-9 ( $\delta_{\text{C}}$  165.4), from the methylene proton 7-H to a hydroxyimino carbon C-8 ( $\delta_{\text{C}}$  153.8) and to the amide carbonyl carbon C-9, together with IR absorptions assignable to an amide and an imino functional group (1655 and 1620  $\text{cm}^{-1}$ , respectively)<sup>11</sup> revealed that two tetrasubstituted benzene substructures were connected through a 2-(hydroxyimino)acetamide moiety<sup>11</sup> as shown in Figure 2. This structure was also supported by the  $^{13}\text{C}$  chemical shifts of the amide and imino carbons and IR absorptions observed in aplysamine 4.<sup>14</sup> From the molecular formula of **1**, four bromine atoms were determined to be substituted at the position of C-2, C-4, C-14 and C-16, and a remaining hydroxyl group was assigned to an oxime functional group at the imino moiety. The geometry of C-8 at oxime moiety was elucidated as *E* from the up-field  $^{13}\text{C}$  chemical shift of C-7 ( $\delta_{\text{C}}$  28.7) because of the  $\gamma$ -effect of the hydroxyl group of the oxime function. The different  $^{13}\text{C}$  chemical shifts between *E* ( $\delta_{\text{C}}$  27.5) and *Z* ( $\delta_{\text{C}}$  35.7) observed in (*E,Z*)-*N,N'*-Bis[3-(3'-bromo-4'-hydroxyphenyl)-2-oximidopropionyl] cystamine,<sup>17</sup> of which positions corresponded to C-7 in **1**, supported the stereochemistry at C-8.

The cytotoxic effects of **1** and aplysamine 4 against human cervical carcinoma HeLa cells were determined by WST-8 colorimetric assay

**Table 1**  $^1\text{H}$  and  $^{13}\text{C}$  NMR spectral data for **1** and aplysamine 4

No.	<b>1</b>		Aplysamine 4	
	$^{13}\text{C}$	$^1\text{H}$ (J/Hz)	$^{13}\text{C}$	$^1\text{H}$ (J/Hz)
1	134.4	7.52 (1H, s)	134.2	7.47 (1H, s)
2	118.6		118.5	
3	152.0		152.1	
4	118.6		118.6	
5	134.4	7.52 (1H, s)	134.4	7.47 (1H, s)
6	137.3		137.2	
7	28.7	3.87 (2H, s)	28.7	3.82 (1H, s)
8	153.8		153.6	
9	165.4		165.2	
10	41.7	3.45 (2H, t, 7.09, 7.33)	41.3	3.43 (2H, t, 7.09, 7.33)
11	34.9	2.73 (2H, t, 7.09, 7.33)	35.1	2.75 (2H, t, 7.09, 7.33)
12	134.6		139.9	
13	133.6	7.36 (1H, s)	134.4	7.38 (1H, s)
14	112.1		118.7	
15	150.7		152.0	
16	112.1		118.7	
17	133.6	7.36 (1H, s)	134.4	7.38 (1H, s)
18			71.6	4.06 (2H, t, 5.8)
19			28.9	2.18 (2H, tt, 5.8, 7.8)
20			38.7	3.29 (2H, t, 7.8)
MeO	61.0	3.85 (3H, s)	60.9	3.81 (3H, s)

$^1\text{H}$  (500 MHz) and  $^{13}\text{C}$  (125 MHz) NMR spectra were taken on an NMR System 500 NB CL (Varian, Palo Alto, CA, USA) in  $\text{CD}_3\text{OD}$ , and the solvent peak was used as an internal standard ( $\delta_{\text{C}}$  49.0,  $\delta_{\text{H}}$  3.30).

(Dojindo, Kumamoto, Japan). HeLa cells were treated for 48 h with various concentrations of **1** and aplysamine 4, which showed the cytotoxic effects in a dose-dependent manner with the  $\text{IC}_{50}$  values of 3.7 and 3.4  $\mu\text{M}$ , respectively. These results indicate that a 3-aminopropanol chain structure at C-15 does not affect cytotoxic activity. As **1** is a structurally interesting compound, it is expected to be a potential candidate for a novel anti-cancer drug targeting new molecules. Studies on detailed biological activities are now underway.

#### ACKNOWLEDGEMENTS

This work was supported in part by the New Energy and Industrial Technology Development Organization of Japan (NEDO) and by a Grant-in-Aid for Scientific Research (20380070 to KS) from The Japan Society for the Promotion of Science (JSPS).

- 1 James, D. M., Kunze, H. B. & Faulkner, D. J. Two New Brominated Tyrosine Derivatives from the Sponge *Druinella* (= *Psammaplysilla*) *purpurea*. *J. Nat. Prod.* **54**, 1137–1140 (1991).
- 2 Nakamura, H. *et al.* Puralin, a novel enzyme activator from the Okinawan marine sponge *Psammaplysilla purea*. *Tetrahedron Lett.* **26**, 4517–4520 (1985).
- 3 Takito, J. *et al.* Puralin, a novel stabilizer of smooth muscle myosin filaments that modulates ATPase activity of dephosphorylated myosin. *J. Biol. Chem.* **261**, 13861–13865 (1986).
- 4 Nakamura, Y. *et al.* Puralin, a novel activator of skeletal muscle actomyosin ATPase and myosin EDTA-ATPase that enhanced the superprecipitation of actomyosin. *Eur. J. Biochem.* **167**, 1–6 (1987).
- 5 Wu, H., Nakamura, H., Kobayashi, J., Ohizumi, Y. & Hirata, Y. Lipopurealins, novel bromotyrosine derivatives with long chain acyl groups, from the marine sponge *Psammaplysilla purea*. *Experientia* **42**, 855–856 (1986).
- 6 Kobayashi, J., Honma, K., Tsuda, M. & Kosaka, T. Lipopurealins D and E and Puralidin H, New Bromotyrosine Alkaloids from the Okinawan Marine Sponge *Psammaplysilla purea*. *J. Nat. Prod.* **58**, 467–470 (1995).
- 7 Ishibashi, M., Tsuda, M., Ohizumi, Y., Sasaki, T. & Kobayashi, J. Puralidin A, a new cytotoxic bromotyrosine-derived alkaloid from the Okinawan marine sponge *Psammaplysilla purea*. *Experientia* **47**, 299–300 (1991).
- 8 Kobayashi, J. *et al.* Puralidins B and C, new bromotyrosine alkaloids from the okinawan marine sponge *psammaplysilla purea*. *Tetrahedron* **47**, 6617–6622 (1991).
- 9 Tsuda, M., Shigemori, H. & Ishibashi, H. Puralidin D, a new pyridine alkaloid from the okinawan marine sponge *psammaplysilla purea*. *Tetrahedron Lett.* **33**, 2597–2598 (1992).
- 10 Tsuda, M., Shigemori, H., Ishibashi, M. & Kobayashi, J. Puralidins E-G, New Bromotyrosine Alkaloids from the Okinawan Marine Sponge *Psammaplysilla purea*. *J. Nat. Prod.* **55**, 1325–1327 (1992).
- 11 Tabudravu, J. N. & Jaspars, M. Puralidin S and Purpuramine J, Bromotyrosine Alkaloids from the Fijian Marine Sponge *Druinella* sp. *J. Nat. Prod.* **65**, 1798–1801 (2002).
- 12 Roll, D. M. *et al.* Structure of the psammaplysins. *J. Am. Chem. Soc.* **107**, 2916–2920 (1985).
- 13 Yagi, H., Matsunaga, S. & Fusetani, N. Purpuramines A-I, new bromotyrosine-derived metabolites from the marine sponge *Psammaplysilla purpurea*. *Tetrahedron* **49**, 3749–3754 (1993).
- 14 Jurek, J., Yoshida, W. Y., Scheuer, P. J. & Kelly-Borges, M. Three New Bromotyrosine-Derived Metabolites of the Sponge *Psammaplysilla purpurea*. *J. Nat. Prod.* **56**, 1609–1612 (1993).
- 15 Carney, J. R., Scheuer, P. J. & Kelly-Borges, M. A New Bastadin from the Sponge *Psammaplysilla purpurea*. *J. Nat. Prod.* **56**, 153–157 (1993).
- 16 Longeon, A., Guyot, M. & Vacelet, J. Araplysillins-I and-II: biologically active dibromotyrosine derivatives from the sponge *Psammaplysilla Arabica*. *Experientia*. **46**, 548 (1990).
- 17 Arabshahi, L. & Schmitz, F. J. Brominated tyrosine metabolites from an unidentified sponge. *J. Org. Chem.* **52**, 3584–3586 (1987).

## NOTE

# Astaxanthin dirhamnoside, a new astaxanthin derivative produced by a radio-tolerant bacterium, *Sphingomonas astaxanthinifaciens*

Dalal Asker<sup>1</sup>, Sho-ichi Amano<sup>1</sup>, Kaori Morita<sup>1</sup>, Kazuya Tamura<sup>1</sup>, Shohei Sakuda<sup>2</sup>, Naoya Kikuchi<sup>2</sup>, Kazuo Furihata<sup>2</sup>, Hiroshi Matsufuji<sup>3</sup>, Teruhiko Beppu<sup>1</sup> and Kenji Ueda<sup>1</sup>

*The Journal of Antibiotics* (2009) 62, 397–399; doi:10.1038/ja.2009.50; published online 26 June 2009

**Keywords:** antioxidant activity; astaxanthin dirhamnoside; carotenoid; *Sphingomonas astaxanthinifaciens*

Astaxanthin (**2**) (Figure 1) is a red carotenoid renowned for a high antioxidant activity.<sup>1</sup> Owing to the protective function as well as the profitable effect on organoleptic properties, the use of this carotenoid benefits consumer acceptance of commercial products. Currently, it is extensively used as feed additives for fish, lobsters and chickens. Astaxanthin is also used as a nutraceutical and medicinal ingredient against degenerative diseases, such as cancer, skin-related illness and heart diseases.<sup>2–4</sup> An astaxanthin-containing microalga has provided a new strategy in treatment against *Helicobacter pylori* infection.<sup>5</sup> Thus, this carotenoid species provides wide application in agricultural, medicinal and pharmaceutical industries.<sup>3</sup>

We previously reported the isolation of carotenoid-producing bacteria from Misasa (Tottori, Japan), a region known for high radioactivity content, and their marked phylogenetic diversity.<sup>6</sup> The frequent isolation of carotenoid producers made us assume that there is some correlation between productivity of the protective pigment and persistence in a radioactive environment of microorganisms.<sup>6</sup> Recently, we taxonomically characterized one of the radio-tolerant isolates (strain TDMA-17), and validated it to be *Sphingomonas astaxanthinifaciens*, a novel species of the gram-negative bacterial genus *Sphingomonas*.<sup>7</sup>

The amount of carotenoids produced by *S. astaxanthinifaciens* was significantly high (2.8 mg g<sup>-1</sup> dry cells); interestingly, the HPLC analysis showed that the red pigment fraction of this strain contained astaxanthin (24.6%) and dihydroxyastaxanthin (7.5%) as minor components and an unknown substance (carotenoid **1**) as a major component (58.4%).<sup>7</sup> The unknown component was assumed to be an astaxanthin derivative, as it showed a similar absorption maximum as astaxanthin at around 470 nm. In this study, we isolated the major carotenoid **1** produced by *S. astaxanthinifaciens*, and determined its chemical structure.

To isolate the major carotenoid pigment, *S. astaxanthinifaciens* NBRC102146 was cultured in PE medium (containing (g l<sup>-1</sup>): Bactopeptone (Difco, Detroit, MI, USA), 4; Bactoyeast extract (Difco), 2; NaCl, 5; fish meat extract, (Kyokuto, Tokyo, Japan) 2; MgSO<sub>4</sub>, 2 and maltose 10 (pH 7.2)) (chemicals were purchased from Kokusan, Tokyo, Japan, if not indicated otherwise) shaken at 180 rpm for 2 days at 37 °C. The cells of *S. astaxanthinifaciens* were harvested by centrifugation at 9000×g, suspended in five times volume of methanol, and shaken at 180 rpm for 30 min at 28 °C and filtrated. This extraction process was repeated three times. Then, the filtrates were combined, dried up by evaporation and dissolved in CHCl<sub>3</sub>. The CHCl<sub>3</sub> solution was then applied to Purif-pack silica-gel chromatography (Moritex, Tokyo, Japan). After washing the column with CHCl<sub>3</sub>, the pigment was eluted with CHCl<sub>3</sub>/methanol (9:1). The eluate was dried up, dissolved in an adequate volume of CHCl<sub>3</sub>/methanol (9:1) and applied onto a preparative C18-TLC (Whatman, Maidstone, UK) developed with CHCl<sub>3</sub>/methanol (4:1) to isolate the final principle. By this process, ~56 mg carotenoid **1** and 4.7 mg astaxanthin were obtained. All procedures were performed under dim light.

The UV-vis absorption spectra in the HPLC eluent of MeOH were measured with a Shimadzu SPD-M10AVP photodiode array spectrophotometer (Shimadzu, Kyoto, Japan). NMR spectra were recorded on a Varian Unity INOVA 500 (Varian, Palo Alto, CA, USA) or JEOL JMN-600 spectrometer (JEOL, Tokyo, Japan). Electrospray ionization-time of flight mass (ESI-TOFMS) spectra were recorded using a JEOL JMS-T100LC AccuTOF (JEOL). IR and CD spectra were measured with an FT/IR 4000 spectrometer (JASCO, Tokyo, Japan) and J-720 spectropolarimeter (JASCO), respectively. The analytical data of carotenoid **1** were as follows: Vis in ether/2-methylbutane/ethanol (5:5:1) λ<sub>max</sub> (ε) 471 (130 000); CD in ether/2-methylbutane/ethanol

<sup>1</sup>Life Science Research Center, College of Bioresource Sciences, Nihon University, Fujisawa, Japan; <sup>2</sup>Department of Applied Biological Chemistry, Graduate School of Agriculture and Life Sciences, The University of Tokyo, Bunkyo-ku, Tokyo, Japan and <sup>3</sup>Department of Food Bioscience and Biotechnology, College of Bioresource Sciences, Nihon University, Fujisawa, Japan  
Correspondence: Dr K Ueda, College of Bioresource Sciences, Life Science Research Center, Nihon University, 1866 Kameino, Fujisawa 252–8510, Japan.  
E-mail: ueda@brs.nihon-u.ac.jp

Received 24 April 2009; revised 18 May 2009; accepted 27 May 2009; published online 26 June 2009



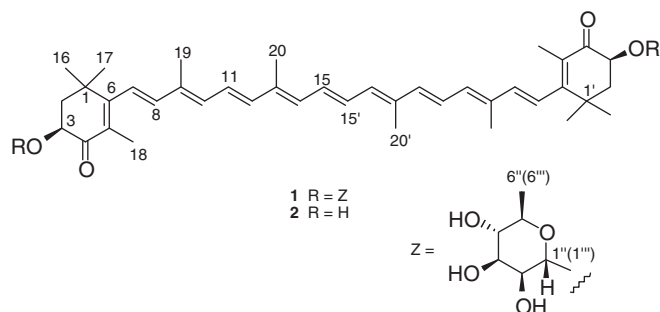


**Figure 1** Chemical structure of astaxanthin dirhamnoside (**1**) and astaxanthin (**2**).

(5:5:1)  $\Delta\epsilon_{381}=1.5$ ,  $\Delta\epsilon_{351}=0$ ,  $\Delta\epsilon_{310}=-18.1$ ,  $\Delta\epsilon_{282}=0$ ,  $\Delta\epsilon_{274}=6.5$ ,  $\Delta\epsilon_{253}=0$ ,  $\Delta\epsilon_{245}=-15.0$ ;  $^1\text{H}$  NMR (DMSO- $d_6$ , 500 MHz) and  $^{13}\text{C}$  NMR (125 MHz), see Table 1; ESI-TOFMS  $m/z$  889 (M+H) $^+$ , 911 (M+Na) $^+$ ; HRESI-TOFMS  $m/z$  911.4878 (M+Na) $^+$  (calcd for  $\text{C}_{52}\text{H}_{72}\text{NaO}_{12}$ , 911.4921); IR (nujol) 3337, 1668, 1039  $\text{cm}^{-1}$ . The  $^1\text{H}$  and  $^{13}\text{C}$  NMR data of **1** in DMSO- $d_6$  (Table 1) indicated the presence of astaxanthin as the carotenoid moiety and two rhamnose residues. The values of  $^3J_{\text{H}-1''(\text{H}-1'''),\text{H}-2''(\text{H}-2''')}$  (1 Hz) $^8$  and  $^1J_{\text{C}-1''(\text{C}-1'''),\text{H}-1''(\text{H}-1''')}$  (171 Hz) $^9$  of rhamnose moieties indicated the  $\alpha$ -glycoside.

To determine the absolute configuration of rhamnose moieties of **1**, methyl 2,3,4-tribenzoyl- $\alpha$ -rhamnopyranoside was derived from **1** and its CD spectrum was compared with that of authentic D-rhamnose. Astaxanthin dirhamnoside **1** (7.2 mg) was hydrolyzed in a sealed tube with 4 M HCl at 105 °C for 3 h. The reaction solution was evaporated to remove HCl and lyophilized. The obtained residue (5.2 mg) was treated with 5% HCl-methanol (3 ml) at room temperature for 1 h and the reaction solution was applied on a Dowex-1 (OH $^-$  type; Wako Pure Chemicals, Osaka, Japan) column. The passed-through solution from the column was evaporated and benzoylated with benzoyl chloride (0.5 ml) in dry pyridine (4 ml) containing 4-dimethylamino-pyridine (2 mg). Water was put into the reaction solution and extracted with ethyl acetate. The ethyl acetate solution was washed with sat. NaCl, sat. NaHCO $_3$  and water, successively, and dried with anhydrous Na $_2$ SO $_4$  and evaporated. The residue was loaded on a silica gel column (Wakogel C-200, 40 g) (Wako) packed with *n*-hexane and eluted stepwise with *n*-hexane-ethyl acetate (95:5, 1.5 l) and ethyl acetate (500 ml). The ethyl acetate fraction (26.5 mg) was washed with sat. NaCl, sat. NaHCO $_3$  and water, successively, and evaporated. The obtained residue (3.3 mg) was purified by HPLC on a 250 $\times$ 20 mm i.d. Capcell-Pak C $_{18}$  column with a gradient of 60–100% acetonitrile in water in 15 min and then isocratic elution of 100% acetonitrile at a flow rate of 5 ml min $^{-1}$  to obtain methyl 2,3,4-tribenzoyl- $\alpha$ -rhamnopyranoside (retention time: 26.7 min; yield: 40  $\mu\text{g}$ ).

Authentic methyl 2,3,4-tribenzoyl- $\alpha$ -D-rhamnopyranoside (2.5 mg) was prepared from  $\alpha$ -D-rhamnose (25.0 mg) by 5% HCl-methanol treatment and benzoylation using the same method mentioned above. The spectral data of authentic methyl 2,3,4-tribenzoyl- $\alpha$ -D-rhamnopyranoside: ESI-TOFMS  $m/z$  513 (M+Na) $^+$ ; CD in acetonitrile  $\Delta\epsilon_{238}=7.3$ ,  $\Delta\epsilon_{227}=0$ ,  $\Delta\epsilon_{221}=-2.3$ ;  $\delta_{\text{H}}$  (CDCl $_3$ , 600 MHz): 7.2–8.2 (15H, Bz), 5.92 (1H, d,  $J=4$  Hz, H-2), 5.63 (1H, t,  $J=10$  Hz, H-4), 5.55 (1H, dd,  $J=10, 4$  Hz, H-3), 4.79 (1H, s, H-1), 3.85 (1H, m, H-5), 3.57 (3H, s, OCH $_3$ ), 1.45 (3H, d,  $J=6$  Hz, H-6). As the retention time on HPLC and ESI-TOFMS, and CD spectra of the derivative from **1** were identical with those of authentic methyl 2,3,4-tribenzoyl- $\alpha$ -D-rhamnopyranoside, the configuration of the rhamnose moieties of **1** was determined as D. The CD spectrum of **2** isolated from the cells of

**Table 1**  $^1\text{H}$  and  $^{13}\text{C}$  assignments of astaxanthin dirhamnoside $^a$

C no.	$\delta_{\text{C}}$	$\delta_{\text{H}}$
1, 1'	36.7	
2, 2'	44.26	1.89, 1.87
3, 3'	71.33	4.36 dd (13, 5.5)
4, 4'	197.80	
5, 5'	127.41	
6, 6'	159.95	
7, 7'	123.81	6.28 d (16)
8, 8'	141.58	6.50 d (16)
9, 9'	134.98	
10, 10'	134.92	6.42 d (12)
11, 11'	125.15	6.71 dd (15, 12)
12, 12'	139.29	6.49 d (15)
13, 13'	136.62	
14, 14'	133.76	6.40 dd (8, 3)
15, 15'	130.98	6.76 dd (8, 3)
16, 16'	26.06	1.28 s
17, 17'	30.09	1.17 s
18, 18'	13.78	1.79 s
19, 19'	12.37	1.99 s
20, 20'	12.62	1.96 s
1'', 1'''	100.29	4.92 d (1)
2'', 2'''	70.25	3.75 ( $J_{2,3}=3.6$ Hz) $^b$
2''-OH, 2'''-OH		4.84 d (4)
3'', 3'''	70.49	3.43 ( $J_{3,4}=9.5$ Hz) $^b$
3''-OH, 3'''-OH	70.4	4.58 d (6)
4'', 4'''	71.94	3.20 ( $J_{4,5}=9.5$ Hz) $^b$
4''-OH, 4'''-OH		4.78 d (5)
5'', 5'''	68.98	3.44
6'', 6'''	17.9	1.14 d (6)

Coupling constants in Hertz are given in parentheses.

$^a$ Spectra were obtained in DMSO- $d_6$ .

$^b$ Obtained by decoupling experiments.

*S. astaxanthinifaciens* indicated the (3*S*,3'*S*) configuration of **2**, strongly suggesting the (3*S*,3'*S*) configuration of **1**. This was confirmed by the CD spectrum of **1** having the minimum or maximum Cotton effects at 310 ( $\Delta\epsilon -18.1$ ), 274 ( $\Delta\epsilon +6.5$ ) and 245 nm ( $\Delta\epsilon -15.0$ ), which was compatible with (3*S*,3'*S*)-**2** or (3*S*,3'*S*)-**2** monoglucoside (314 ( $\Delta\epsilon -18.5$ ), 274 ( $\Delta\epsilon +10.1$ ) and 242 nm ( $\Delta\epsilon -12.0$ )). $^{10}$  Therefore, the structure of the major carotenoid of *S. astaxanthinifaciens* was assigned as (3*S*,3'*S*)-3,3'-bis( $\alpha$ -D-rhamnopyranosyloxy)- $\beta$ , $\beta$ -carotene-4,4'-dione (**1**) (Figure 1).

Antioxidant activity of compound **1** was measured by the inhibition of methyl linoleate hydroperoxide production because of the reaction of methyl linoleate with 2,2'-azobis(2,4-dimethylvaleronitrile) (AMVN). $^{11}$  Reaction mixture (containing ( $\mu\text{l}$ ): methyl linoleate, 50; ethanol, 450; 0.15 mM AMVN, 125 and 1 mM carotenoid in CHCl $_3$ , 125) was incubated at 37 °C for 4 h with reciprocal shaking at 80 rpm under dark conditions. The reactant was analyzed by normal phase HPLC using a Shodex SIL 5B column (4.6 $\times$ 250 mm; Showa Denko, Tokyo, Japan) (mobile phase, *n*-hexane/2-propanol (99:1); flow rate, 1.0 ml min $^{-1}$ ;  $\lambda=235$  nm), and measured for the content of the four kinds of hydroperoxides. The antioxidant activity was expressed as a percentage of inhibition of hydroperoxide production because of the addition of carotenoids. The result showed that 1 mM of astaxanthin, astaxanthin dirhamnoside and  $\beta$ -carotene inhibited methyl linoleate hydroperoxide production at 27, 20 and 16%, respectively (a representative result; though the inhibitory values fluctuated, similar results were obtained in analyses repeated three times). This indicated that

compound **1** shows a distinct antioxidant activity, which is slightly lower than that of astaxanthin.

Compound **1** was also studied for solubility in a water-based solvent by a spectroscopic measurement. First, carotenoid **1** and astaxanthin were dissolved in 100% dimethyl sulfoxide (DMSO), acetone and methanol at 20 mM. The solutions were then added with water at various ratios. After removing the insoluble pigment particles by filtration (pore size, 0.1  $\mu\text{m}$ ; Millipore, Billerica, MA, USA), each solution was measured for absorption at 475 nm. Similarly, the absorption of the above 20 mM solution and its diluted series was measured and used as standards to quantify the amount of solubilized pigment. Astaxanthin dirhamnoside was dissolved in solutions of H<sub>2</sub>O–DMSO (99:1), H<sub>2</sub>O–acetone (99:1) and H<sub>2</sub>O–methanol (99:1) at 13, 6.2 and 5.4  $\mu\text{M}$ , respectively. Solubility of astaxanthin in these water-containing solvents was below the detectable level (<0.1%) (appearance of various solutions is shown in Supplementary Figure S1).

The known carotenoid rhamnosides to date include myxocoxanthin rhamnoside from myxobacterium,<sup>12</sup> and oscillol 2,2'-dirhamnoside<sup>13</sup> and myxol 2'-rhamnoside<sup>14</sup> from blue-green algae. Although these known molecular species were produced as minor components, astaxanthin dirhamnoside (**1**) identified in this study was a major carotenoid of *S. astaxanthinifaciens*. The unique properties of astaxanthin dirhamnoside may expand the application of this kind of carotenoids.

#### ACKNOWLEDGEMENTS

This study was supported by the High-Tech Research Center Project of the Ministry of Education, Culture, Sports, Science and Technology, Japan. DA was supported by a JSPS fellowship.

- 1 Bhosale, P. & Bernstein, P. S. Microbial xanthophylls. *Appl. Microbiol. Biotechnol.* **68**, 445–455 (2005).
- 2 Chew, B. P., Park, J. S., Wong, M. W. & Wong, T. S. A comparison of the anticancer activities of dietary beta-carotene, canthaxanthin and astaxanthin in mice *in vivo*. *Anticancer Res.* **19**, 1849–1853 (1999).
- 3 Guerin, M., Huntley, M. E. & Olaizola, M. Haematococcus astaxanthin: applications for human health and nutrition. *Trends Biotechnol.* **21**, 210–216 (2003).
- 4 Mayne, S. T. Beta-carotene, carotenoids, and disease prevention in humans. *Faseb J.* **10**, 690–701 (1996).
- 5 Wang, X., Willen, R. & Wadstrom, T. Astaxanthin-rich algal meal and vitamin C inhibit *Helicobacter pylori* infection in BALB/cA mice. *Antimicrob. Agents Chemother.* **44**, 2452–2457 (2000).
- 6 Asker, D., Beppu, T. & Ueda, K. Unique diversity of carotenoid-producing bacteria isolated from Misasa, a radioactive site in Japan. *Appl. Microbiol. Biotechnol.* **77**, 383–392 (2007).
- 7 Asker, D., Beppu, T. & Ueda, K. *Sphingomonas astaxanthinifaciens* sp. nov., a novel astaxanthin-producing bacterium of the family Sphingomonadaceae isolated from Misasa, Tottori, Japan. *FEMS Microbiol. Lett.* **273**, 140–148 (2007).
- 8 Yang, S. W. *et al.* Three new ellagic acid derivatives from the bark of *Eschweilera coriacea* from the Suriname rainforest. *J. Nat. Prod.* **61**, 901–906 (1998).
- 9 Bock, K. & Pedersen, C. A study of <sup>13</sup>C coupling constants in hexopyranoses. *J. Chem. Soc. Perkin Trans. II*, 293–297 (1974).
- 10 Yokoyama, A., Adachi, K. & Shizuri, Y. New carotenoid glucosides, astaxanthin glucoside and *adonixanthin glucoside*, isolated from the Astaxanthin-producing marine bacterium, *Agrobacterium aurantiacum*. *J. Nat. Prod.* **58**, 1929–1933 (1995).
- 11 Terao, J. Antioxidant activity of beta-carotene-related carotenoids in solution. *Lipids* **24**, 659–661 (1989).
- 12 Kleinig, H., Reichenbach, H., Achenbach, H. & Stadler, J. Carotenoid pigments of *Sorangium compositum* (Myxobacterales) including two new carotenoid glucoside esters and two new carotenoid rhamnosides. *Arch. Mikrobiol.* **78**, 224–233 (1971).
- 13 Hertzberg, S. & Liaaen-Jensen, S. Carotenoids of blue-green algae: 5. The structure of oscillaxanthin. *Phytochemistry* **8**, 1281–1292 (1969).
- 14 Halfen, L. N. & Francis, G. W. The influence of culture temperature on the carotenoid composition of the blue-green alga, *Anacystis nidulans*. *Arch. Mikrobiol.* **81**, 25–35 (1972).

Supplementary Information accompanies the paper on The Journal of Antibiotics website (<http://www.nature.com/ja>)

## NOTE

# Sch 1385568, a new azaphilone from *Aspergillus* sp.

Shu-Wei Yang, Tze-Ming Chan, Joseph Terracciano<sup>1</sup>, David Loebenberg, Mahesh Patel<sup>2</sup>, Vincent Gullo<sup>3</sup> and Min Chu<sup>1</sup>

*The Journal of Antibiotics* (2009) 62, 401–403; doi:10.1038/ja.2009.51; published online 26 June 2009

**Keywords:** *Aspergillus* sp.; azaphilone; Sch 1385568; structure elucidation

In the course of our continuing search for novel antimicrobial agents,<sup>1,2</sup> we have identified a novel azaphilone Sch 1385568 (**1**) (Scheme 1) from an *Aspergillus* sp. culture (SPRI-0814). Various azaphilones and hydrogenated azaphilones have been isolated mainly from fungal species, such as *Emericella* sp.,<sup>3–5</sup> *Penicillium* sp.,<sup>6–8</sup> *Phomopsis* sp.,<sup>9</sup> *Chaetomium* sp.,<sup>10</sup> *Pseudohalonectria* sp.<sup>11</sup> and *Annu-lohyphoxylon* sp.<sup>12</sup> Some of them have been described to show biological activities against various targets related to the different therapeutic areas, including cardiovascular, lipid metabolism, inflammatory, anti-infectious and antitumor areas. More specifically, azaphilones have been reported to display inhibitory activity against the following targets: acyl-CoA: cholesterol acyltransferase,<sup>6</sup> endothelin receptor,<sup>8</sup> cholesteryl ester transfer protein,<sup>13</sup> platelet-derived growth factor,<sup>14</sup> gp120-CD4,<sup>15</sup> monoamine oxidase,<sup>16</sup> phospholipase A<sub>2</sub><sup>17</sup> and nitric oxide production.<sup>18</sup> Some azaphilones have also been reported to display antitumor<sup>10,19</sup> and antimicrobial activities.<sup>10–12</sup> In this communication, we describe the fermentation, isolation, structure elucidation and antimicrobial activity of **1**.

Fermentation of *Aspergillus* sp. culture SPRI-0814 was conducted in shake flasks. Stock cultures were maintained as frozen whole broths at –80 °C in a final concentration of 10% glycerol. The germination medium contained proteus peptone 5.0 g, NaCl 5.0 g, KH<sub>2</sub>PO<sub>4</sub> 5.0 g, yeast extract 3.0 g, cerelose 20 g and soybean grits 5.0 g in 1.0 l tap water with pH 7.0 before autoclaving. Each 250 ml flask containing 70 ml of this medium was inoculated with 2 ml of the stock culture. The flasks were incubated at 24 °C on a rotary shaker at 250 rpm for 4 days to obtain the first stage seed. The above procedure was repeated using the first stage seed to obtain the second stage seed. This second stage seed was then used to inoculate the fermentation medium at 5% v/v. The fermentation was carried out in 500 ml flasks, each containing 100 ml of the fermentation medium, which consisted of neopeptone 10 g and cerelose 40 g in 1.0 l tap water. The pH was adjusted to 7.4, and CaCO<sub>3</sub> (4 g l<sup>-1</sup>) was added. The flasks were incubated at 24 °C in a rotary shaker at 250 rpm for 7 days.

The harvested fermentation broth (10 l) was mixed with NaCl (2 kg) and acetonitrile (MeCN, 20 l) for 15 min. The organic layer was separated and concentrated to a slurry, and then the slurry material was absorbed onto the polymeric resin, CG161 (~200 ml, Tosoh Biosep LLC, Montgomeryville, PA, USA). The salts and hydrophilic substances were removed by washing with water (20 l). Then, the absorbed organic material was eluted with 85% aq. MeOH (4 l) to yield ~2.4 g of dried material after concentration *in vacuo*. Part of this organic material was purified on a semi-preparative ODS-A HPLC column (YMC, 120 Å, S-7, 20×250 mm; Waters HPLC, Millennium System (Milford, MA, USA), equipped with a photodiode array detector). The column was eluted with a gradient of MeCN-H<sub>2</sub>O: 5–100% MeCN in 50 min, and then held isocratically with 100% MeCN for an additional 15 min with a flow rate of 15 ml min<sup>-1</sup>. All fractions were collected and analyzed on the basis of a UV chromatogram. Pure **1** (~5 mg) was obtained from three injections of the enriched material (40 mg each).

The structure of **1** was mainly elucidated by extensive one- and two-dimensional NMR analyses. In the <sup>1</sup>H-NMR spectrum, a total of 17 carbon-attached protons were detected. Three methyl and one methine signals were observed in the aliphatic region, and eight resonances were observed in the low-field region. In the <sup>13</sup>C NMR spectrum, 21 carbon signals were detected, in which a conjugated ketone functionality (C-6, δ 200.0) was identified. The molecular ion *m/z* 385, [M+H]<sup>+</sup> was observed on an electrospray ionisation-MS instrument (Applied Biosystem, Foster City, CA, USA, API-150Ex spectrometer), and therefore the molecular formula of **1** was calculated as C<sub>21</sub>H<sub>20</sub>O<sub>7</sub>. From the analyses of NMR and MS data, three hydroxyl groups were proposed to be present in the molecule based on only 17 protons observed in the <sup>1</sup>H-NMR spectrum. The azaphilone skeleton was mainly determined by <sup>1</sup>H–<sup>13</sup>C long-range correlations measured in a heteronuclear multiple bond correlation (HMBC) experiment. The methyl group showing a doublet–doublet resonance (H<sub>3</sub>-3', δ 1.88, dd, *J*=7.0, 1.7 Hz) in <sup>1</sup>H-NMR was determined to be

Schering-Plough Research Institute, Kenilworth, NJ, USA

<sup>1</sup>Current address: Cubist Pharmaceuticals, Inc. 65 Hayden Ave., Lexington, MA 02421, USA.

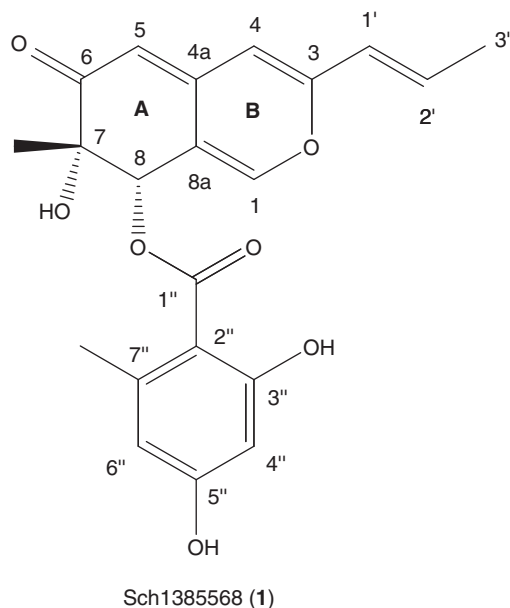
<sup>2</sup>Current address: SMP International LLC, 42 Brentwood Drive, Verona, NJ 07044, USA.

<sup>3</sup>Current address: Drew University, Charles A. Dana Research Institute, 36 Madison Ave., Madison, NJ 07940, USA.

Correspondence: Dr S-W Yang, Schering-Plough Research Institute, 2015 Galloping Hill Road, Kenilworth, NJ 07033-1300, USA.

E-mail: shu-wei.yang@spcorp.com

Received 22 April 2009; revised 26 May 2009; accepted 1 June 2009; published online 26 June 2009



Scheme 1 Structure of 1.

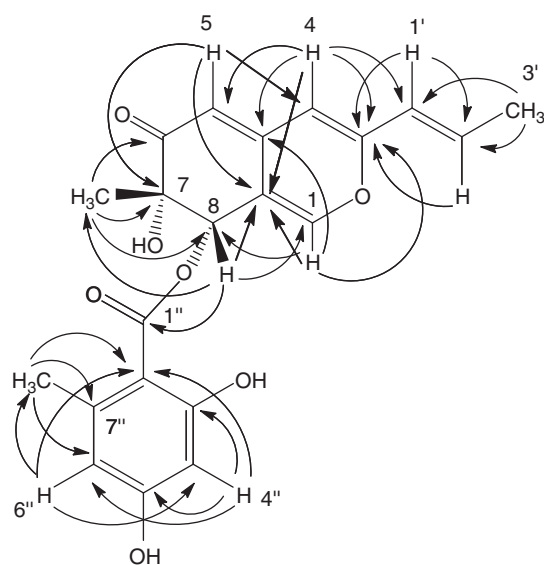


Figure 1 HMBC correlations of 1.

adjacent to a double bond consisting of two olefinic methine carbons (C-1' and C-2') because of the observation of the correlations between H<sub>3</sub>-3' and C-1' ( $\delta$  124.4) and C-2' ( $\delta$  136.0). This double bond was conjugated to the additional two double bonds and further extended to the ketone (C-6) at the other end on the basis of the following correlations: H-1' to C-3; H-2' to C-3; H-4 to C-3, C-4a, C-5, and C-1'; H-5 to C-4 and C-7; CH<sub>3</sub>-7 to C-6 and C-7 (Figure 1). The NOE correlations observed between H-1' and H<sub>3</sub>-3', H-1' and H-4', and H-4 and H-5 established linear conjugation and regiochemistry of the ketone-triene moiety. The oxygenated olefin proton signal (H-1,  $\delta$  7.75) showed correlations to the oxygenated olefinic C-3 ( $\delta$  157.5), C-4a ( $\delta$  146.7) and C-8a ( $\delta$  117.3) assembling a pyran moiety (ring B). The second methyl group (7-CH<sub>3</sub>,  $\delta$  1.36, s) substituted on an oxygenated quaternary carbon (C-7,  $\delta$  75.3) was located adjacent to

Table 1 NMR spectral data for compound 1 in CD<sub>3</sub>OD<sup>a</sup>

C/H no.	<sup>1</sup> H ( $\delta$ )	<sup>13</sup> C ( $\delta$ ) <sup>b</sup>	<sup>1</sup> H- <sup>1</sup> H COSY
1	7.75, 1H, d, <i>J</i> =1.2	150.9 d	H-5
3		157.5 s	
4	6.25, 1H, s	103.9 d	
4a		146.7 s	
5	5.44, 1H, d, <i>J</i> =1.2	105.9 d	
6		200.0 s	
7		75.3 s	
7-Me	1.36, 3H, s	24.6 q	
8	5.88, 1H, s	76.2 d	
8a		117.3 s	
1'	6.11, 1H, dq, <i>J</i> =15.8, 1.7	124.4 d	H-2'
2'	6.57, 1H, dq, <i>J</i> =15.8, 7.0	136.0 d	H-1', H-3'
3'	1.88, 3H, dd, <i>J</i> =7.0, 1.7	18.7 q	H-2'
1''		172.3 s	
2''		105.7 s	
3''		166.5 s	
4''	6.11, 1H, d, <i>J</i> =2.5	101.8 d	H-6''
5''		164.3 s	
6''	6.13, 1H, d, <i>J</i> =2.5	112.8 d	H-4''
7''		145.2 s	
7''-Me	2.25, 3H, s	24.7 q	

<sup>a</sup>Recorded on a Varian Unity 500 NMR instrument (Varian, Palo Alto, CA, USA) at 500 MHz for <sup>1</sup>H and 125 MHz for <sup>13</sup>C, using standard Varian pulse sequence programs (VNMR Version 6.1 Software).  $\delta$  in ppm; *J* in Hz.

<sup>b</sup>The proton-attached carbon signals showed cross peaks with its corresponding proton signals in the HSQC-COSY spectrum.

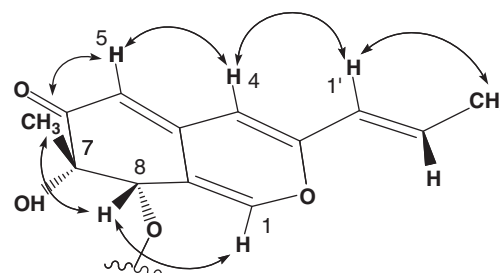


Figure 2 The relative configuration of 1 and NOE correlations observed in NOESY spectrum (represented by double arrows).

the conjugated ketone (C-6) and an aliphatic oxygenated methine carbon (C-8,  $\delta$  76.2) because of the significant coupling of CH<sub>3</sub>-7 and C-7, C-6 and C-8. C-8 was further identified to connect to C-8a based on the following long-range correlations: H-8 to C-1 and C-8a; H-1 to C-8. Therefore, the six-member ring A was constructed on the basis of these evidences. Thus, the 7,8-dihydro-6H-isochromen-6-one ring skeleton was determined.

The remaining seven carbons were constructed to represent a 2,4-dihydroxy-6-methyl-benzoyl moiety based on the following observation: correlations H-4'' to C-2'', C-3'', C-5'' and C-6''; H-6'' to C-2'', C-4'', C-5'' and CH<sub>3</sub>-7''; CH<sub>3</sub>-7'' to C-2'', C-6'' and C-7''. The <sup>13</sup>C chemical shifts of the highly substituted benzoyl moiety were identical to the data of the same benzoyl moiety reported in the literature.<sup>20</sup> The benzoyl group was unambiguously assigned to the 8-O position based on the correlation of H-8 and C-1'' ( $\delta$  172.3). Thus, the two-dimensional structure of 1 was determined, and the unambiguous assignment of the <sup>1</sup>H and <sup>13</sup>C chemical shifts was accomplished on the basis of the two-dimensional NMR data analyses including <sup>1</sup>H-<sup>1</sup>H COSY, HSQC and HMBC as detailed in Table 1.

The stereochemistry of **1** was established by the analyses of  $^1\text{H}$ - $^1\text{H}$  coupling constants and NOESY. The double bond  $\Delta 1',2'$  was determined as *trans* because of the typical large coupling constant ( $J=15.8$  Hz). The relative stereochemistry on C-7 and C-8 was assigned as *cis* configuration on the basis of the NOE correlations between H-8 and  $\text{CH}_3$ -7 as shown in Figure 2. The highly conjugated system and the double bond  $\Delta 1,8a$  led to the flat bicyclic ring system, causing pseudoaxial orientation of the 7-methyl group, sterically close to H-8. The absolute configuration of **1** was not studied because of the limited amount of the sample.

Most of the previously reported azaphilones possess benzoyl substitution on the C-7 position.<sup>3-5</sup> Benzoyl substitution on C-8 for azaphilone is rare.<sup>6,7,21</sup> To the best of our knowledge, Sch1385568 (**1**) represents the fourth example of a C-8 benzoyl-substituted azaphilone. It is a close analog of Sch 725680 and mitorubrinic acid B. Sch 725680 is a 1,8a-dihydroazaphilone derivative of **1**<sup>21</sup> and mitorubrinic acid B is an oxidative acidic analog of **1** at the 3' position.<sup>7</sup>

Sch1385568 (**1**) was evaluated for its antimicrobial activity. It displayed antifungal activity against *Saccharomyces cerevisiae* (PM503)<sup>22</sup> with an MIC of  $32\ \mu\text{g ml}^{-1}$ , and it was inactive against *Candida albicans* (C43) with an MIC of  $256\ \mu\text{g ml}^{-1}$ . In addition, **1** did not show antibacterial activity against *Staphylococcus aureus* at  $256\ \mu\text{g ml}^{-1}$ .

#### ACKNOWLEDGEMENTS

We are grateful to Mr Lewis B Fan for extract preparation and to Mr Ross Yang for MS measurement.

- 1 Yang, S. W. *et al.* A new 5-alkenylresorcinol Sch 725681 from *Aspergillus* sp. *J. Antibiot.* **59**, 190–192 (2006).
- 2 Yang, S. W. *et al.* Structure elucidation of Sch 725674 from *Aspergillus* sp. *J. Antibiot.* **58**, 535–538 (2005).
- 3 Itabashi, T. *et al.* Falconensins A, B, C, and D, new compounds related to azaphilone, from *Emericella falconensis*. *Chem. Pharm. Bull.* **40**, 3142–3144 (1992).
- 4 Itabashi, T., Nozawa, K., Nakajima, S. & Kawai, K. A new azaphilone, falconensin H, from *Emericella falconensis*. *Chem. Pharm. Bull.* **41**, 2040–2041 (1993).
- 5 Itabashi, T., Ogasawara, N., Nozawa, K. & Kawai, K. Isolation and structures of new azaphilone derivatives, falconensins E-G, from *Emericella falconensis* and absolute configurations of falconensins A-G. *Chem. Pharm. Bull.* **44**, 2213–2217 (1996).
- 6 Arai, N. *et al.* Isochromophilones III~VI, inhibitors of Acyl-CoA: cholesterol acyl-transferase produced by *Penicillium multicolor* FO-3216. *J. Antibiot.* **48**, 696–702 (1995) (Erratum: 48, C2 (1995)).
- 7 Natsume, M., Takahashi, Y. & Marumo, S. Mitorubrinic acid, a morphogenic substance inducing chlamydospore-like cells, and its related new metabolite, (+)-mitorubrinic acid B, isolated from *Penicillium funiculosum*. *Agric. Biol. Chem.* **49**, 2517–2519 (1985).
- 8 Pairet, L. *et al.* Azaphilones with endothelin receptor binding activity produced by *Penicillium sclerotiorum*: taxonomy, fermentation, isolation, structure elucidation and biological activity. *J. Antibiot.* **48**, 913–923 (1995).
- 9 Yu, B. Z. *et al.* Phomoeuphorbins A-D, azaphilones from the fungus *Phomopsis euphorbiae*. *Phytochemistry* **69**, 2523–2526 (2008).
- 10 Phonkerd, N. *et al.* Bis-spiro-azaphilones and azaphilones from the fungi *Chaetomium cochliodes* VTh01 and *C. cochliodes* CTh05. *Tetrahedron* **64**, 9636–9645 (2008).
- 11 Dong, J. *et al.* New nematocidal azaphilones from the aquatic fungus *Pseudohalonestria adversaria* YMF1.01019. *FEMS Microbiol. Lett.* **264**, 65–69 (2006).
- 12 Quang, D. N., Stadler, M., Fournier, J., Tomita, A. & Hashimoto, T. Cohaerins C-F, four azaphilones from the xylariaceous fungus *Annulohypoxylon cohaerens*. *Tetrahedron* **62**, 6349–6354 (2006).
- 13 Tomoda, H. *et al.* Structure-specific inhibition of cholesteryl ester transfer protein by azaphilones. *J. Antibiot.* **52**, 160–170 (1999).
- 14 Toki, S. *et al.* RP-1551s, a family of azaphilones produced by *Penicillium* sp., inhibit the binding of PDGF to the extracellular domain of its receptor. *J. Antibiot.* **52**, 235–244 (1999).
- 15 Matsuzaki, K. *et al.* New brominated and halogen-less derivatives and structure-activity relationship of azaphilones inhibiting gp120-CD4 binding. *J. Antibiot.* **51**, 1004–1011 (1998).
- 16 Fujimoto, H., Matsudo, T., Yamaguchi, A. & Yamazaki, M. Two new fungal azaphilones from *Talaromyces luteus*, with monoamine oxidase inhibitory effect. *Heterocycles* **30**, 607–616 (1990).
- 17 Nakamura, K., Kino, T., Niko, K., Kyotou, S. & Okuhara, M. Phospholipase A<sub>2</sub> inhibitors containing sclerotiorin from *Penicillium sclerotiorum* for treatment of inflammatory pancreatitis, and allergy JP 02255615 A2, 16 October (1990).
- 18 Quang, D. N. *et al.* Inhibition of nitric oxide production in RAW 264.7 cells by azaphilones from xylariaceous fungi. *Biol Pharm Bull* **29**, 34–37 (2006).
- 19 Yasukawa, K. *et al.* Azaphilones inhibit tumor promotion by 12-O-tetradecanoylphorbol-13-acetate in two-stage carcinogenesis in mice. *Oncology* **51**, 108–112 (1994).
- 20 Quang, D. N., Hashimoto, T., Stadler, M. & Asakawa, Y. Dimeric azaphilones from the xylariaceous ascomycete *Hypoxylon rutilum*. *Tetrahedron* **61**, 8451–8455 (2005).
- 21 Yang, S. W. *et al.* A new hydrogenated azaphilone Sch 725680 from *Aspergillus* sp. *J. Antibiot.* **59**, 720–723 (2006).
- 22 Yang, S. W. *et al.* Structure elucidation of a new antifungal sterol sulfate, Sch 575867, from a deep-water marine sponge (Family: *Astroscleridae*). *J. Antibiot.* **56**, 186–189 (2003).